NASA/CR—2005-213584/VOL4

Critical Propulsion Components
Volume 4: Inlet and Fan/Inlet Accoustics Team

Pratt & Whitney
West Palm Beach, Florida

General Electric Aircraft Engines
Cincinnati, Ohio

May 2005

The NASA STI Program Office . . . in Profile

Since its founding, NASA has been dedicated to the advancement of aeronautics and space science. The NASA Scientific and Technical Information (STI) Program Office plays a key part in helping NASA maintain this important role.

The NASA STI Program Office is operated by Langley Research Center, the Lead Center for NASA's scientific and technical information. The NASA STI Program Office provides access to the NASA STI Database, the largest collection of aeronautical and space science STI in the world. The Program Office is also NASA's institutional mechanism for disseminating the results of its research and development activities. These results are published by NASA in the NASA STI Report Series, which includes the following report types:

- TECHNICAL PUBLICATION. Reports of completed research or a major significant phase of research that present the results of NASA programs and include extensive data or theoretical analysis. Includes compilations of significant scientific and technical data and information deemed to be of continuing reference value. NASA's counterpart of peer-reviewed formal professional papers but has less stringent limitations on manuscript length and extent of graphic presentations.

- TECHNICAL MEMORANDUM. Scientific and technical findings that are preliminary or of specialized interest, e.g., quick release reports, working papers, and bibliographies that contain minimal annotation. Does not contain extensive analysis.

- CONTRACTOR REPORT. Scientific and technical findings by NASA-sponsored contractors and grantees.

- CONFERENCE PUBLICATION. Collected papers from scientific and technical conferences, symposia, seminars, or other meetings sponsored or cosponsored by NASA.

- SPECIAL PUBLICATION. Scientific, technical, or historical information from NASA programs, projects, and missions, often concerned with subjects having substantial public interest.

- TECHNICAL TRANSLATION. English-language translations of foreign scientific and technical material pertinent to NASA's mission.

Specialized services that complement the STI Program Office's diverse offerings include creating custom thesauri, building customized databases, organizing and publishing research results . . . even providing videos.

For more information about the NASA STI Program Office, see the following:

- Access the NASA STI Program Home Page at ***http://www.sti.nasa.gov***

- E-mail your question via the Internet to help@sti.nasa.gov

- Fax your question to the NASA Access Help Desk at 301–621–0134

- Telephone the NASA Access Help Desk at 301–621–0390

- Write to:
  NASA Access Help Desk
  NASA Center for AeroSpace Information
  7121 Standard Drive
  Hanover, MD 21076

NASA/CR—2005-213584/VOL4

Critical Propulsion Components
Volume 4: Inlet and Fan/Inlet Accoustics Team

Pratt & Whitney
West Palm Beach, Florida

General Electric Aircraft Engines
Cincinnati, Ohio

Prepared under Contract NAS3–27235

National Aeronautics and
Space Administration

Glenn Research Center

May 2005

Document History

This research was originally published in September 2000.

Available from

NASA Center for Aerospace Information
7121 Standard Drive
Hanover, MD 21076

National Technical Information Service
5285 Port Royal Road
Springfield, VA 22100

Available electronically at http://gltrs.grc.nasa.gov

Abstract

Several studies have concluded that a supersonic aircraft, if environmentally acceptable and economically viable, could successfully compete in the 21st century marketplace. However, before industry can commit to what is estimated as a 15-to-20 billion dollar investment, several barrier issues must be resolved. In an effort to address these barrier issues, NASA and Industry teamed to form the High-Speed Research (HSR) program. As part of this HSR program, the Critical Propulsion Components (CPC) element was created and assigned the task of developing those propulsion component technologies necessary to: (1) reduce cruise emissions by a factor of 10 and (2) meet the ever-increasing airport noise restrictions with an economically viable propulsion system. The CPC-identified critical components were ultra-low-emission combustors, low-noise/high-performance exhaust nozzles, low-noise fans, and stable/high-performance inlets. Propulsion cycle studies (coordinated with NASA–Langley sponsored airplane studies) were conducted throughout this CPC program to help evaluate candidate components and select the best concepts for the more complex and larger scale research efforts. The propulsion cycle and components ultimately selected were a mixed-flow turbofan (MFTF) engine employing a lean, premixed, prevaporized (LPP) combustor coupled to a two-dimensional mixed compression inlet and a two-dimensional mixer/ejector nozzle.

The CPC program began in 1994 and was planned for completion in 2002. Unfortunately, in 1999 NASA chose to prematurely end the HSR program. Although terminated early, the HSR program demonstrated that an economically viable and environmentally acceptable supersonic aircraft (and propulsion system) was achievable. The purpose of this document is to document the CPC findings in support of those visionaries in the future who have the courage to once again pursue a supersonic passenger airplane.

Due to the large amount of material presented in this report, it was prepared in four volumes:

Volume 1: Section 1 – Summary
Section 2 – Introduction
Section 3 – Propulsion System Studies

Volume 2: Section 4 – Combustor

Volume 3: Section 5 – Exhaust Nozzle

Volume 4: Section 6 – Inlet
Section 7 – Fan/Inlet Acoustic Team

Table of Contents

Table of Contents (Continued)

Table of Contents (Concluded)

List of Illustrations

List of Illustrations (Continued)

List of Illustrations (Continued)

List of Illustrations (Continued)

List of Illustrations

CG	Center of gravity
CG1	Turbomachinery center of gravity
CG2	Exhaust nozzle center of gravity
CG3	Overall engine center of gravity
CM	Coordination memo
CMC	Ceramic-matrix composite
CMMR	Critical major milestone review
CMT	CPC management team
CO	Carbon monoxide
COTR	Contracting Officer's Technical Representative
CPC	Critical Propulsion Components
CPR	Compressor pressure ratio
CR	Contractor report
CRAFT	Combustion Research and Flow Technology Inc.
CTOL	Conventional takeoff and landing
dB	Decibels
DEN	Double-edge notch
$\Delta H/T$	Specific work
DOC	Direct operating cost
DOC+I	Direct operating cost + interest
DoD	Department of Defense
DOE	Design of experiments
DOSS	Design optimization synthesis system (Boeing)
DP	Pressure drop or differential
DPC	Circumferential pressure distortion
DPC/Pmx	Circumferential-distortion parameter (total pressure)
DPE	Perfluoroalkyldiphenylether
DPR	Radial pressure distortion
DPR/Pmx	Radial-distortion parameter (total pressure)
DR&O	Design requirements and objectives (Boeing document)
DRD	Documentation requirements document
DS	Directionally solidified
DSM	Downstream mixer (exhaust nozzle)
DTR	Diffuser test rig
DVM	Discrete-vortex method
EB	Electron beam
EDM	Electrical-discharge machining (or machined)
EFH	Engine flight hour(s)
EI	Emissions index: g of pollutant per kg of fuel burned; also, environmental impact
EICO	CO emissions index: g CO/kg fuel
EIHC	HC emissions index: g of unburned hydrocarbons per kg of fuel burned
EINOx	NOx emissions index: g of NOx/kg fuel
EPM	Enabling Propulsion Materials
EPNdB	Effective perceived noise decibels
EPNL	Effective perceived noise level
ER	Extraction ratio: P_{16}/P_{56}
ESF	Engine scale factor
ESP	Electronically scanned pressure
ETA (η)	Efficiency
f/a	Fuel/air ratio
F/C	Fan/core
FA&M	Florida Agricultural and Mechanical University
FADEC	Full-authority digital electronic control
FAR	Fuel/air ratio, also Federal Aviation Regulation
FC	Fixed chute (mixer/ejector nozzle)
FCG	Fatigue crack growth
FCM	Fixed-chute mixer
FCN	Fixed-chute nozzle
FEGV	Fan exit guide vane
FEM	Finite-element model
FENTD	Full-scale engine nozzle technology demonstration/demonstrator (more frequently called FSD)

FH	Flight hour(s)
FIAT	Fan inlet/acoustics team (ITD team)
FLABI	"FLADE" bypass injector valve
FLADE	Fan-on-blade HSCT engine concept
FN, F_N, F_n	Net thrust
FNAA	Fan average
FNDAB	Net thrust with afterbody drag removed
FNP	Fixed chute, no plug; unsuppressed primary (idle) thrust; uninstalled net thrust
FNS	Full Navier–Stokes
$F_{n\ sup}$	Net thrust with nozzle in noise-suppression mode
FOD	Foreign-object damage
FPR	Fan pressure ratio
FSD	Full-scale demonstrator
FSN	Fluid-shield nozzle
FSPSTD	Full-scale propulsion system technology demonstrator
FTR	Formal test report
γ	Gamma titanium aluminide (TiAl)
GC/MS	Gas chromatography/mass spectrometry
GE AE	GE Aircraft Engines
GFY	Government fiscal year
GI	Ground idle
GOCAP	Goals, objectives, challenges, approaches, and programs
GOTCHA	Goals, objectives, technical challenges, and approaches
GRA	Geared rotary actuator
GRC	Glenn Research Center
HAM	Hot acoustic model
HART	Hot acoustic rig test
HARW	High aspect ratio wing
HC	Hydrocarbons (unburned, in exhaust gas)
HCF	High-cycle fatigue
HEAT	High-lift engine aeroacoustic technology
HIN	HEAT isolated nacelle
HISCAT	Highly integrated supersonic cruise airplane technology
HMMRA	Highly mixed multistage radial/axial
HP	High pressure, also horsepower
HPC	High-pressure compressor
HPT	High-pressure turbine
HPX	Horsepower extraction
HPXH	Customer (aircraft) power extraction
HPX(2)	Customer (aircraft) power extraction plus engine parasitic requirements
HS	High speed; also, Hamilton Sundstrand
HSCT	High Speed Civil Transport
HSR	High Speed Research
HSS	HEAT semispan
IBR	Integrally bladed rotor
ICAO	International Civil Aviation Organization
ICD	Interface control document
ID	Inner diameter
IFV	Inverter flow valve
IGV	Inlet guide vane(s)
IHPTET	Integrated High Performance Turbine Engine Technology
ILT	Interlaminar tension
IMFH	Integrated mixer/flameholder
IML	Increased mixer length (exhaust nozzle)
IMT	Industry method test-bed
IR&D	Independent Research and Development
IRR	Internal rate of return
ITD	Integrated technology development
JBTS	Jet burner test stand (UTRC facility)
JER	Jet exit rig
JN8, Jn8B2	Jet-noise prediction models (P&W)

JNL	Jet Noise Laboratory (NASA–Langley
KCAS	Knots, calibrated air speed
KEAS	Knots, equivalent air speed
KIVA II	A multidimensional CFD code
KONA	NASA database Unix server
KTAS	Knots, true air speed
L/D	Lift/drag ratio, also length/diameter ratio
LAPIN	Large-amplitude perturbation inlet (model)
LaRC	Langley Research Center
LBO	Lean blowout
LCF	Low-cycle fatigue
LDI	Lean direct (fuel) injection
LDV	Laser doppler velocimeter
LE, Le	Leading edge
LeRC	Lewis Research Center
LET	Large Engine Technology
LF	Linked flap
LHV	Latent heat value
LOL, LoL	Lobe on lobe
LP	Low pressure
LPC	Low-pressure compressor (main engine fan)
LPP	Lean premixed/prevaporized
LPT	Low-pressure turbine
LSAF	Low-speed aeroacoustic facility (Boeing)
LSAWT	Low-speed aeroacoustic wind tunnel
LSM	Large-scale model
LSMS	LSM similitude
LSWT	Low-speed wind tunnel
LTO	Landing/takeoff
LV	Laser velocimeter
M	Mach number
M_∞	Ambient Mach number
M_0	Free-stream Mach number
M14	Mach number at bypass duct inlet
M15	Mach number at bypass duct average area
M155, $M_{15.5}$	Maximum Mach number in fan duct (bypass duct over rear frame)
M16, M_{16}	Mach number at fan duct mixing plane (fan/core mixer duct side)
M2	Mach number at engine inlet
M21ID	Mach number at fan discharge ID
M21OD	Mach number at fan discharge OD
M25	Mach number at compressor inlet
M3	Mach number at compressor discharge
M36	Mach number at combustor inlet
M4	Mach number at HPT vane inlet
M49	Mach number at LPT rotor 1 inlet
M5	Mach number at LPT exit
M54	Mach number at rear frame/diffuser average area
M55	Mach number at mixer entrance, core stream
M56	Mach number at mixer exit, core stream
M68	Mach number at miniaugmentor exit
MAR	Mixing area ratio (duct)
MCP	Modular component predictor
MCTCB	Mixed compression translating centerbody (inlet)
MDA	McDonnell Douglas Aircraft
MDC	McDonnell Douglas Corporation
MDO	Multidiscipline optimization
M–E, M/E	Mixer/ejector (exhaust nozzle)
MFTF	Mixed-flow turbofan
MIDIS	Mixer/ejector inlet distortion study
MIT	Massachusetts Institute of Technology
MITCFA	MIT compound flow analysis (computer program)
MMC	Metal-matrix composite
Mn	Mach number

MPC	Multiple-component predictor
MRA	Multistage radial/axial
M&S	Materials and structure
MTF	Mid-tandem fan
MTOGW	Maximum takeoff gross weight
MTOW	Maximum takeoff weight
N1	Low-pressure rotor speed
N1C2	Low-pressure rotor speed corrected to station 2
N2C2.5	High-pressure rotor speed corrected to station 25 (compressor inlet)
N4	HP spool speed
N5	LP spool speed
NASA	National Aeronautics and Space Administration
NASA LaRC	NASA Langley Research Center
NASA LeRC	NASA Lewis Research Center (now NASA Glenn)
NASTRAN	Computer modeling software
NATR	Nozzle acoustic test rig
Nc, N_c	Corrected engine (shaft) speed
NCP	National cycle program
NFM	Nearly fully mixed
NOx	Oxides of nitrogen
Noy	Acoustic annoyance parameter
NPD	Noise power distance
NPSS	Numerical propulsion-system simulation
NPR	Nozzle pressure ratio
NRA	NASA Research Announcement
OAC	Optimized aeroelastic concept
OD	Outer diameter
OEW	Operating empty weight (no fuel, oil, etc.)
OEW–PR	OEW minus propulsion-system weight
OGV	Outlet guide vane(s)
OML	Outer mold line
OPR	Overall pressure ratio
P_{16}	Pressure exiting bypass duct
P16Q56	Extraction ratio
P_{56}	Pressure exiting core engine
PAI	Propulsion/airframe integration
PAIT	Propulsion/airframe integration technology
PC	Power code
PCC	Precision Castparts Co.
PDF	Probability density function
PDPA	Phase Doppler particle analyzer
PDR	Preliminary design (or data) review
PFPAE	Perfluoropolyakylether
PH3	Tri-perfluoropolyalkylether-phenyl-phosphine
PIC	Pressure-infiltration casting
PLIF	Planar laser-induced fluoresence
PLR	Programmable lapse rate
PMT	Propulsion Management Team
PMC	Polymer-matrix composite
PNLT	Tone-controlled perceived noise level
P&O	Performance and operability
PSET	Propulsion System Evaluation Team
PSI	Propulsion system integration, also Pressure Systems Inc.
PST	Propulsion selection team
PT, P_T	Total pressure
PT8	Exhaust gas total pressure at nozzle throat
PT14	Total pressure at bypass duct inlet
PT15	Total pressure at bypass duct average area
PT155	Total pressure at bypass duct over turbines and rear frame (mixer entrance)
PT16	Total pressure at mixer exit, bypass stream side
PT21	Total pressure at fan discharge
PT21A	Average total pressure at fan discharge

PT21ID	Total pressure at fan discharge inner diameter
PT21ID	Total pressure at fan discharge outer diameter
PT25	Total pressure at compressor inlet
PT3	Total pressure at compressor discharge
PT36, P_{T36}	Total pressure at compressor inlet
PT4	Total pressure at HPT vane inlet
PT5	Total pressure at LPT exit
PT55	Total pressure at mixer entrance, core stream side
PT56	Total pressure at mixer exit, core stream side
PT68	Total pressure at miniaugmentor exit
PT7	Total pressure at convergent nozzle inlet
PT8	Total Pressure at nozzle throat
PTC	Preliminary technology configuration
Q	Dynamic pressure
R1	First-stage rotor
R2	Second-stage rotor
R3	Third-stage rotor
RAN	Reynolds-averaged Navier–Stokes
RC	Round convergent (exhaust nozzle)
RM	Relative “mixedness”
ROM	Rough order of magnitude
RPM	Revolutions per minute
RQL	Rich (burn), quick (quench), lean (burn)
RR	Rolls Royce
RSQ	Reduced-scale quench
RTI	Reversing through inlet
RTO	Refused takeoff
Rx4	HPT pitch reaction
S/MTD	STOL and maneuvering technology demonstratior
S1	First-stage stator
S2	Second-stage stator
S3	Third-stage stator
SAE	Society of Automotive Engineers
SAR	Suppressor area ratio
SAVE	Systematic approach to value engineering
SCC	Sizing-code calibration
SCID	Supersonic cruise integrated design
SCN	Sliding-chute nozzle
SD	Stepped dome
SDOF	Single degree of freedom
SERN	Single-expansion-ramp nozzle
SFC	Specific fuel consumption: lbm of fuel per hour per lbf
SFCDAB	SFC based on FNDAB
SI_{cp}	Stability index
SLA	Stereolithographic apparatus
SLS	Sea-level static
SLTO	Sea level takeoff
SMFAN	Stall margin, fan
SOAPP	State-of-the-art performance program (P&W)
SPFDB	Superplastic formed, diffusion bonded
SPL	Sound power level
SRP	Separate reverser port
SSC	Supersonic cruise
SST	Supersonic transport
STMT	System technology management team
STOL	Short takeoff and landing
SW	Sidewall
SWET	Substrate welding at elevated temperature
SW	Toal wing planform area
SwRI	Southwest Research Institute
SWT	Supersonic wind tunnel
T/b	Thickness-to-chord ratio
T/O	Takeoff

T_3	High-pressure compressor exit temperature
T_4	Combustor exit temperature
T_{41}, $T_{4.1}$	High-pressure turbine rotor inlet temperature
TAC	Total accumulated cycles
TBC	Thermal-barrier coating
TBE	Turbine bypass engine
TC	Technology configuration
TCA	Technology concept aircraft
TCB	Translating centerbody (inlet)
TCE	Technology concept engine
TCLA	Turbine cooling air
TCS	Turbulence control structure, also technology concept solution
TE	Trailing edge
TF	Turbofan
TF–IFV	Turbofan-inverter flow valve
TI	Technical integration (team)
TIC	Transient inlet/compressor (model)
TJ	Turbojet
TJ–IFV	Turbojet-inverter flow valve
TLID	Thrust-lapse parameter
TMT	Technology management team
TOBI	Tangential on-board bleed injection
TOC	Top of climb
TOGW	Takeoff gross weight
TP3	GEAE performance-analysis software
TPS	Thermal-protection system, also turbulence-prevention structure
TRF	Turbine rear frame
TRL	Technology readiness level
TSI	Triton Systems Inc.
TT, T_T	Total temperature
TT3	Compressor discharge total temperature
TT4	Total temperature at HPT vane inlet
TT4.1	High-pressure turbine rotor inlet total temperature
T_{T7}	Augmentor-exit total temperature
TT8	Exhaust gas total temperature at nozzle throat
TTC	Technology transition (or tracking) chart
TTR	Total-temperature ratio
UHB	Ultrahigh bypass
UHC	Unburned hydrocarbons
UPS	Universal propulsion simulator
UTRC	United Technology Research Center
VABI	Variable-area bypass injector
VAM	Variable-area mixer
VAMP	Variable-area mixing plane
VCE	Variable-cycle engine
VCF	Variable-capacity fan
VDC	Variable-diameter centerbody
VDVP	Variable-displacement vane pump
VEN	Variable exhaust nozzle
VFX	Variable-capacity fan, experimental
VG	Variable geometry
VJIP	Primary ideal jet velocity
VPI	Virginia Polytechnic Institute
W2AR	Engine corrected airflow
W5GR	LPT exit gas flow function
W_a	Airflow
WAE, W_{AE}	Engine airflow
WB3	Customer bleed
WBS	Work breakdown structure
W_c	Corrected airflow, also coolant flow
WG	Air (gas) flow
WG36	Airflow at combustor inlet
W_p	Primary flow, lbm/s
W_s	Secondary flow, lbm/s
XNH	Rotor speed (high-pressure spool)
XNL	Rotor speed (low-pressure spool)

6.0 Inlet

It is appropriate to acknowledge the significant impact of the cutting-edge advances in inlet testing and data processing made by NASA on the results reported herein.

- Operation of the "Virtual Control Room" during inlet testing in the "GRC 10×10 Supersonic Wind Tunnel" (SWT) essentially permitted on-site test participation while remaining off site at different contractor facilities.
- Reduced and plotted translating centerbody (TCB) and two-dimensional bifurcated (2DB) inlet test data access via the supporting electronic data network was thorough and exceedingly prompt.
- The GRC "Rapid Analysis of Dynamic Data" system provided near-real-time inlet dynamic distortion data with report-quality output during 2DB inlet testing.
- The "Subsonic Diffuser Test Facility" at GRC provided opportunity for critical subsonic diffuser technology development without the added expense and time associated with obtaining such data from supersonic windtunnel testing of a complete mixed-compression inlet.
- The Dryden "Heated and Pressurized Test Chamber" used for cyclic durability testing of flight-type variable-diameter centerbody (VDC) inlet component hardware was designed, fabricated, and made operational in record time.

These advances not only contributed significantly to our technology base, they also increased our productivity in the course of such technology development.

6.1 Overview

A high-performance, supersonic inlet is required for achieving HSCT aircraft range with an acceptable maximum takeoff weight (MTOW) and enough passengers to provide adequate airline profit. While high-performance, supersonic inlets might be considered state-of-the-art for military aircraft, simultaneously reducing approach noise levels to those of comparable gross weight subsonic aircraft, while achieving the high performance and reliability required for commercial operation, requires new inlet technology. State-of-the-art supersonic fighter inlet designs tend toward external compression schemes, but the stringent dictates of long-duration supersonic cruise preclude the use of traditional external inlet designs. Historically, above about Mach 2.2, use of mixed-compression inlets has been deemed necessary because of their higher inlet total pressure recovery at lower levels of cowl drag. However, such performance improvement adds the challenge of minimizing the risk and implications of inlet unstart — particularly in commercial operation. Consequently, significant HSR resources were expended to evolve the mixed-compression inlet scheme.

The following discussions reflect significant progress towards development of a commercial mixed-compression inlet that can meet the technical and economic criteria for a viable HSCT. Subsection 6.1.1 summarizes the specific goals, objectives, challenges, and approach. Subsection 6.1.2 summarizes program logic, and Subsection 6.1.3 summarizes progress relative to specific goals. Features of the VDC, the 2DB, and the TCB candidate inlet concepts are discussed in Subsection 6.2. Subsection 6.2 documents the final downselect decision from the candidate concepts. The remainder of Section 6 provides further details of the progress summarized in 6.1.3 for these three unique mixed compression inlets.

6.1.1 Approach

Figure 1 illustrates that key objectives in achieving the goal of a commercial mixed-compression inlet include reliability of only one inlet unstart per million fleet hours — representing an operability technology challenge — and cruise total pressure recovery of 93% with only 3% boundary layer bleed — representing performance, length, and weight challenges. Note that the performance goals were increased to reflect the success of the experimental testing. With the exception of full-scale design studies, controls development, and operability technology, the approach for accomplishing such objectives varies significantly among the three candidate inlet concepts because they each represent unique characteristics.

The first task is to identify the most promising inlet geometry concepts. Prior work suggested that an axisymmetric inlet would offer inherent advantages. During initial planning stages, some promising rectangular inlet concepts were identified as well. Three concepts were chosen for subsequent development effort: the VDC, the 2DB, and the TCB inlets.

Windtunnel data for the VDC inlet concept (6.5.2, page 29) were available early in the CPC program as a result of supporting technology activities. The unique technology development required for the VDC inlet was evaluating mechanical feasibility of the untried and complex mechanisms associated with centerbody diameter change.

The 2DB inlet was designed, fabricated, and tested in the CPC program (6.5.3, page 34) both in the "cold pipe" mode (inlet alone, no engine) and with a J85 engine. Coupling it with a J85 engine permitted attainment of critical unstart data (6.10, page 54) as well as low-speed auxiliary inlet results (6.5.3, page 34). It was also the focus of subsonic-diffuser development work (6.8, page 44)

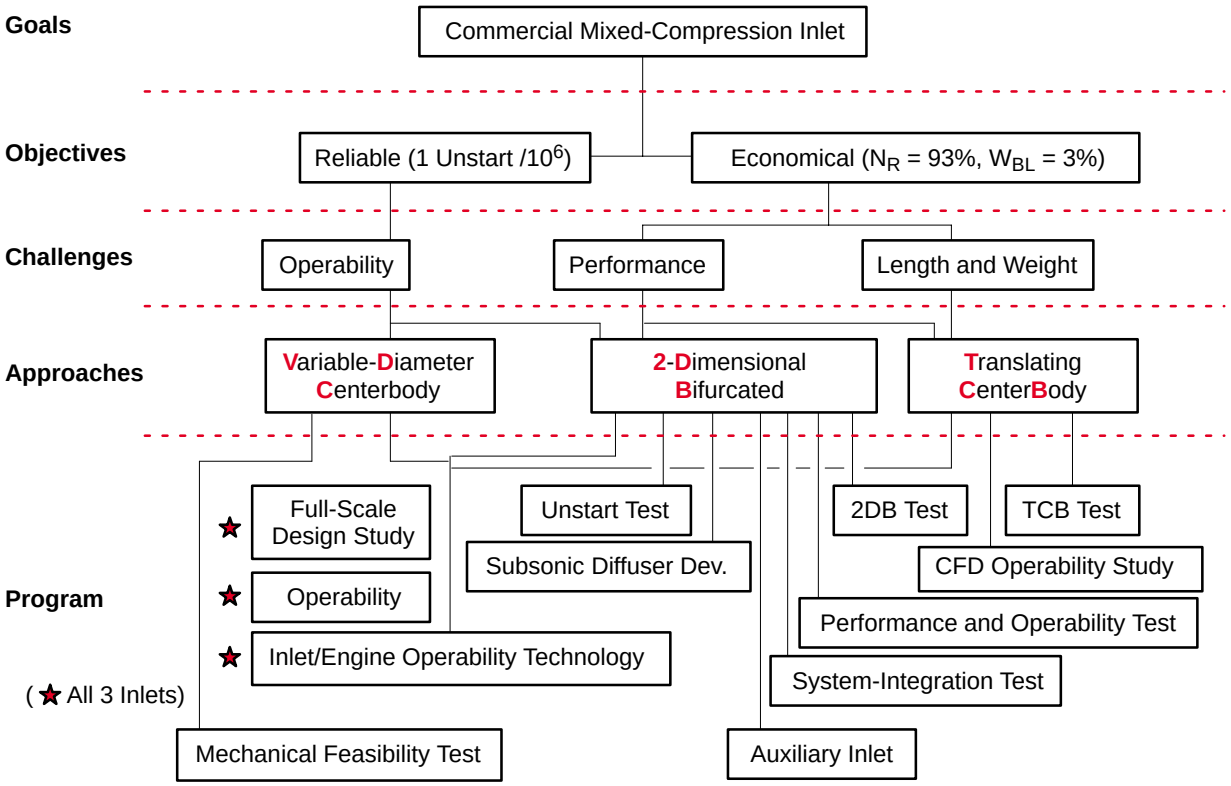

Figure 1. CPC Inlet Program Approach

due to conflicting requirements for a short subsonic diffuser in spite of the additional length required for transition from the two-dimensional inlet flowpath to the round engine. As the winner in the downselect process (6.3, page 11), the 2DB inlet concept was scheduled for additional development technology design and testing (6.4, page 20).

The TCB inlet model was existing Boeing hardware, tested during the CPC program in the NASA–Glenn 10×10 SWT under a Space Act Agreement. These test results were the catalyst for a subsequent computational fluid dynamics (CFD) operability study focused on decreasing flow angularity sensitivity.

In summary, the formulated inlet technology development approach, by being tailored for each inlet concept, provided a sound basis for selecting and validating the best inlet concept.

6.1.2 Inlet Logic

Figure 2 illustrates how the different work packages, and key external activities implemented the program approach of the previous figure and supported the Level 2 milestones. The "6.X" annotations identify the subsections where such work is discussed in the text that follows. Initial CPC program work benefited from propulsion/airframe integration technology (PAIT) studies as well as from bifurcated, two-stage, supersonic inlet (BTSSI) and VDC inlet testing. The fan inlet/acoustics test (FIAT) integrated technology development (ITD) team, propulsion system integration (PSI) team, and technology integration (TI) team all provided key input in meeting Level 2 milestones. The Configuration Aerodynamics team provided under-the-wing-inlet flowfield definition used in design of the wing/diverter simulator. The percent gray coloring within a particular box or circle indicates the degree of activity completion before phase-out at CPC program termination. Those items crossed out were abruptly cancelled early in the CPC program termination process. Work in a few selected areas was permitted to continue to the end of the CPC termination process; these primarily involved test data analyses and completing fabrication of the wing/diverter simulator hardware for future use in NASA–Glenn 10×10 SWT test programs.

6.1.3 Inlet Metrics

Five metrics were identified for tracking mixed-compression inlet technology development progress relative to CPC inlet program goals. (The first three metrics apply at Mach 2.4 flight conditions.)

1. Inlet total pressure recovery
2. Inlet boundary layer bleed as a percent of inlet capture flow
3. Circumferential and radial inlet dynamic distortion
4. Inlet weight per unit airflow
5. Inlet unstart probability

Figures 3 through 7 track inlet technology progress for these metrics as a function of time. The grayed-out region in each figure identifies technology development areas eliminated by CPC program cancellation, thus limiting results (including Technology Readiness Levels) to status values at cancellation. The vertical bars on the far-right side of each chart span the judged range bridging "most likely" and "best conceivable" final values.

Figures 3 and 4 indicate that the projected year 2001 inlet total pressure recovery and boundary layer bleed goals were both met or exceeded with the 2DB inlet. The TCB and VDC inlets also exceeded

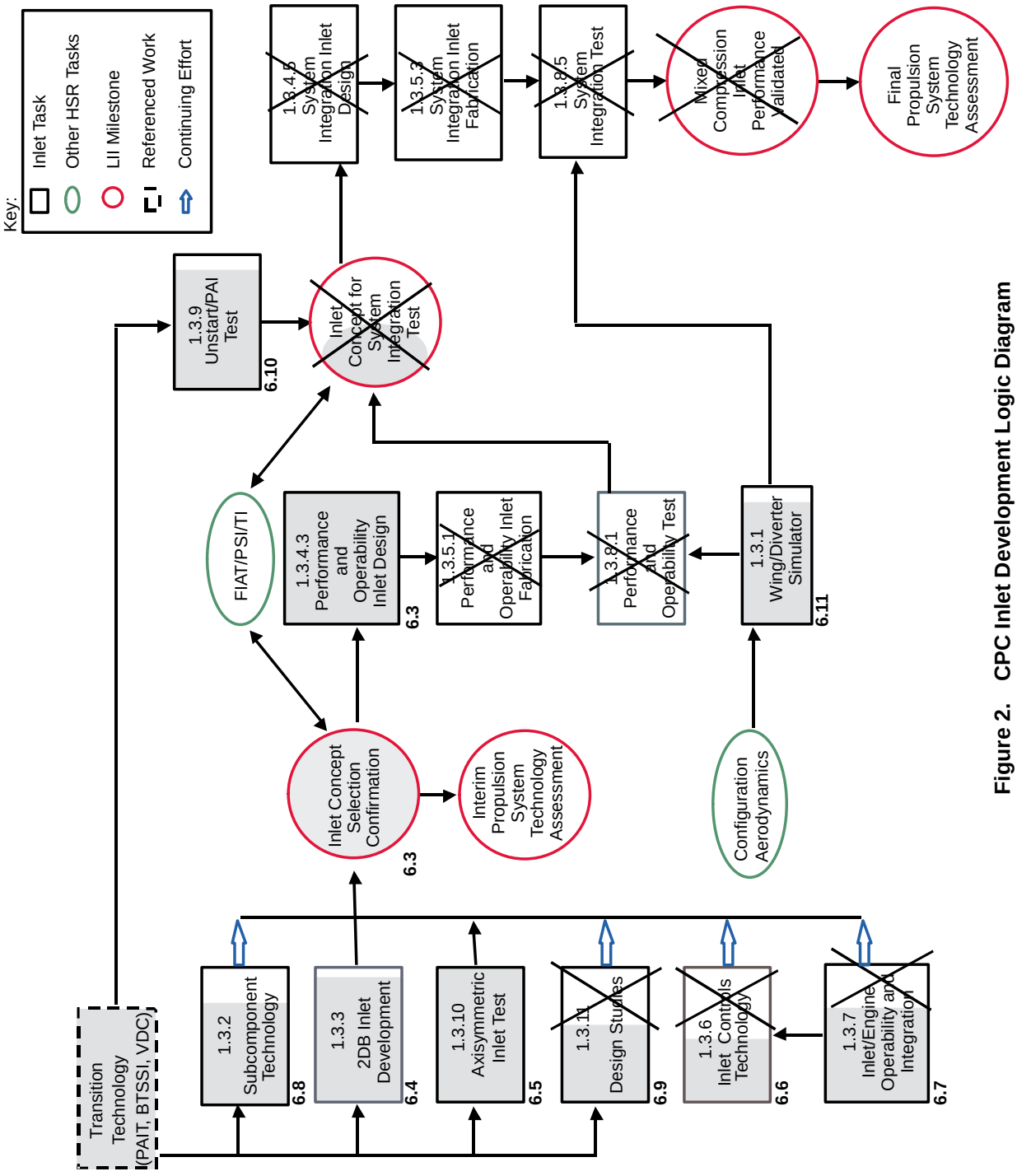

Figure 2. CPC Inlet Development Logic Diagram

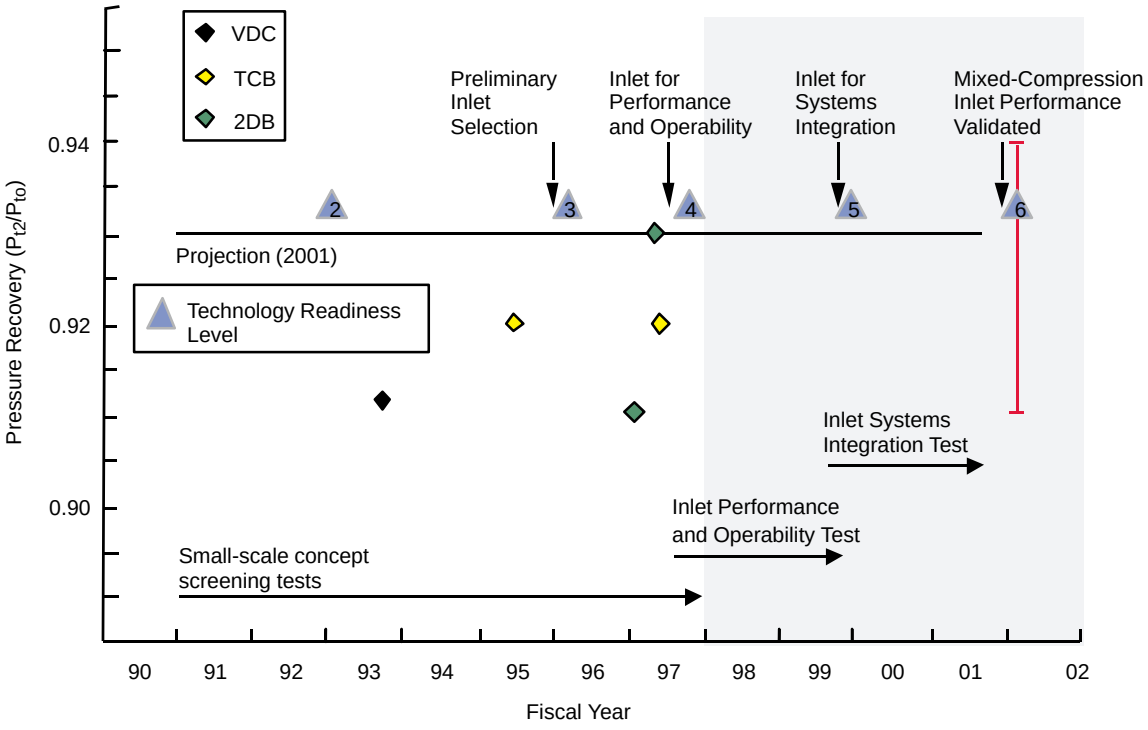

Figure 3. Inlet Total Pressure Recovery Technology Metric

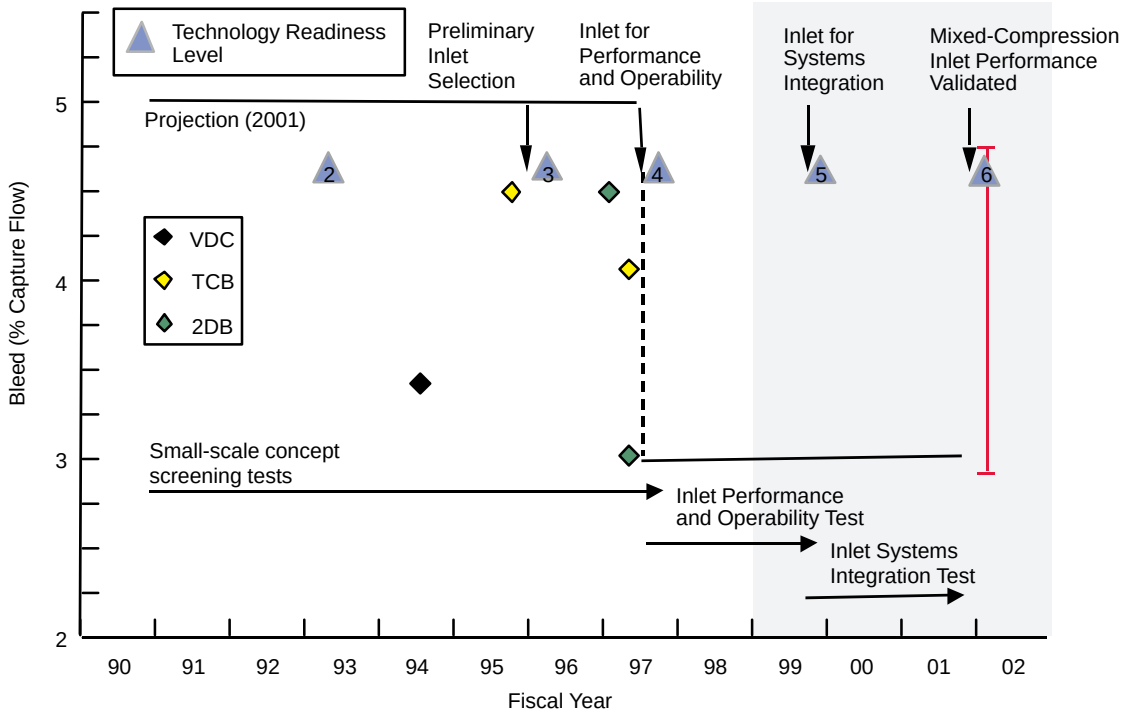

Figure 4. Inlet Boundary Layer Bleed Technology Metric

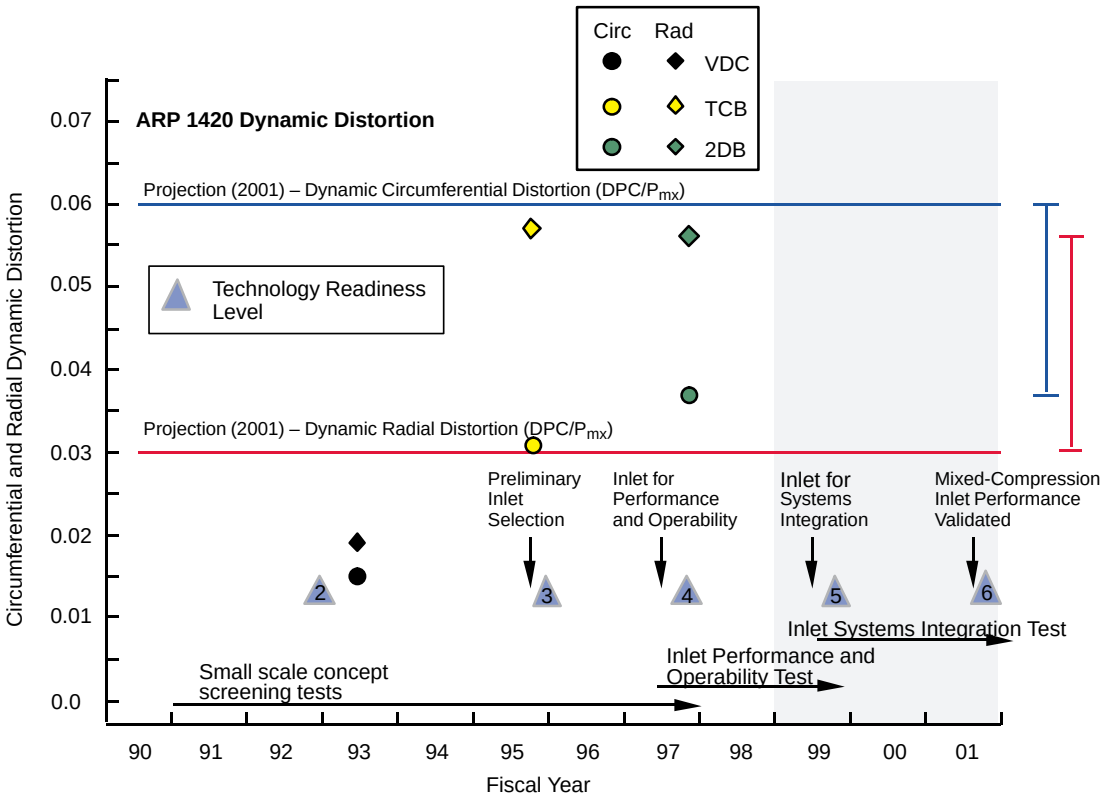

Figure 5. Inlet Dynamic Distortion Technology Metric

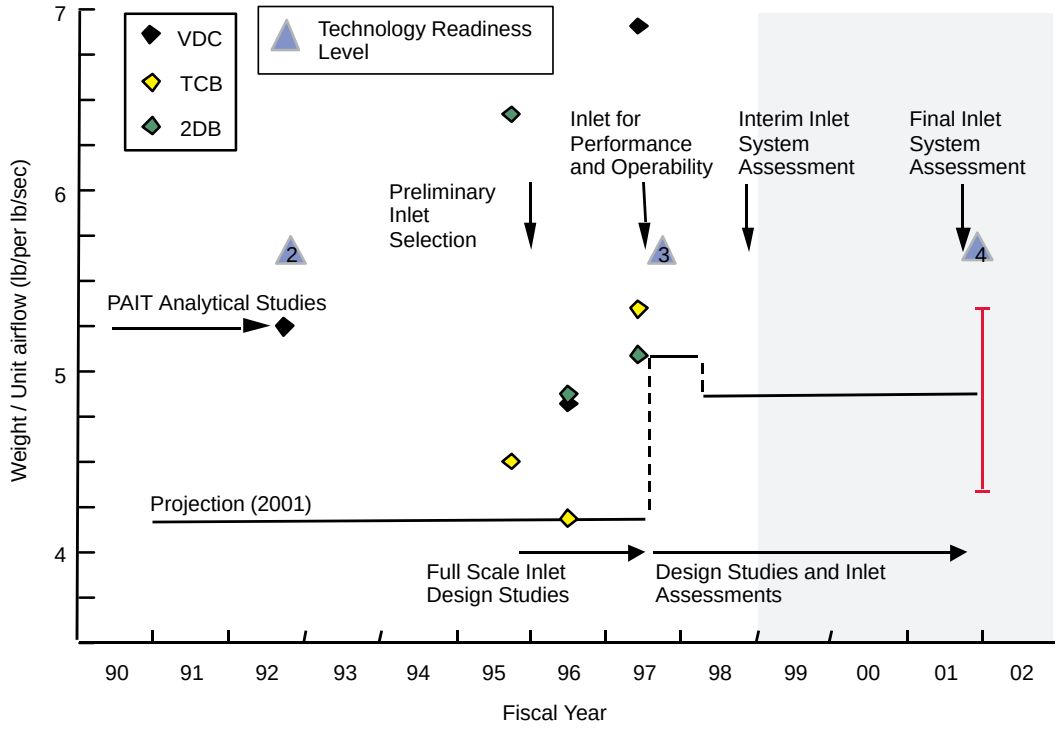

Figure 6. Inlet Weight/Engine Airflow Technology Metric

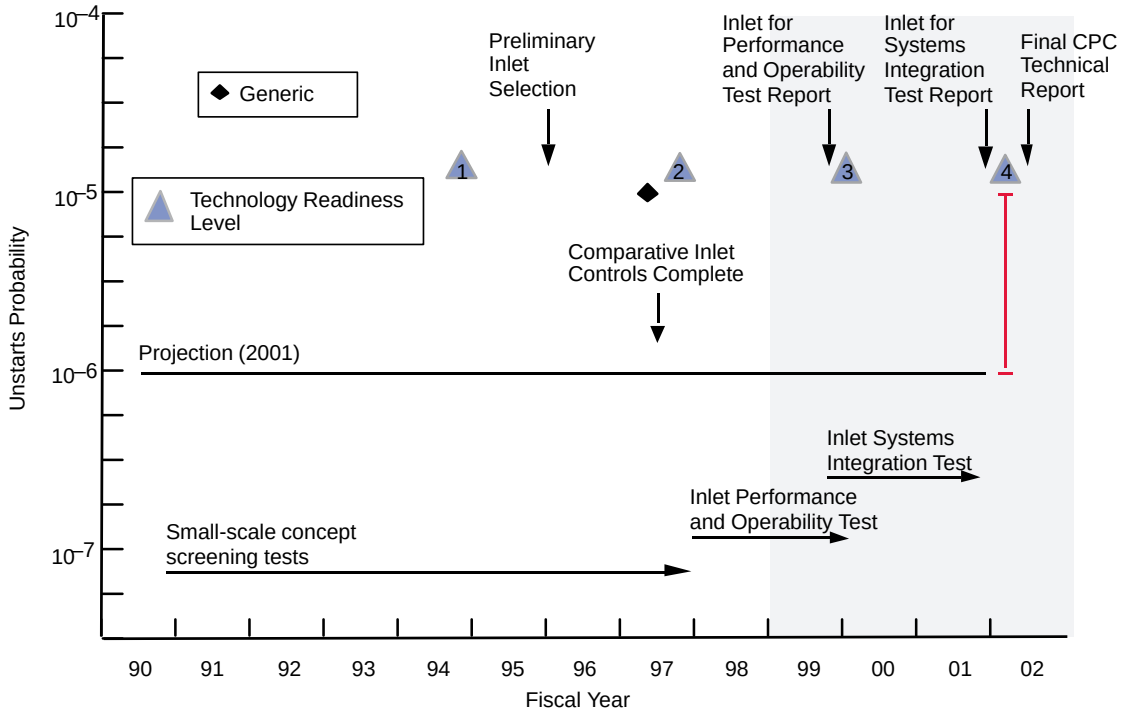

Figure 7. Inlet Unstart Probability Technology Metric

the boundary layer bleed goal, but they did not achieve the total pressure recovery goal. Note that the TCB and VDC inlet test articles represent an earlier generation of mixed-compression inlet technology. With additional effort in a balanced ranking, the axisymmetric inlets may provide aerodynamic performance superior to that of the 2DB concept. However, the HSR program required a downselect decision rather than an optimized inlet, and the 2DB inlet was selected. The planned 2DB inlet performance and operability (P&O) testing followed by the planned inlet systems integration testing were to subsequently increase the Technology Readiness Levels from 4 to 6 in order to provide full mixed-compression inlet performance validation.

Figure 5 indicates, for both the 2DB and TCB inlets, that the circumferential dynamic distortion goal was met and exceeded; whereas, the radial dynamic distortion goal had not been met. The VDC inlet, however, is seen in Figure 5 to have met and exceeded both of these dynamic distortion goals.

Scale-model testing provided the basis for evaluating the first three metrics. For the two remaining metrics, assessments are limited to analytical studies and thus reflect lower Technology Readiness Levels. Figure 6 indicates that the 2DB inlet met the revised weight/unit airflow goal, whereas the TCB and VDC inlets did not. Figure 7 indicates that the very challenging unstart-probability goal had yet to be met.

6.2 Concepts

Preliminary studies (Transition Technology, Figure 2, page 4) investigated both external and mixed-compression inlets of different configurations. Results indicated that mixed-compression inlet configurations tend to enable lower TOGW aircraft with higher installed performance relative to external-compression inlet configurations. The three mixed-compression inlet concepts depicted in Figure 8 were selected for more detailed evaluation in the CPC program: the TCB, 2DB, and VDC.

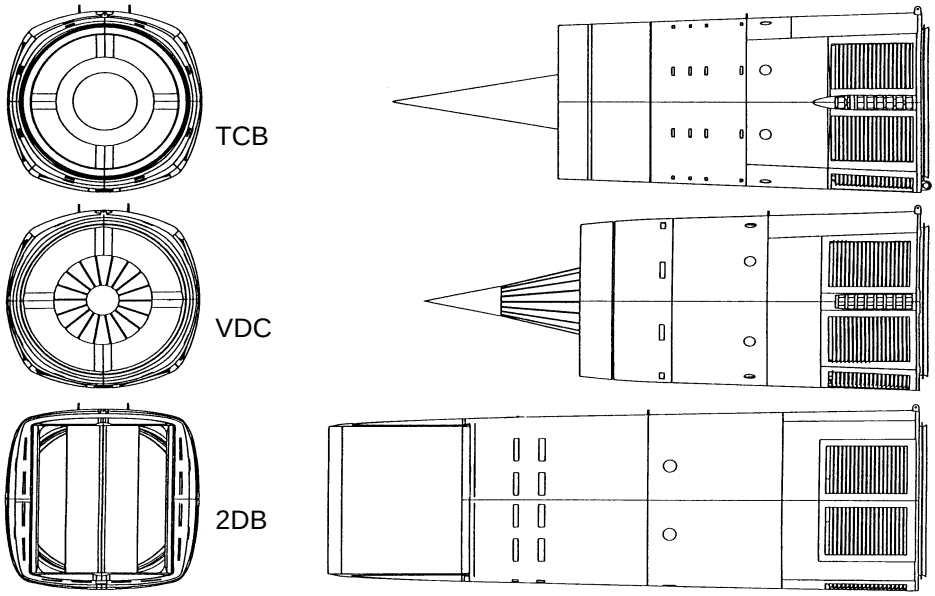

Figure 8. Candidate Inlet Concepts

Each concept has unique features and unique risks. Figure 9 summarizes the initial (August 1995) relative CPC ranking of the concepts in 11 key areas.

The TCB — with low drag, low weight, and low manufacturing and maintenance costs — was judged to also represent significant risk in the areas of transonic-flow capability, operability, and unstart potential.

Parameter	TCB	2DB	VDC
Recovery	2	3	2
Distortion	2	1	3
Bleed	2	1	3
Drag	3	**1**	2
Transonic Flow	**1**	3	2
Noise	3	2	2
Operability	**1**	2	3
Unstart Severity	**1**	3	2
Weight	3	**1**	2
Producibility	3	2	**1**
Maintenance	3	2	**1**

Figure 9. Initial Ranking of Candidate Inlet Concepts *Highest numerical ranking indicates most merit; highlighted cells indicate potentially significant but presently unquantified risk.*

The 2DB — with higher recovery, higher transonic-airflow capability, and lower unstart probability — was judged to also represent potentially higher drag and heavier weight.

The VDC — with lower bleed, lower distortion, and better operability — was judged to also represent significantly higher manufacturing and maintenance costs.

Early CPC Inlet effort focused on technology development and improved risk quantification in the more critical areas, indicated in Figure 9, which would permit a creditable downselection to a single concept. Late in the CPC program, a unique external-compression concept was considered; this concept offered the potential for cruise performance approaching that of the mixed-compression inlets without the complexity of inlet unstart behavior.

6.2.1 Translating Centerbody

Figure 8 depicts the TCB inlet as configured early in the CPC program. Internal contraction of this axisymmetric inlet is controlled through axial translation of the centerbody (full aft at supersonic cruise and full forward during transonic operation). The TCB inlet has the highest internal contraction of the three inlet concept candidates. This high degree of internal contraction at supersonic cruise permits a lower external cowl lip angle that reduces cowl drag, but the associated kinematics limit the throat area increase that can be achieved for transonic operation. The latter restriction, however, also produces a slightly higher throat Mach number at approach, thus providing a small noise-suppression advantage. High internal contraction can also reduce tolerance to capture-flow gradients that in turn can increase flow distortion at the aerodynamic-interface plane (AIP) and increase the probability and severity of inlet unstart.

The flowpath from the cowl lip aft permits efficient flow compression in a relatively short distance, thus contributing to reduced weight and cost. The structural efficiency of the round pressure vessel also contributes to reduced weight and cost. The design symmetry and simplicity (modest number of moving parts, seals, and linkages) contributes to reduced maintenance cost as well as reduced manufacturing cost.

6.2.2 Variable-Diameter Centerbody

Figure 8 depicts the VDC inlet as configured early in the CPC program. With more external compression and less internal contraction compared to the TCB, the VDC is slightly shorter. Ability to vary the centerbody diameter permits high overall contraction ratio at supersonic cruise while providing more transonic throat area than is possible with the TCB. The increased external contraction can reduce sensitivity to incoming flow gradients, thus enhancing operability and reducing distortion at the AIP. The overall aerodynamic attributes of the VDC could be considered the best of the three concepts.

The mechanical complexity of the VDC, however, is the highest of the three concepts. Diameter is varied by using overlapping leaves on the centerbody forward and aft sections. This introduces new design challenges in minimizing leakage, seal wear, seal-replacement interval, actuation (ability to accurately position each section for consistently achieving concentricity with the axisymmetric flowpath of the fixed outer wall), etc. Solutions to these design challenges are required to enable the aerodynamic benefits attributed to the VDC, and they must be accomplished in a manner that permits acceptable manufacturing and maintenance costs.

6.2.3 Two-Dimensional Bifurcated

The higher recovery attributed to the 2DB is achieved through two major design features. First, the inviscidly developed aerodynamic lines employ isentropic compression on the variable-curvature, bifurcated-ramp surfaces to reduce shock losses. Second, a variety of bleed patterns and vortex-generator configurations were optimized during an extensive wind tunnel test program. The design philosophy of the 2DB was an outcome of modern CFD development verifying years of design and testing experience. The final configuration represents a new generation of high-performance, mixed-compression inlets.

Other design features of the 2DB inlet concept include hinged ramp surfaces permit ramp positioning for both high inlet contraction ratio and large transonic throat area. Internal contraction is slightly higher than that of the VDC but still significantly less than that of the TCB. Transitioning from the two-dimensional, supersonic diffuser to the round AIP adds length compared to the TCB and VDC, which can increase external drag. Corner-flow losses and two-dimensional-to-round transition in the subsonic diffuser suggest potential for increased boundary layer bleed and increased distortion at the AIP. Extensive test optimization greatly reduced the need for increased bleed.

The extra length of the 2DB compared to that of the TCB and VDC (as evident in Figure 8), and the less structurally efficient noncircular sections, make the 2DB design inherently the heaviest of the three inlet concepts. However, the acoustic treatment to mitigate fan/inlet noise caused this disadvantage to disappear in the final inlet downselect. Unstart loads should be more easily absorbed by the bifurcated ramps, which are axially supported by the frame, relative to a centerbody cantilevered from the struts as in the case of the axisymmetric concepts. Consequently, the 2DB was judged to be the best of the three concepts relative to unstart severity.

6.2.4 Waverider External Compression

The waverider inlet concept depicted in Figure 10 reintroduced consideration of an external compression design scheme. This novel design preserves high performance while eliminating the complications and risks associated with unstart of mixed-compression inlets. As flight Mach number increases, higher flow angles are needed to externally compress the airflow. This compression lowers the Mach number so that high total pressure recovery is achieved through the normal shock. At flight above (nominally) Mach 2.2, such flow angles historically produce high cowl drag and spill drag. While such compression/flow angle physics also apply to waverider inlet concepts, the unique

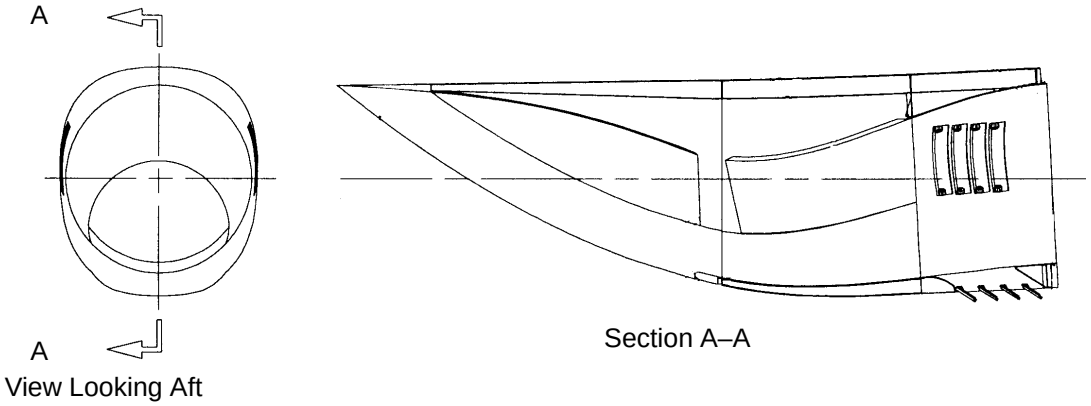

Figure 10. Preliminary Waverider Concept

manner in which waverider cowl lips are generated requires that only a fraction of the lip perimeter be at a steep angle. Consequently, an opportunity exists for significant drag reduction. The forward supersonic and aft subsonic hinged ramps provide the contraction ratio change required for good performance at reduced flight Mach numbers, similar to that of the 2BD inlet. Unlike the 2DB inlet, however, rotation of laterally curved ramp surfaces can introduce steps and gaps into the flowpath, introduce additional side-wall sealing problems, and produce high loads at points of rotation.

Work on this concept was not funded under the CPC program and has only recently been initiated (under the HSR airframe contract). Consequently, it is not discussed in detail in this CPC report. Due to the promising performance and challenging three-dimensional design, the inlet team members funded under the CPC contract recommended these further efforts in increase the technical maturity of the waverider concept.

6.3 1997 Inlet Downselect

A scheduled *Inlet Downselect* was conducted in August of 1995. Most CPC Inlet work was not far enough along to provide significant input. Because existing models were used, windtunnel data were available for the VDC and TCB inlets, but fabrication had just been initiated on the 2DB. Based on such a limited amount of information, a downselect decision was made that would later be changed. The general perspective is reflected in Figure 9 (page 8). The consensus decision was to choose an axisymmetric or "round" inlet as the initial *Downselect* result. Discrimination between the VDC and TCB concepts could not be discerned. Provided an opportunity for a *Downselect Confirmation* in April of 1997, the inlet team replanned and accelerated their effort to make a more comprehensive database available.

The scope of the comprehensive technology effort launched to support the *Downselect Confirmation* is summarized in Figure 11. Included among the most important issues to be resolved was establishing specific operability and design requirements against which to evaluate each candidate inlet, obtaining windtunnel data on the 2DB inlet, and completing full-scale design studies for each of the three candidates. The latter was required in order to establish consistent weight and cost estimates.

A wide spectrum of input from outside the expertise of the Inlet Team was also obtained. The FIAT would provide approach-noise assessments, the PSI team would provide aircraft sizing input, Boeing would retest TCB design improvements, and a *Red Team* would conduct an independent audit of the full-scale inlet mechanical designs for the TCB, VDC, and 2DB inlets.

6.3.1 Criteria

Figure 12 summarizes the inlet performance goals that were subsequently established. For gradients in inlet capture flow angle of at least 2° and gradients in capture flow Mach number of at least 0.05, the inlet was to provide a minimum of 92% total pressure recovery with no more than 5.5% boundary layer bleed. This was to be accomplished while maintaining at least 2% stability margin and producing no more than the indicated nominal values of flow distortion at the AIP Stability margin can be measured as inlet stability index (the maximum reduction of inlet corrected flow ratioed to operating-point corrected flow). All of these goals were to be achieved without any active control of the flowpath geometry ("static" mode associated with cruise flight).

During maneuvering flight, active control of inlet flowpath geometry was permitted. The flow angularity gradient capability was increased to 4° minimum, the maximum distortion levels were increased to the indicated "maneuver" values, and a minimum of 10% stability margin was required.

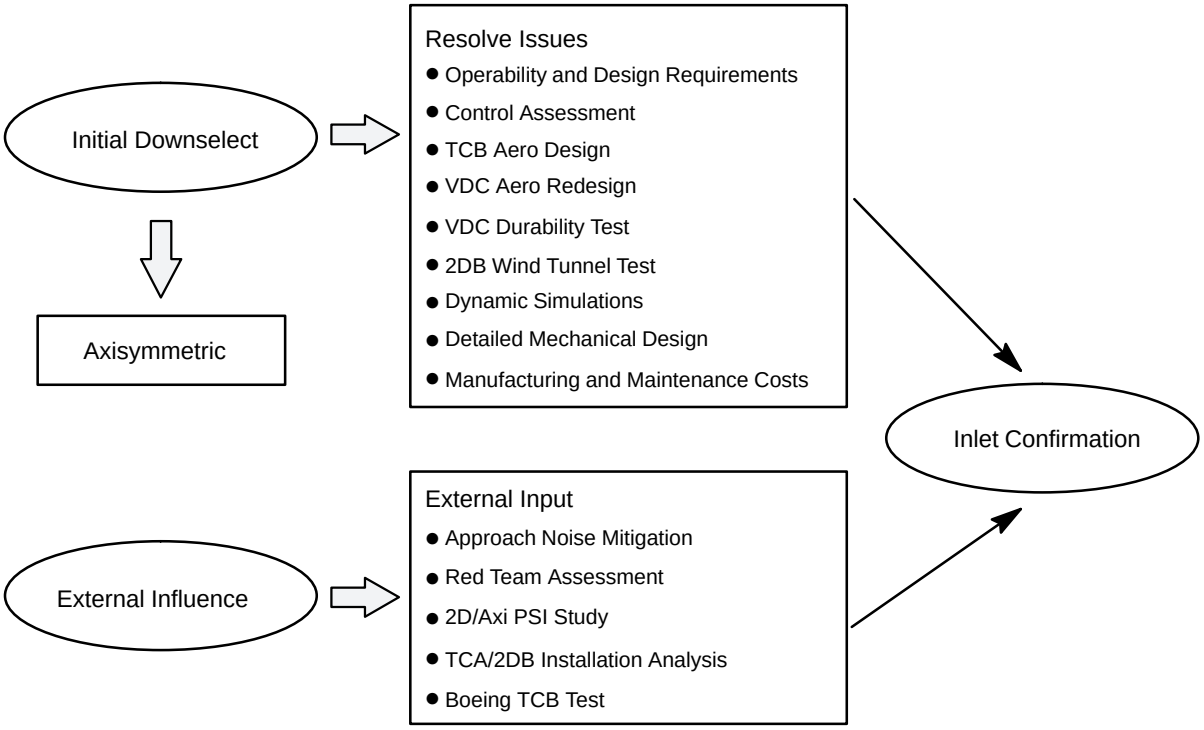

Figure 11. Inlet Technology Development

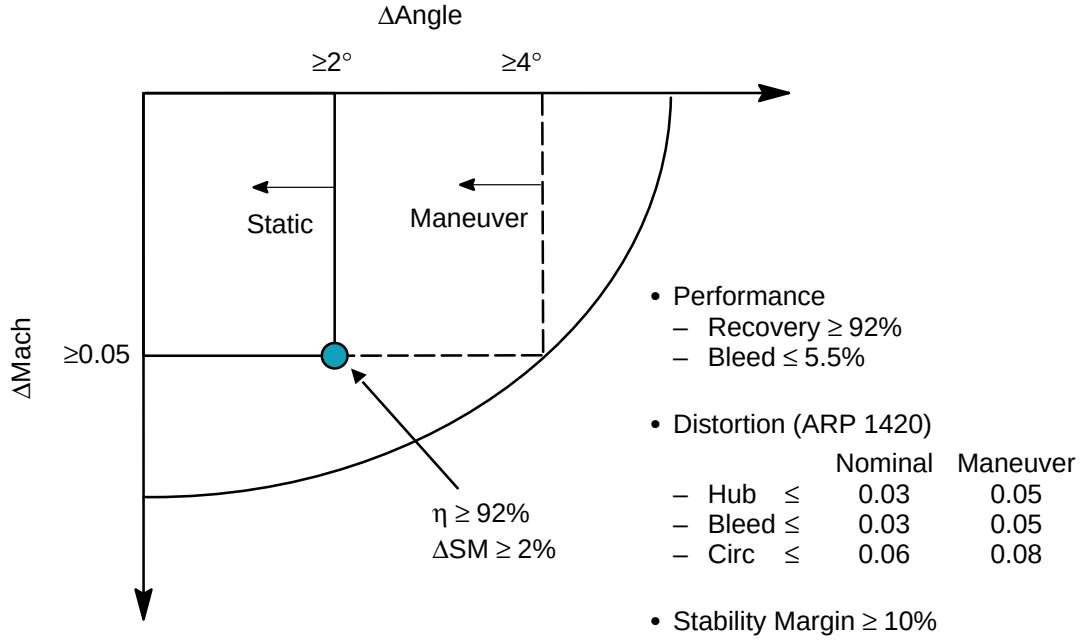

Figure 12. Inlet Performance Goals

While the full-scale design studies (6.9, page 51) were able to use recently formulated aerodynamic and mechanical design groundrules, such was not the case for the earlier TCB, VDC, and 2DB windtunnel models. Those were based not only on different design guidelines but also were built to different scale and complexity. Consequently, performance and operability characteristics are to some extent affected by the different historical backgrounds. The final downselect decision was made in this context with the goal of maintaining the overall program schedule.

6.3.2 Process

As illustrated in Figure 13, the inlet downselect confirmation process was system focused. The objective was to determine which of the three candidate inlet concepts was most likely to permit the best HSCT considering weight, cost, and risk. This was accomplished using the *Technology Concept Aircraft* (TCA) as the baseline HSCT and comparing weight and cost results against risk for each of the three inlet concepts.

Figure 14 illustrates the process for evaluating weight and cost. The seven indicated inlet properties were assessed using a "status" basis. "Status" implied results already demonstrated by applicable test data, CFD, design studies, etc. The intent of this approach was to achieve a higher degree of objectivity than might result from adjusting "status" results to less objective "potential" or "growth" levels — requiring perhaps even more arguable amounts of additional funding and time to pursue. Opportunity was provided for individually prepared written positions on such projections should this become a major issue; however, it did not. The PSI (propulsion systems integration) team provided sensitivities of MTOW and ΔDOC+I (incremental *direct operating cost* plus *interest*) to the seven inlet properties for the TCA, Figure 14. The process for evaluating ΔDOC+I is illustrated in Figure 15. The TCA (on design mission) was individually resized for each of:

- 1% change in inlet total pressure recovery
- 1% change in boundary layer bleed
- one count in total nacelle drag
- 100 lbm weight change per inlet

Economic mission calculations made with the resized TCA then provided corresponding ΔDOC+I values (from the TCA baseline level) that were used in creating the necessary sensitivity derivatives. Increments were then calculated relative to the TCA baseline for each concept in terms of database recovery, bleed, drag, weight, manufacturing cost, and maintenance. Combining the latter with the ΔDOC+I derivatives then produced the total ΔDOC+I value for each inlet.

Areas that were difficult to assess from a weight or cost standpoint were considered "risk areas." Figure 16 identifies the six risk areas and summarizes the risk methodology. In striving to maintain the highest objectivity, the inlets were compared only within each risk area, thus avoiding less objective and more arguable "weighting factors" required for combining all risk areas in order to arrive at a single risk value for each inlet.

Two key elements were used in arriving at inlet risk values within each risk area: (1) relative probability of a problem and (2) relative impact of having to fix the problem. The "relative probability risk" was estimated using probability distributions fit through assigned "anchor points." If risk was considered "low" at a particular anchor point of the selected independent variable, then 5% relative risk was assigned. If risk was instead considered to be moderate, then 25% relative risk was

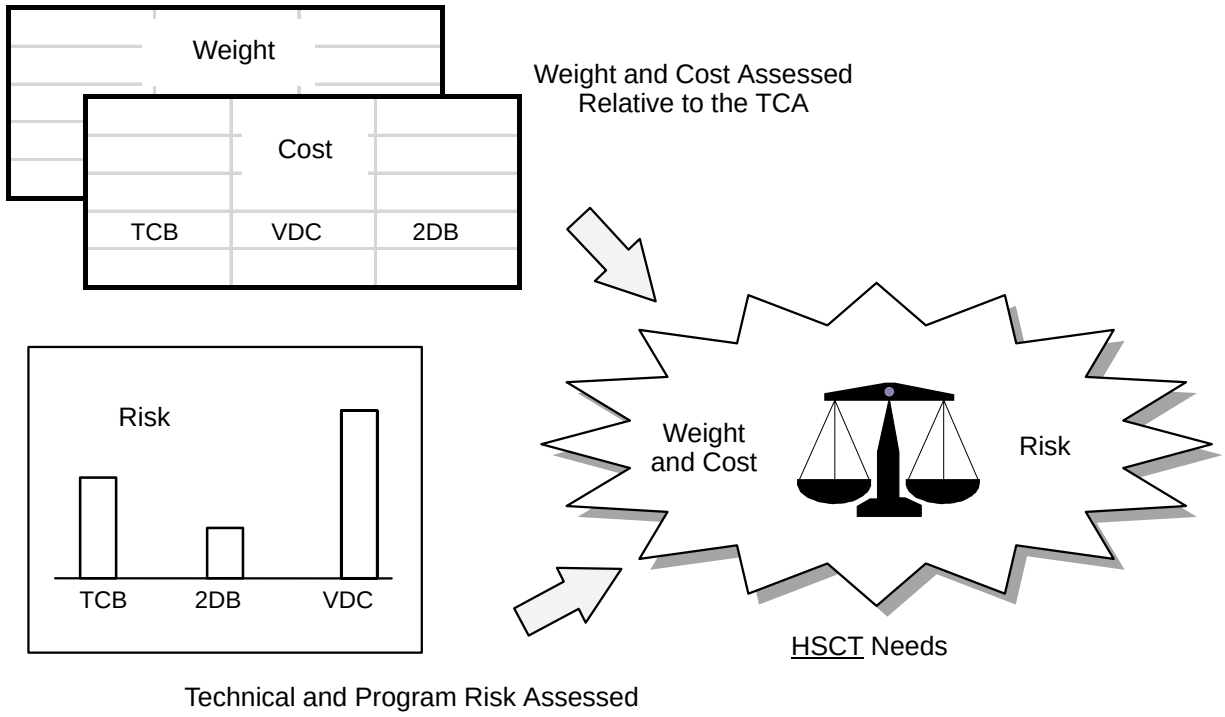

Figure 13. System Focused Inlet Downselect Process

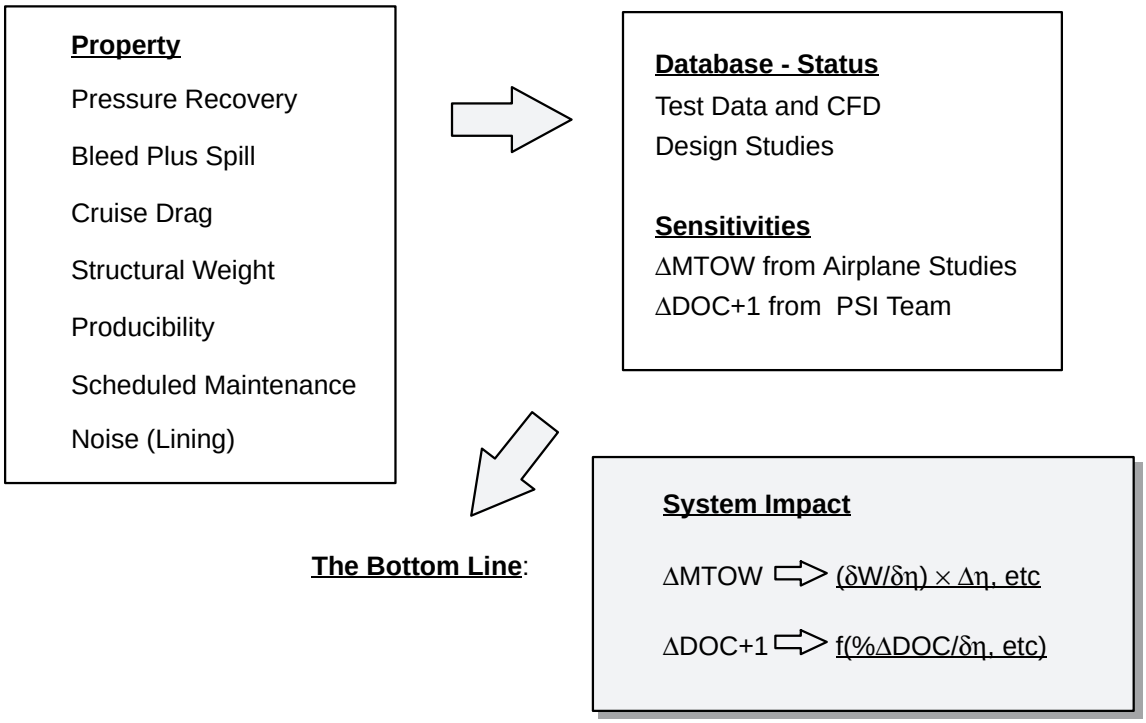

Figure 14. Weight and Cost Process

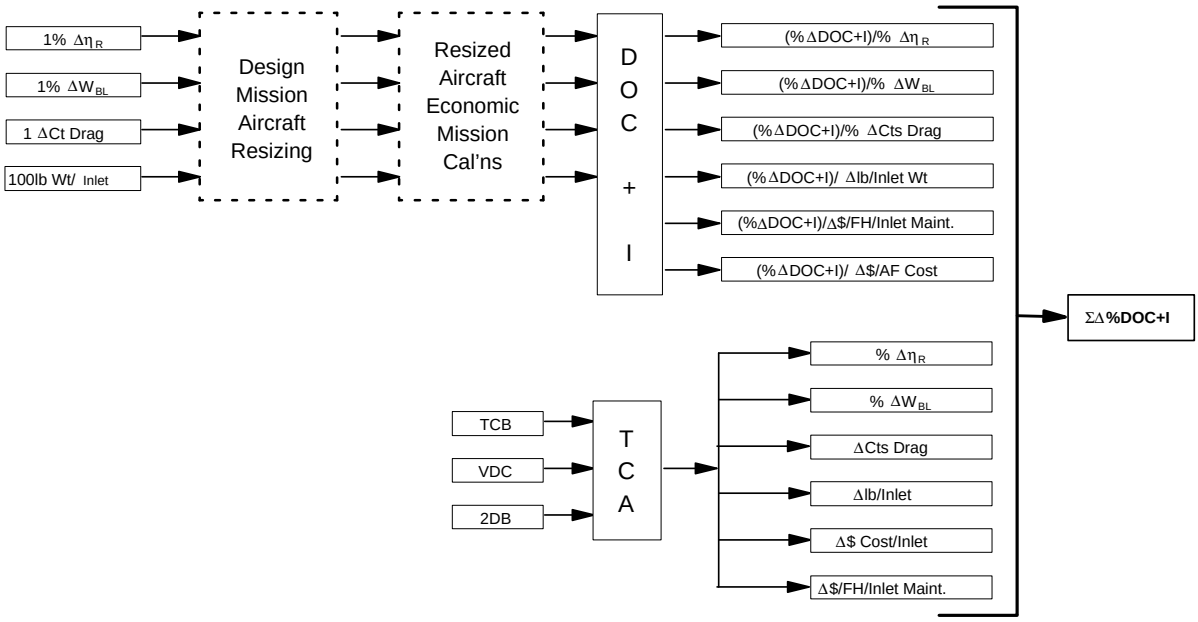

Figure 15. Cost-Assessment Approach

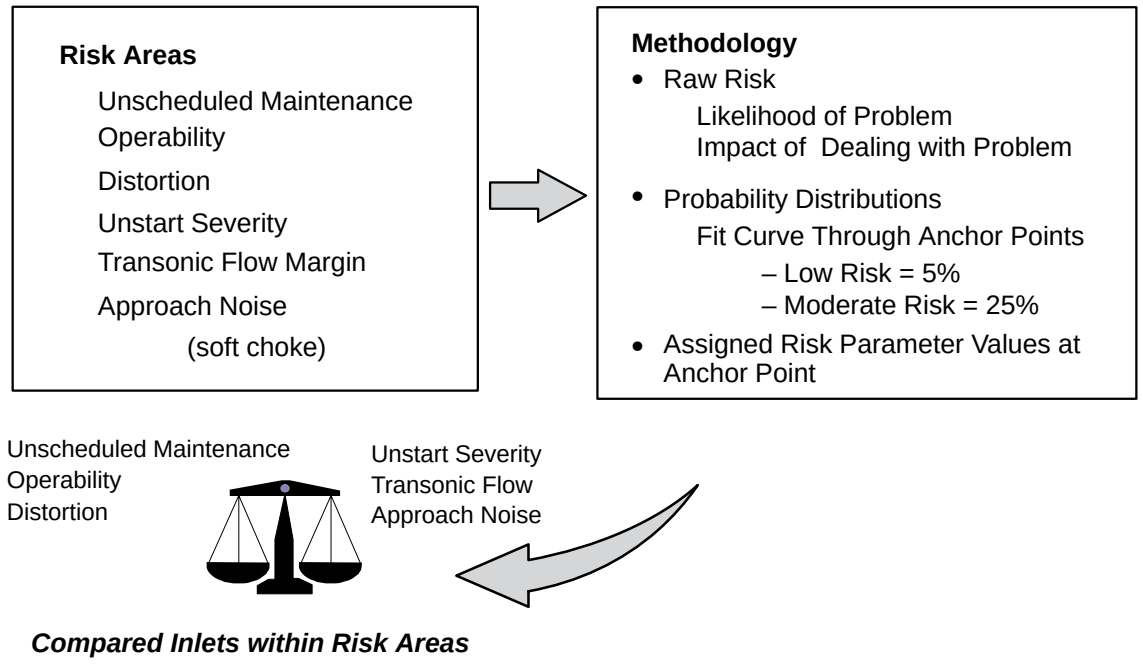

Figure 16. Risk-Assessment Process

assigned. At other values of the independent variable, the relative probability risk could then be read from the thus anchored probability distribution curve. However, if it was also considered that the program impact of fixing such a problem was significantly different between inlets within a particular risk area, then a raw risk table was used to establish the "impact raw risk." In such cases, the percent relative risk was then the product of the impact raw risk and the relative probability risk.

6.3.3 Results

Using inlet geometry results from the full-scale design studies (6.9, page 51), FIAT added noise treatment inside each of the inlets on a space-available basis (accounted for in the inlet weight) and then estimated the approach noise reduction with each inlet relative to the requirement. Even factoring in the projection of 3-dB effective perceived noise level (EPNL) reduction from the proposed *Low Noise Fan* program, as seen in Figure 17, none of the three inlets initially met the noise-reduction goal. With the latter being a firm requirement for the HSCT, it was decided that the best course of action was to increase the lengths of the inlets to provide additional surface area for installing enough treatment that each inlet would then permit the noise-reduction goal to be met. (Additional treatment area was found in the 2BD inlet such that an increase in its length was not required.) The result, as also summarized in Figure 17, was that the length of the two axisymmetric inlets had to be increased essentially to that of the 2DB if they were to also meet the approach noise-reduction goal. Initial weight and cost increments were adjusted accordingly.

The MAR97 FIAT projections indicated the following Approach Fan Noise shortfalls *assuming their proposed Low Noise Fan program delivers –3-dB ΔEPNL*:

	TCB(1)	VDC(1)	2DB(1)	2DB(2)
ΔEPNL Goal	–14.0	–14.0	–14.0	–14.0
Projected Total ΔEPNL	–12.2	–11.5	–10.8	–14.0
ΔEPNL Shortfall	1.8	2.5	3.2	0.0

(1) L/Di and other geometry based on Full Scale Design Study

(2) Additional 128 ft^2 treatment added within existing length, representing a 190 lb weight increase per inlet which is included in the COST ΔDOC+I analyses.

The L/Di increases to accommodate the required increased treatment area would be approximately:

	L/Di Current(1)	ΔL/Di	New L/Di
TCB	2.17	0.78	2.95
VDC	2.06	1.09	3.15
2DB	2.93	0.00	2.93

suggesting no significant relative drag differences (same nominal L/Di), but relative weight and manufacturing cost increases which were factored into the ΔDOC+I COST Evaluation.

Thus: All inlets same noise risk with ΔL/Di

Figure 17. Common Approach Noise Requirement Impact

Weight assessments are summarized in Figure 18. The 2DB, VDC, and TCB database values for the five cost criteria are tabulated in the top section, in addition to corresponding values for the baseline TCA. In the middle section, the differences from the TCA are tabulated in addition to the appropriate

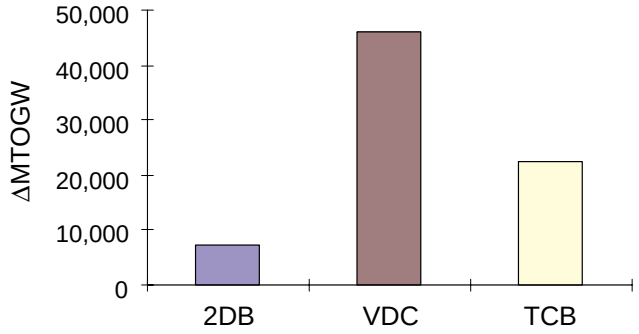

Cost Criteria			Raw Scores		Baseline
	Units	2DB	VDC	TCB	TCA
Recovery	Ptav / Pt0	93.0	91.2	92.0	93.0
Bleed	%Wcapture	3.0	3.4	4.1	4.1
Cruise Drag	A/P cts / inlet	2.1	2.1	2.1	2.1
Structural Weight	lb / inlet	4,070	3,840	3,310	3,360
Acoustic Lining Weight	lb / inlet	0	1,680	960	0
		Variation from Baseline			
		2DB	VDC	TCB	Sensitivity
Recovery	Ptav / Pt0	0.0	–1.8	–1.0	–5,000 lb / %
Bleed	%Wcapture	–1.1	–0.7	0.0	5,800 lb / %
Cruise Drag	A/P cts / inlet	0.0	0.0	0.0	24,800 lb / 4 cts
Structural Weight	lb / inlet	710	480	–50	19 lb / lb
Acoustic Lining Weight	lb / inlet	0	1,680	960	19 lb / lb
		Individual Ranking			
		2DB	VDC	TCB	
Recovery	lb MTOW	0	9,000	5,000	
Bleed	lb MTOW	–6,380	–4,060	0	
Cruise Drag	lb MTOW	0	0	0	
Structural Weight	lb MTOW	13,490	9,120	–950	
Acoustic Lining Weight	lb MTOW	0	31,920	18,240	
		Overall Ranking			
		2DB	VDC	TCB	
	Δ MTOW	7,110	45,980	22,290	

Assessment of 2DB inlet includes effect of hinge modification for reduced transonic drag.

Figure 18. Weight-Assessment Results

sensitivities obtained from the PSI Team. The bottom section combines the differences from the TCA with the PSI provided sensitivities to establish the MTOW increments for each of the inlet concepts relative to the baseline TCA. While all three concepts result in MTOW increases relative to the TCA, the 2BD was determined to be the lightest of the three candidate concepts. An important caveat to this conclusion is that the subsonic diffuser of the 2DB inlet for the weight studies was significantly shorter (and thus lighter) than the diffuser tested — an important risk factor. The risk was to be addressed by additional planned testing that was subsequently cancelled; see Subsection 6.4.2 for details. This result is opposite to the August 1995 assessment summarized in Figure 9 (page 8) and reflects the improved database resulting from the full-scale design studies (6.9, page 51), 2DB windtunnel data (6.5.3, page 34), and the decision to require that approach noise reduction with all three inlet candidates meet the HSCT program goals.

Cost assessments are summarized in Figure 19. Five of the independent variables and the database values are repeated from Figure 18 but are evaluated here using cost instead of weight sensitivities. The TCB does not achieve full capture flow at cruise; thus, the resulting spill drag incurs a slight cost penalty. Inlet candidate database values for the other independent variables are from the full-scale design studies (6.9, page 51). In the lower part of Figure 19, independent variable differences from the TCA, corresponding cost sensitivities provided by the PSI team, and the resulting ΔDOC+I increments are tabulated. As seen from the sums of the latter, the total ΔDOC+I calculated for the 2DB is the lowest of the three candidate concepts and represents a slightly better DOC+I than that calculated for the TCA baseline. The primary reasons for this different result, as compared to the August 1995 assessment summarized in Figure 9 (page 8), is again the improved database

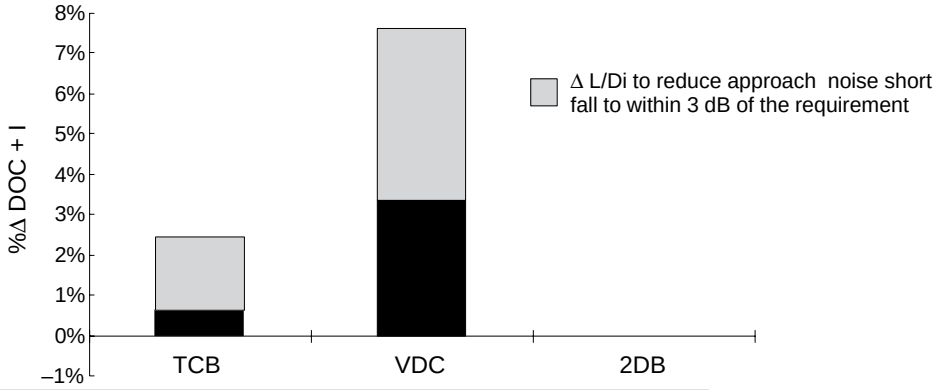

	Units	TCB	VDC	2DB	TCA
Recovery	% Pt_{2AVG}/Pt_0	92.0%	91.2%	93.0%	93.0%
Bleed	% Capture Flow	4.1%	3.4%	3.0%	4.1%
Spillage	% Capture Flow	0.47%	0.0%	0.0%	0.0%
Cruise Drag	Δ Cts./Aircraft	0.26	Base	Base	Base
Structural Wt.	lb/inlet	3310	3840	4070	3360
Producibility	$M/inlet	1.352	1.329	1.424	1.352
Sched. Maint.	$/FH/inlet	36	142	21	36
Noise (Lining)	dB shortfall	1.8	2.5	0	0
Wt ΔL/Di	lb/inlet	960	1680	0	0
Prod. ΔL/Di	$M/inlet	0.427	0.657	0	0
Maint. ΔL/Di	$/FH/inlet	11	70	0	0
Drag ΔL/Di	Cts./Aircraft	0	0	0	0

	Derivatives		Δ DOC+ I	Δ DOC+ I	Δ DOC+ I
	Value	Δ DOC+ I	TCB	VDC	2DB
Recovery	–1%	0.46%	0.46%	0.83%	0.00%
Cruise Drag	1	0.85%	0.22%	0.00%	0.00%
Bleed	1%	0.67%	0.00%	–0.47%	–0.74%
Structural Wt.	100	0.14%	–0.07%	0.67%	0.99%
Producibility	0.250	0.14%	0.00%	–0.01%	0.04%
Sched. Maint.	25	0.55%	0.00%	2.33%	–0.33%
Noise (Lining)					
Wt ΔL/Di	100	0.14%	1.34%	2.35%	0.00%
Prod. ΔL/Di	0.250	0.14%	0.24%	0.37%	0.00%
Maint. ΔL/Di	25	0.55%	0.24%	1.54%	0.00%
Drag ΔL/Di	1	0.85%	0.00%	0.00%	0.00%
TOTAL %Δ DOC+ I			**2.44%**	**7.61%**	**–0.03%**

No matter how it is stacked, the 2DB inlet has the lowest DOC + I.

Figure 19. Cost-Assessment Results

resulting from the full-scale design studies (6.9, page 51), the 2DB windtunnel data (6.5.3, page 34), and the decision to require that approach noise reduction with all three inlet candidates meet the HSCT program goals.

Risk assessment results are summarized in Figure 20. In each of the six risk areas, the 2DB was evaluated as having low or comparable risk and thus judged to have the lowest overall risk. The TCB was evaluated as the highest risk in four areas: operability, distortion, unstart severity, and transonic flow; therefore, the TCB was judged to have the lowest overall robustness. The VDC was evaluated to have the highest risk in only two areas: random failures and approach noise. Both of these, however, are critical. VDC random failures were considered likely to be more time consuming and costly to correct since this inlet concept has not only a significantly higher parts count but also a substantially higher percentage of new parts. This assessment is also in agreement with conclusions reached in the independent *Red Team* audit.

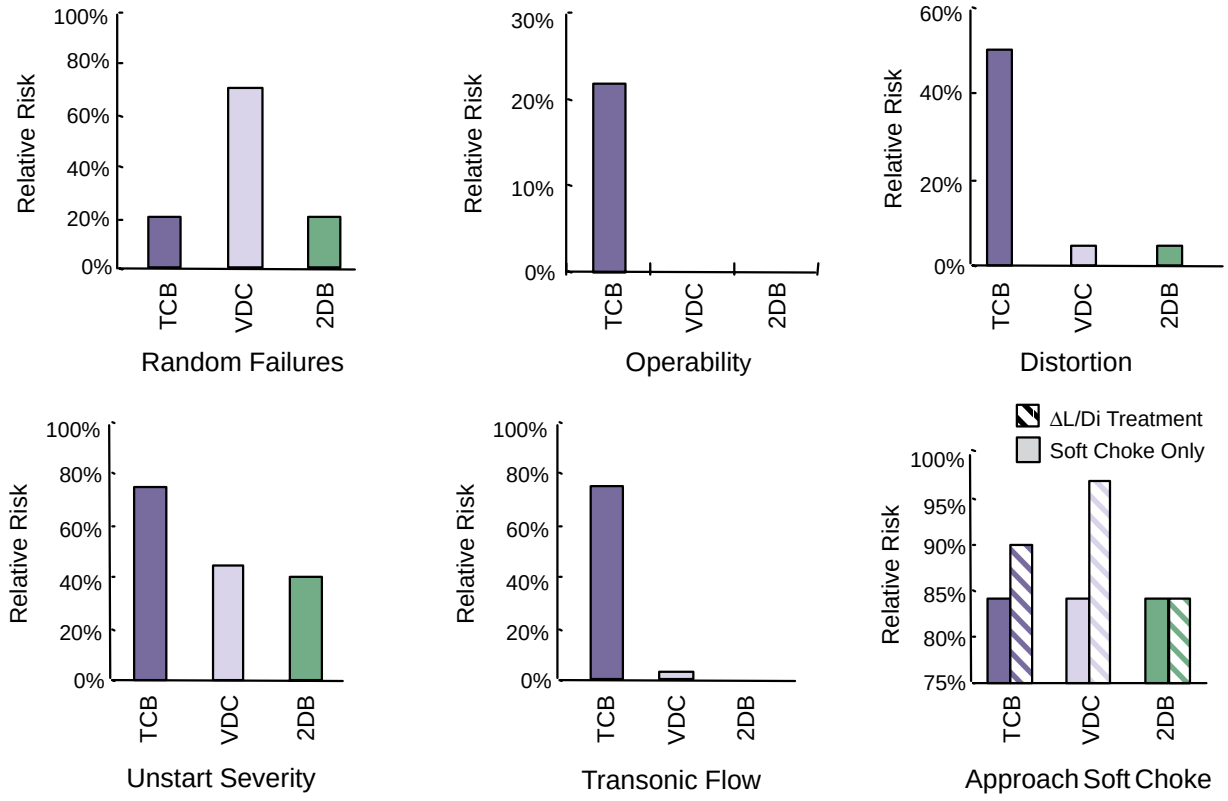

- *The **2DB** is Judged to have the Lowest Overall Risk*
- *The **TCB** is Judged to have the Lowest Overall Robustness*
- *The **VDC** is Judged to have the Highest Relative Risk in two Critical Areas:*

  (1) Potential Random Failures

  (2) Approach Noise

Figure 20. Risk-Assessment Results

The second critical risk area for the VDC involves approach noise levels from the fan. An alternative to increasing the lengths of the TCB and VDC inlets, to allow installation of additional acoustic treatment, is the use of soft choke during approach. As seen in the acoustic lining weight values of Figure 18, the VDC requires considerably more acoustic panels. This is primarily because other design considerations permit less use of internal surface area for acoustic panel installation. Consequently, with less acoustic panel addition, a higher throat Mach number during approach is required to meet the noise-reduction goal. Increased throat Mach number during approach was considered to increase risk. In the event of an aborted landing, the rapidly increasing airflow resulting from a throttle burst could result in an interval of fully choked inlet operation and high distortion. The consequences of the latter could be a lag in acceleration thrust or even engine surge if a high interim level of supercritical inlet operation resulted.

Figure 21 summarizes the *Downselect Confirmation* bottom line. Regardless of whether soft choke or additional acoustic panels are used to meet the approach noise-reduction goal, the 2DB inlet was evaluated to have both the lowest ΔDOC+I, relative to the TCA baseline, and the lowest relative risk. Consequently, the inlet team recommendations were as indicated in Figure 22. The database supported the downselect, and the 2DB was recommended for additional technology development to support a near-term HSCT launch decision. Development cost for the technology required to achieve a viable VDC concept was deemed to be beyond the scope of the CPC program; consequently, it was recommended that it be dropped from consideration. The TCB was considered to be a risk-reduction candidate deserving of a modest continued level of technology development because it was judged to offer higher performance potential — if the robustness concerns could be resolved.

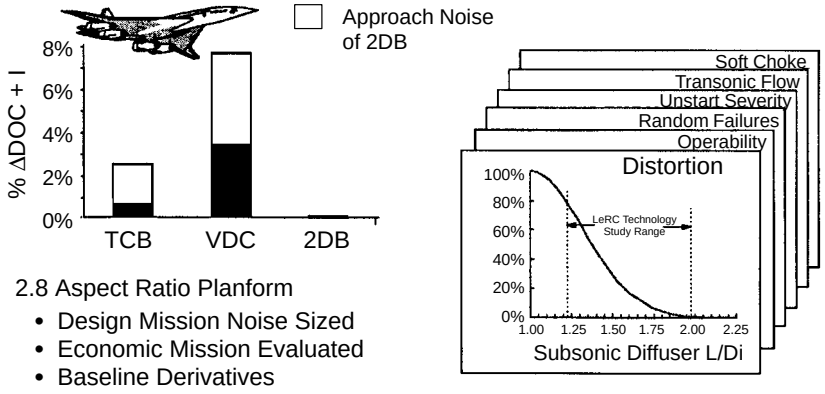

Evaluated Risk Areas	% Relative Risk		
	TCB	VDC	2DB
Random Failures	20	70	20
Operability	22	<1	<<1
Distortion	50	5	5
Unstart Severity	75	55	40
Transonic Flow	75	2	0
Soft Choke	90	97	84

Figure 21. Downselect Confirmation Bottom Line

6.4 2DB Inlet Development

Within the CPC contract, two generations of two-dimensional, bifurcated inlets were designed to achieve the HSCT goals. This effort was driven primarily by perceived aerodynamic concerns and relative shortfalls reflected in the matrix chart of Figure 9 (page 8). As evident from the metric charts (Subsection 6.1, page 1), three of the four applicable goals were met or exceeded (pressure recovery, bleed, and circumferential distortion) with the radial distortion yet to be achieved. Characteristics of the two 2D inlets, sequentially designed to permit achievement of all four of these goals, are discussed in the following paragraphs of this subsection. The first-generation model, the 2DB inlet, was designed and successfully tested. The second-generation model, the P&O inlet, was designed but was not fabricated before the HSR program termination.

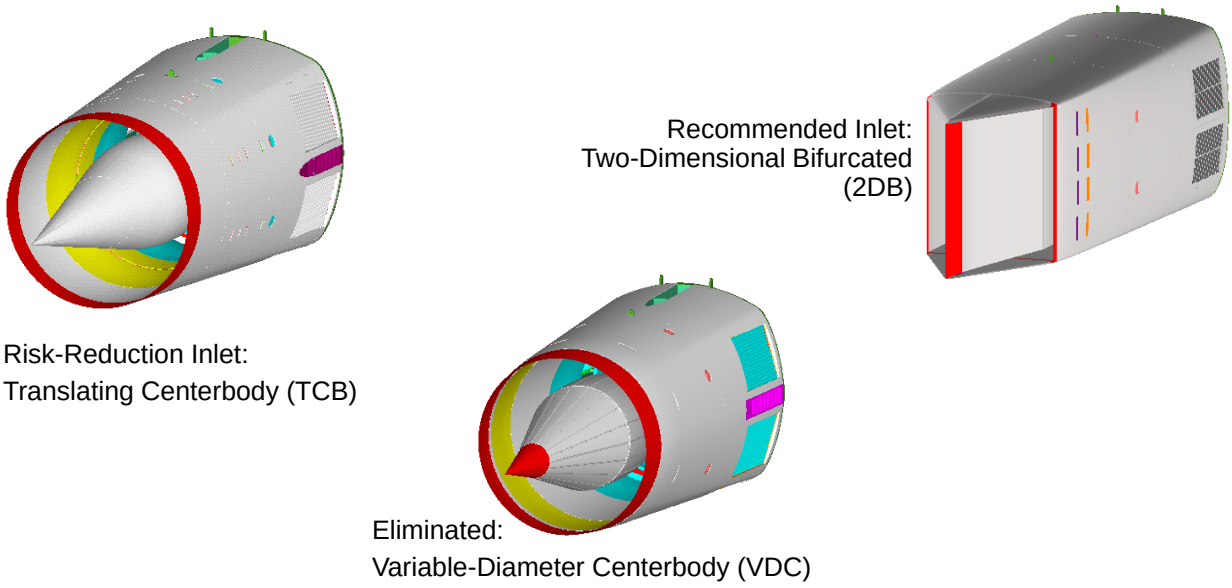

Figure 22. Inlet Team Downselect Recommendation

6.4.1 First Generation, 2DB Test Model

The design-point flowpath geometry and compression system of the 2DB inlet windtunnel test model are shown in Figures 23 and 24 respectively. The basic flowpath comprises two ducts that are mirror images of one another. The two ducts are separated by the compression ramp system along most of the inlet length and merge into a single passage just forward of the engine face. As illustrated in Figure 23, each duct has supersonic and subsonic diffusers. Transition from supersonic to subsonic flow occurs in the throat section. The supersonic diffusers and the throat sections have rectangular cross-sectional shapes. The cross sections of the subsonic diffusers are rectangular at the entry station and transition to half circles to form a full circle where the bifurcated ducts join. The inlet was sized for a J85 engine with a projected capture of 16.316 by 16.07 in. It was approximately ¼ scale to the HSCT inlet.

Figure 24 shows details of the supersonic compression system. The initial compression angle is 3° from the centerline, making a 6° included angle for the ramp leading edge. This was considered the lowest practical value for ease of manufacturing and durability in service. It is desirable to keep the initial turning angle low in order to minimize total pressure losses across the bow shock wave. The bow shock is followed by 8.82° isentropic compression focused at the cowl lip. The ramps include an additional 0.77° compressive turning further downstream. The internal angle of the cowl lip is turned 3° away from the streamwise direction, thereby reducing the strength of, and total pressure losses across, the cowl lip shock. The total turning angle along the cowl is 7°, such that the flow angle at the end of the supersonic compression is 4° toward the inlet centerline.

The supersonic compression system was developed through an extensive parametric design optimization process. Figure 25 shows sample results for selecting the value of the second isentropic compression turn on the ramp. The final choice was based on maximizing total pressure recovery while maintaining the required external-to-internal compression split of at least 60% and keeping the throat angle at not more than 4° to preclude a second throat in the subsonic diffuser during

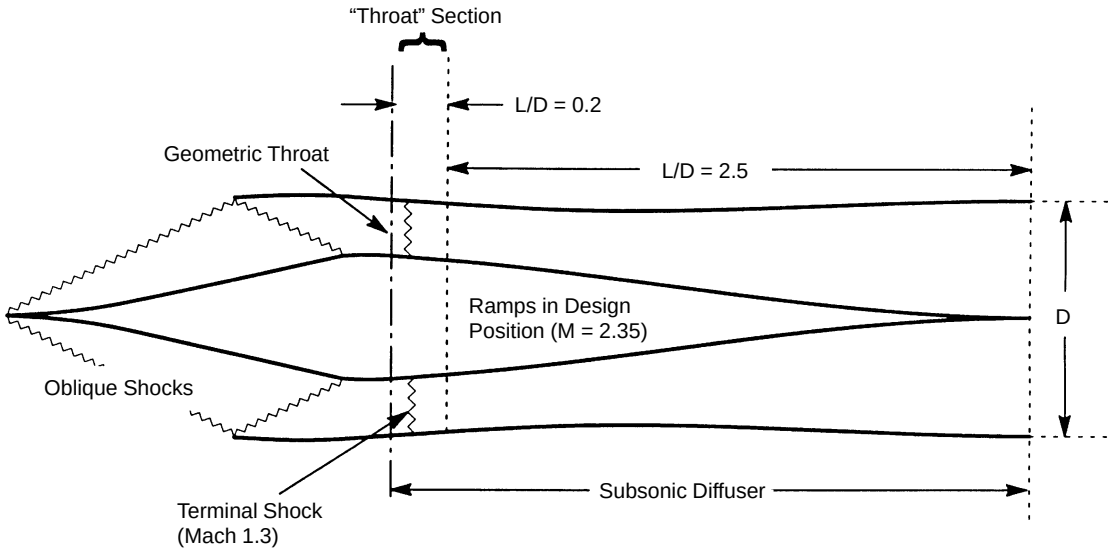

Figure 23. Design Point 2DB Inlet Flowpath

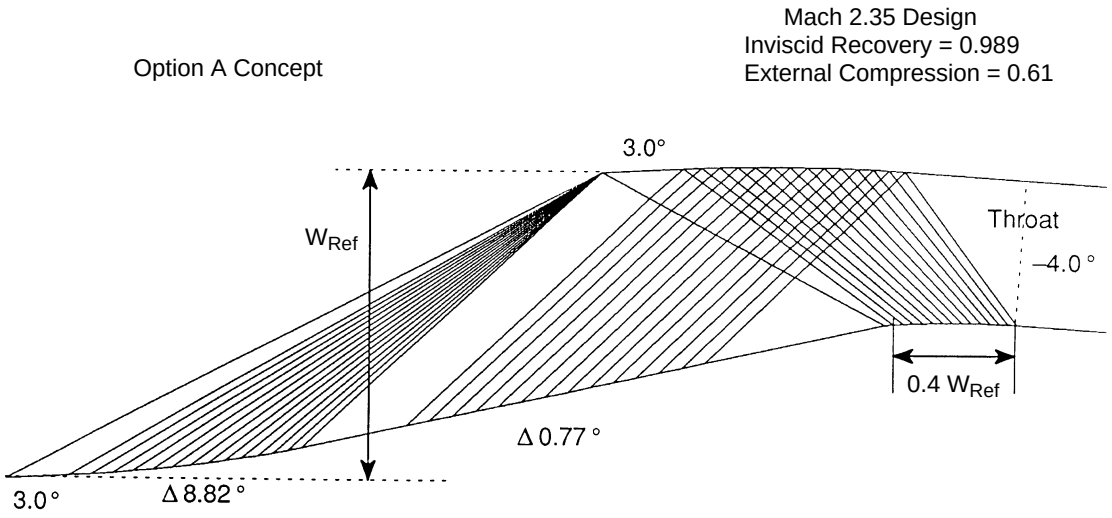

Figure 24. Design Point 2DB Inlet Supersonic Compression System

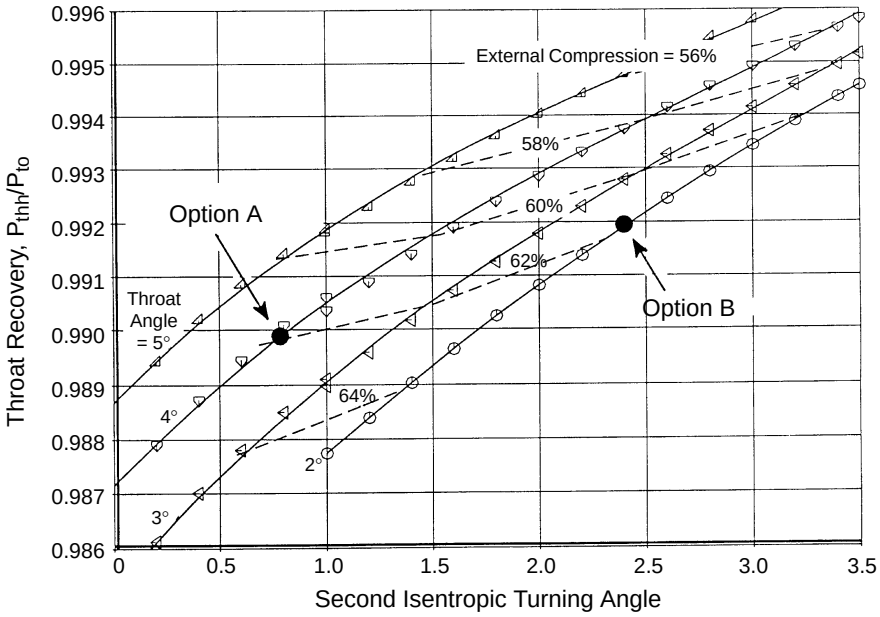

Figure 25. Optimization of 2DB Inlet Supersonic Diffuser

low-speed operation. After final selection of the parametric values shown in Figure 23, the design point total pressure recovery of the 2DB inlet model supersonic diffuser was predicted to be about 99% as shown in Figure 25. The selected design (Option A) and an alternative (Option B) were evaluated using CFD tools. The selected design had a slightly cleaner flowfield at off-design conditions and was therefore incorporated into the mechanical design of the model.

The 2DB model bleed system is illustrated in Figure 26. The porous regions on the cowl, sidewalls, and ramp were designed to allow tailoring of the distribution of bleed for optimum performance. In any given bleed configuration, only part of the bleed holes were open — the remainder being plugged.

The inlet model was designed to allow testing with fixed bleed exits as well as with variable bleed exits. For the majority of testing, the exit area was varied with remotely controlled variable-position plug valves for all bleed exits — except the forward cowl bleed where fast-response sliding louvers were used to control bleed exit area. For part of the testing, throat bleed exits were controlled with poppet valves originally designed for the SR–71 airplane. Figure 27 is a schematic of a poppet valve.

Design of the inlet model followed a modular approach to allow parametric optimization of features considered to involve technical risk not easily resolved through theoretical analysis. The length of the region where flow from the two inlet ducts mixed in front of the engine face was identified to be one of these risks. Modules were provided to make possible testing with three mixing-region lengths. In terms of engine face radius (R), the available lengths were 0, 1R, and 2R. Model drawings of the three optional mixing-region configurations are shown in Figure 28.

Supersonic inlets require sharp cowl lips to minimize drag during supersonic cruise. The sharp cowl lip leads to excessive total pressure loss and distortion during low-speed operation. Traditionally, the most common approach to improving low-speed performance is to incorporate auxiliary inlets. An alternate approach of increasing the contraction ratio of the inlet by varying the cowl lip has been tried successfully on the B–1A *Lancer* inlets. A variable cowl lip was designed for the 2DB model

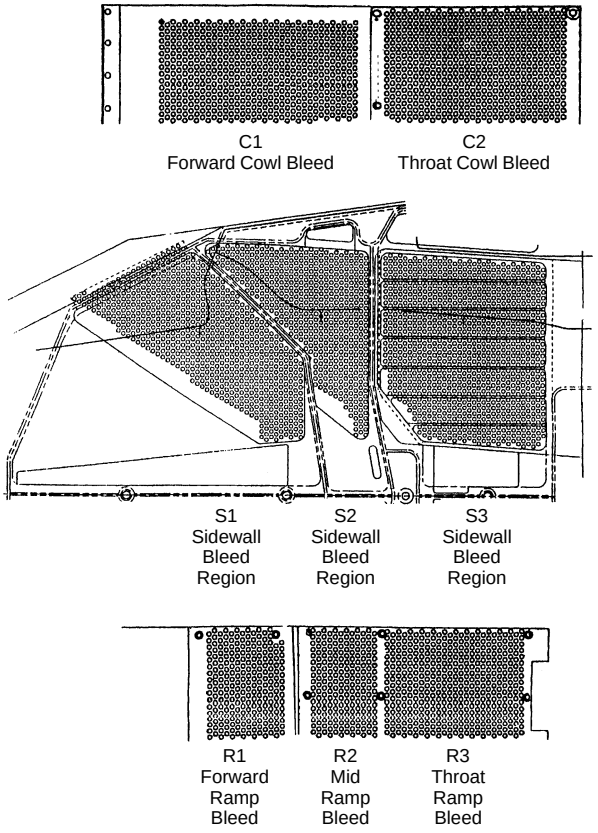

Figure 26. Basic Bleed Patterns for the 2DB Inlet Model

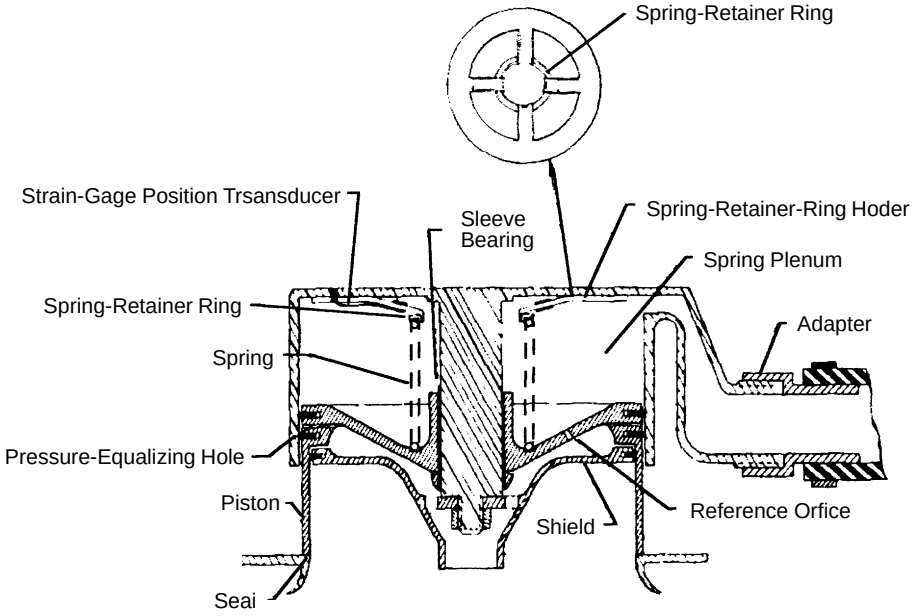

Figure 27. Poppet Valve Schematic

based on the B–1A inlet. For purposes of the test, the cowl lip variation is achieved with replaceable inserts as shown in Figure 29.

A plan view drawing in Figure 30 illustrates salient features of the 2DB inlet wind tunnel test model. Figure 30 also shows the lines of the second-generation (P&O) model (which is discussed in the next subsection). For the 2DB inlet, the leading edge of the ramps is a 6° wedge, providing an initial compression angle of 3° for each ramp. The forward ramp extends from the leading edge to the forward hinge. The fixed wedge is followed by a flexible segment providing additional distributed compression. Next is a rigid portion ending at the forward hinge. The middle ramp segment is supported by the forward and middle hinges. The aft ramp extends from the middle hinge to a sliding hinge where the left- and right-hand ramps rejoin. A vertical splitter along the model centerline separates the volume between the ramps into two compartments that contain independently controllable ramp-position actuators and bleed plenum dividers.

Each inlet cowl is provided with fast-acting actuators to control the forward cowl bleed overboard exit areas. The bypass cavity is an annular plenum forward of the engine bellmouth. The cowl surfaces away from the inlet centerline at the ramp trailing edge station form the forward wall of the bypass plenum.

The bypass exits are overlapping sliding louvers, similar to the forward cowl bleed exits. Each of the four sets of bypass exit louvers was provided with remotely controlled position actuators.

The engine face total pressure rakes were of the standard 40-probe design recommended by the S16 committee of the Society of Automotive Engineers (SAE). In addition to the engine face instrumentation, several crossduct and boundary layer total pressure rakes were installed on the ramp and cowl surfaces. Flush-mounted static pressure taps were installed on the ramp, cowl, and sidewall surfaces.

6.4.2 Performance and Operability Model

The second-generation test model of the 2DB concept was called the *performance and operability* (P&O) model. The P&O model was intended to update the 2DB inlet design to address changes dictated by the evolution of the HSCT airplane, as well as the of the overall propulsion system, and to incorporate improvements indicated by the preceding 2DB inlet model test. The major differences between the P&O and 2DB model flowpaths are primarily in the design of the subsonic diffuser:

Parameter	Existing Model	Mixed-Flow Turbofan
Engine Face Mach Number	0.35	0.31
Diffuser Area Ratio	1.6	1.9 ▲
Diffuser Length/Diameter Ratio	2.7	2.3 ▼

The change in diffuser area ratio is the driven by a change in the engine cycle; the change in the diffuser length-to-diameter ratio is driven by system study results indicating airplane performance benefits attributable to a lower overall inlet length.

Features of the design point compression system of the P&O model are illustrated in Figure 31. It is similar to the 2DB inlet compression system discussed in Subsection 6.4.1 (page 21). The main analytical design difference is that the throat section of the P&O model has been shortened somewhat relative to the 2DB model. The difference in mechanical design is that the supersonic diffuser has been rescaled to accommodate the reduced capture area required by the new subsonic diffuser (Figure 30).

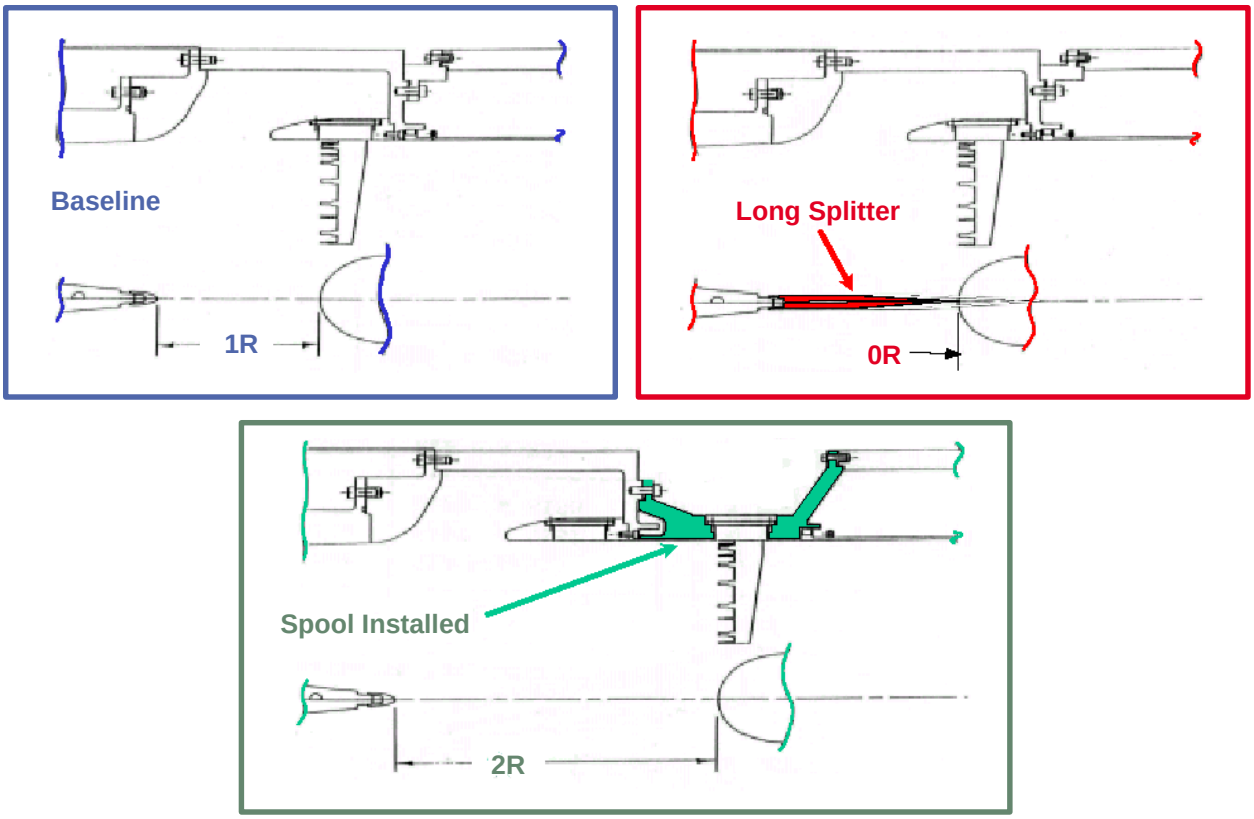

Figure 28. Subsonic Diffuser Mixing-Length Configurations

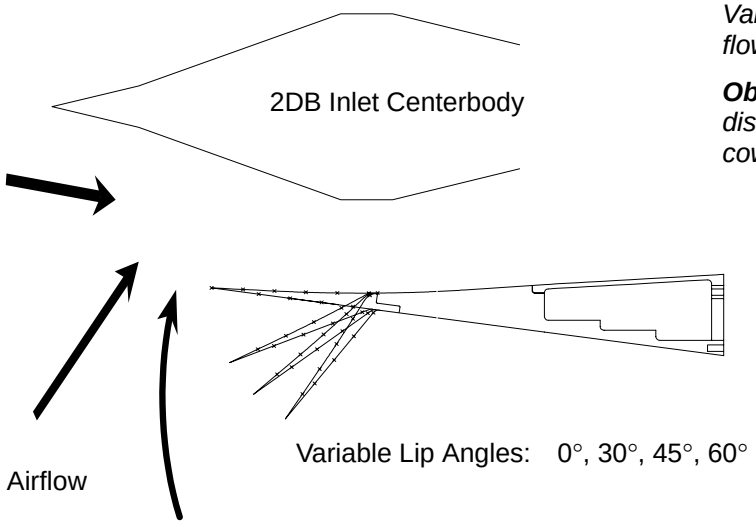

Variable cowl lip test evaluates alternate flow-augmentation approach.

Objective: *Assess 2DB inlet recovery and distortion at static conditions for various cowl lip configurations.*

Figure 29. Variable Cowl Lip

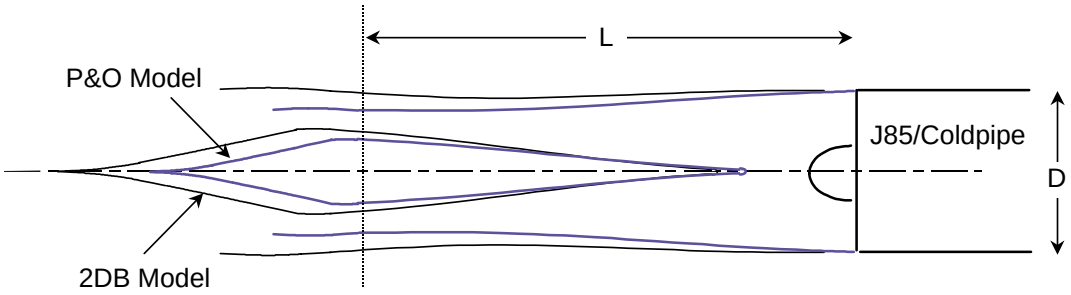

Figure 30. Centerline Cross Section of 2DB Inlet Model

- Focused Ramp Compression on Cowl
- Cancelled Cowl Shock on Shoulder
- Distributed Compression From Shoulder to Throat
- Sidewalls Parallel from Ramp Leading Edge to Engine Face, Width = Engine Diameter

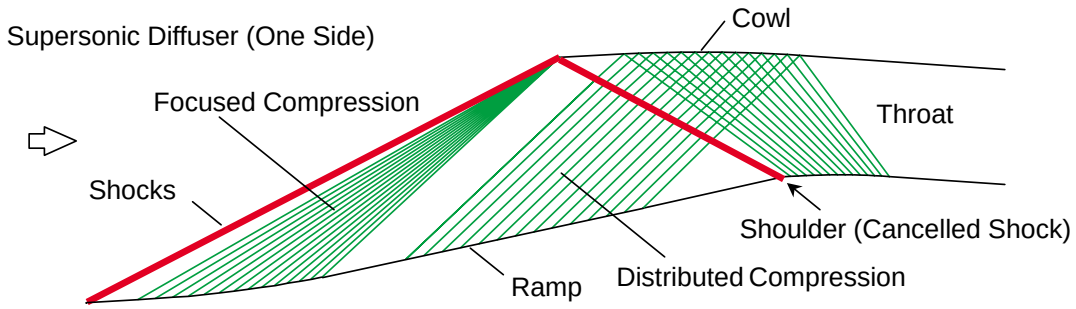

Figure 31. Performance and Operability Model – Inlet Type

The P&O model bleed system is illustrated in Figures 32 and 33, along with the nomenclature used for the compartmented bleed regions and associated bleed exit valves. As in the 2DB model, each exit valve was designed for independent remote control to allow optimization of the bleed system.

The supersonic diffusers of the P&O and 2DB inlet models share nearly the same aerodynamic design. Thus, the predicted total pressure recovery of the P&O inlet supersonic diffuser is 99% as it is for the 2DB model. As noted earlier, the primary difference between the two models is in the design of the subsonic diffuser. An analytical study to predict subsonic diffuser performance was conducted at NASA. Results of the CFD analyses are summarized in Figure 34. Since boundary layer blockage at the inlet throat is a function of throat bleed rate, the analysis was conducted assuming a range of diffuser entry blockage values. Presenting the results in this way makes possible a trade of total pressure recovery versus throat bleed flow rate.

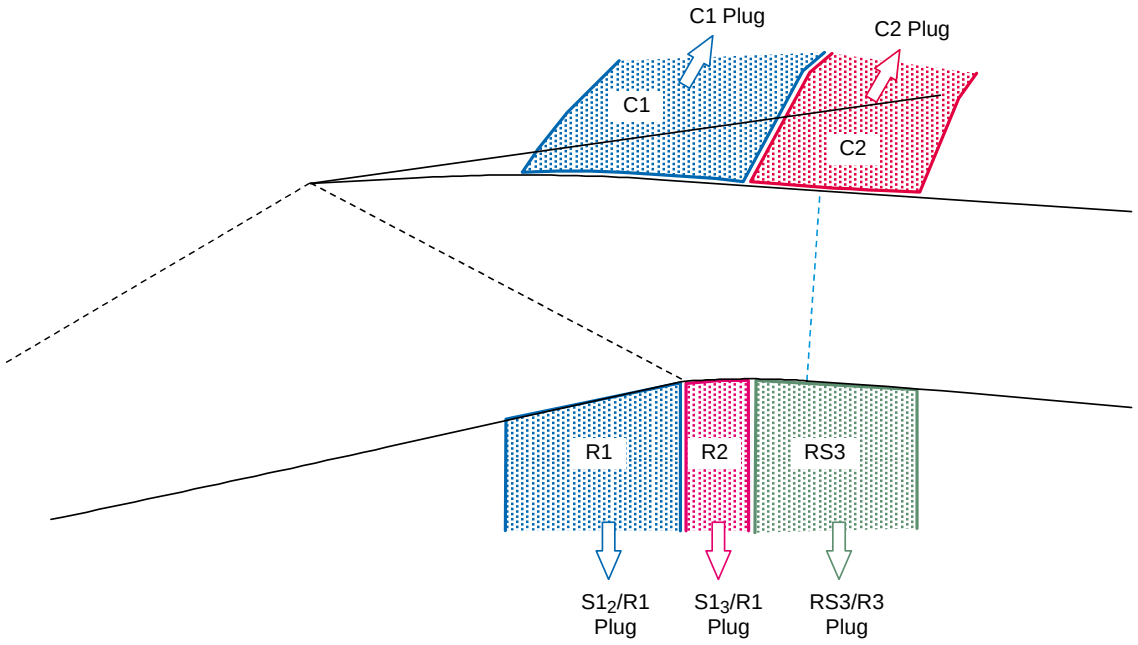

Figure 32. Ramp and Cowl Bleed Regions

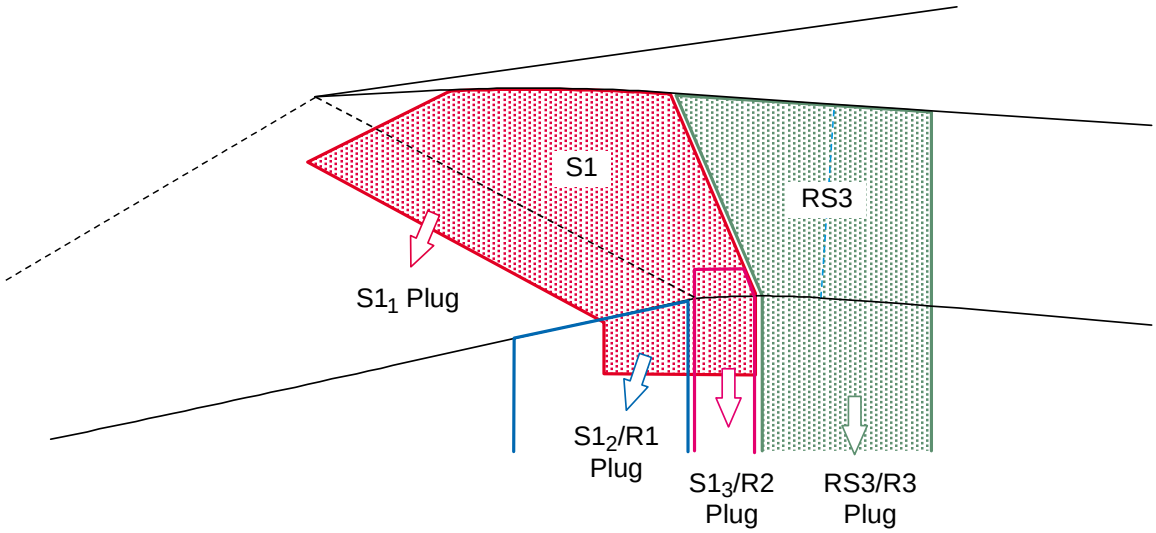

Figure 33. Sidewall Bleed Regions

6.5 Scale-Model Test Results

This subsection presents key aerodynamic and controls results for the three downselected candidate inlets. All testing was conducted in the NASA–Glenn 10×10-ft SWT.

6.5.1 TCB

The TCB inlet wind tunnel test model was designed and built under Boeing IR&D funds. It was provided to NASA for testing under a Space Act Agreement between Boeing and NASA. The testing was conducted by NASA with Boeing support in the GRC 10×10-ft SWT. Since the results of the test were part of the inlet downselect process, they are mentioned here for the sake of completeness.

The test model had a cowl lip diameter of 8.9 in and was approximately 1/9 scale to the HSCT inlet. Wind tunnel experiments used a cold-flow pipe and plug valve to vary the inlet backpressure. Design-point total pressure recovery and distortion along with pitch, yaw, and Mach tolerance of the TCB inlet model are summarized in Figure 35. The figure also shows goal values for these parameters, illustrating the shortcomings of the inlet as designed. Since the 2DB model (discussed in Subsection 6.5.3, page 34) demonstrated higher total pressure recovery, lower distortion, and more flow stability, further development of the TCB inlet was abandoned under the CPC contract.

6.5.2 VDC

Background – The VDC inlet concept dates back to the initial *Supersonic Transport* (SST) effort in the 1960's. NASA–Glenn (then NASA–Lewis) developed VDC concepts and several model hardware builds to verify the aerodynamic and operability of the concept. An important model that had full variable-geometry capability was funded intermittently through the decades and finally finished as the HSR program was beginning. Formally, this inlet was then successfully tested and reported under a earlier contract, Propulsion/Airframe Integration Technology (PAIT), Task 5 (NAS3–25965) by Boeing – Long Beach (then known as McDonnell Douglas Aerospace, MDA), see Reference 1. A pending NASA report gives further details on the test program, Reference 2. A section was largely excerpted from the PAIT report to describe the pertinent results for the HSR program. These data are included for background and completeness, as it influenced the inlet downselect decision.

Within the HSR–CPC contract, the VDC data were further examined with an eye towards engine compatibility. Distortion parameters were calculated using the ARP–1420 standard that was eventually adopted by HSR as an inlet metric (Reference 3). A summary figure is included showing the distortion performance of the VDC inlet near the HSCT design Mach number.

The questions of mechanical complexity and reliability were not fully addressed in the previous tests, so an additional test program was added. This "VDC Durability Test" is reported in Subsection 6.9.2 (page 54).

Evaluation of MDA VDC Inlet Based on NASA VDC Inlet Mach 2.325 Results – The VDC inlet was designed for a Mach number of 2.5. Since the HSCT Mach number was 2.4, the inlet was also tested for aerodynamic characteristics at Mach 2.325 (the closest possible test Mach number to the estimated local under-wing Mach number at the inlet location for the MDA Mach 2.4 HSCT). Note that the mismatch in design Mach number would result in some additional spillage; this was considered to have only a very minor effect on recovery or distortion. This test provided data against which

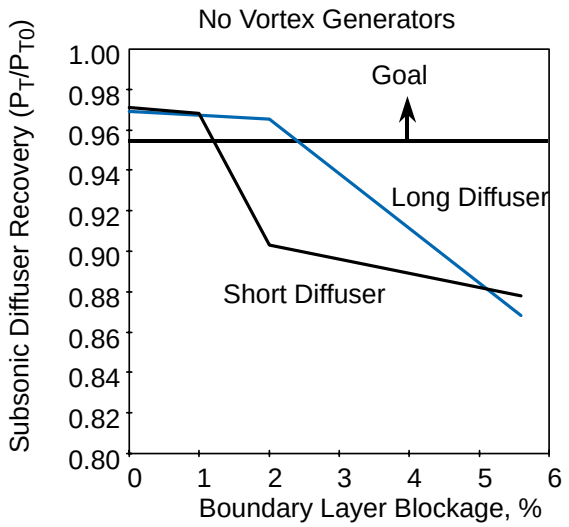

Subsonic Diffuser Blockage Study
(J. Dudek, J. Slater, C. Towne)

- WIND, Navier–Stokes Code
- Spalart–Allmaras Turbulence Model
- Entrance Mach number = 0.79
  (Simulating Mach 1.3 Normal Shock)
- Power Law Boundary Layer Profile
- Goal Recovery Achievable
  - Reduced Blockage Via Increased Bleed
  - Introduction of Vortex Generators to Suppress Separation

Figure 34. Total Pressure Recovery Estimates for the P&O Model Subsonic Diffuser

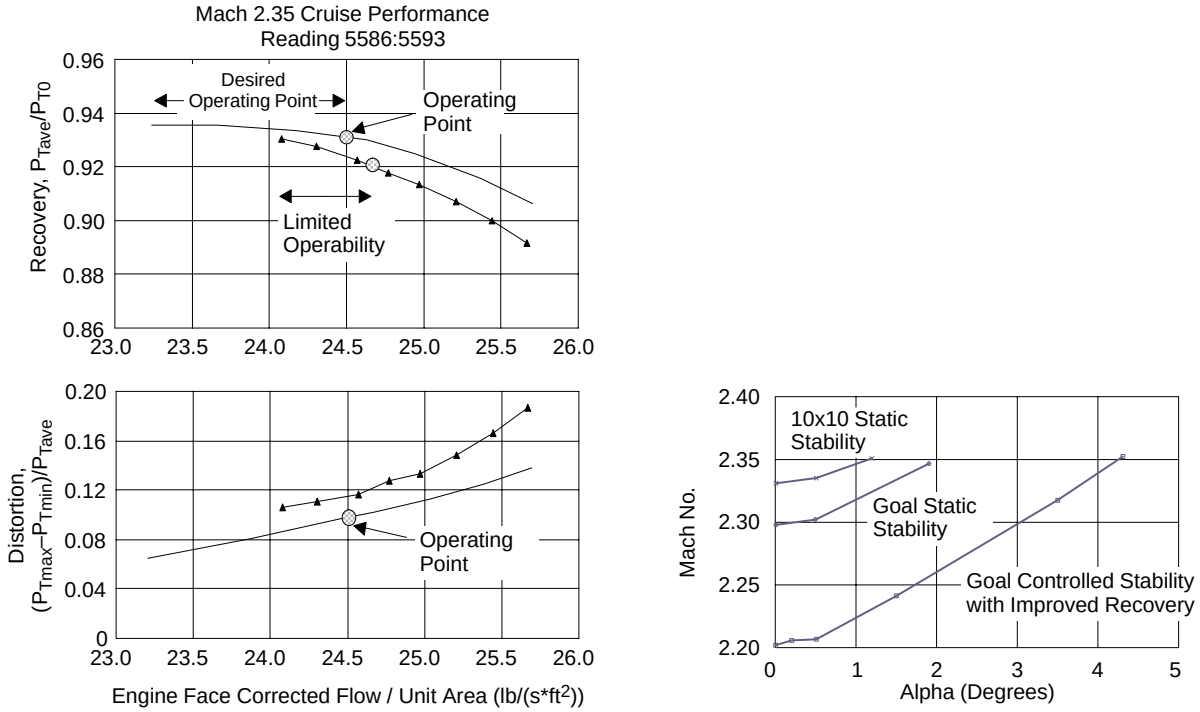

Figure 35. TCB Inlet Performance

to compare the performance estimated for a McDonnell Douglas VDC inlet designed for an inlet configuration trade study (Reference 4). The MDA inlet is similar to the NASA VDC inlet design in that it is also a mixed-compression, bicone inlet with translating-variable-diameter centerbody. It has greater transonic flow capacity than the NASA VDC inlet because it was sized for a GEAE fan-on-blade (FLADE) engine. Estimated operating point performance was 0.899 inlet-pressure recovery, with 0.02 centerbody bleed at 0.22 bleed-pressure recovery and 0.01 cowl bleed at 0.22 bleed-pressure recovery.

The NASA VDC inlet was tested with several centerbody geometries to minimize the amounts of centerbody and cowl bleed. Figure 36 shows plots of total pressure recovery and distortion data for four centerbody geometries. Table 1 lists the features of the four inlet configurations.

Table 1. Inlet Configurations with Centerbody Translation and Diameter Changes

Mach 2.325 Inlet Configuration	I	J	K	L
Centerbody Translation, X_{cb}/R	0.0481	0.0289	0.0	0.0626
Second Cone Angle, Degrees	17.5	17.4	17.4	17.4
Centerbody Bleed Slot Width, DX_{cb}/R	0.1083	0.1083	0.1083	0.1083
$A_{cowl\ bleed\ exit}$ / $A_{capture}$	0.0128	0.0128	0.0128	0.0128
Cowl Bleed Surface Porosity	60%	60%	60%	60%
Cowl Bleed Hole Rows Open	3–11	3–11	3–11	3–11
Supercritical Bleed Mass Flow Ratio	0.018	0.018	0.022	0.014
Supercritical Cowl Bleed Mass Flow Ratio	0.01	0.01	0.01	0.01

Overall the NASA VDC inlet performance at Mach 2.325 is expressed in terms of takeoff gross weight relative to MDA VDC inlet. Takeoff gross weight versus stability index is plotted for the four inlet configurations in Figure 37. Stability index (SI_{cp}) is measured as the ratioed change in corrected airflow while holding constant pressure in the throat bleed plenum. The lowest TOGW configuration was Configuration J, but no angle-of-attack or Mach number sensitivity data were taken for it. Only Configuration I, which had similar performance to J, was tested for angle-of-attack and Mach number sensitivity. It will be shown that the configuration tested had adequate angle-of-attack and Mach number tolerance at $SI_{cp} = 0.05$, and it was thus inferred that the lowest TOGW configuration would also have sufficient angle-of-attack and Mach number tolerance at $SI_{cp} = 0.05$. A comparison of the performance of the lowest TOGW NASA VDC inlet configuration to the MDA VDC inlet at $SI_{cp} = 0.05$ is listed in Table 2.

The similarity in overall performance between the two inlets indicates that the performance that was estimated for the MDA VDC inlet is reasonable. The NASA VDC inlet only had 0.2% higher TOGW despite having higher operating pressure recovery because it also had more centerbody bleed drag (due to lower bleed flow pressure recovery).

Details of the best bleed configuration can be found in the HSCT/VDC inlet reports (References 1 through 3) along with data for ΔMach number and angle tolerances. Several years after these results were reported, a stack-up of the angle and Mach number changes was made (see 6.6.2, page 38). This effort used the atmospheric model in Reference 5 with predictions of wing aeroelasticity, vehicle trim attitude, under-wing flowfield distortion, manufacturing tolerances, etc. to determine the HSCT required inlet operability limits. These are given as 2° angle and 0.05 Δ Mach simultaneously, while maintaining 0.92 recovery and acceptable distortion. The VDC inlet meets these criteria.

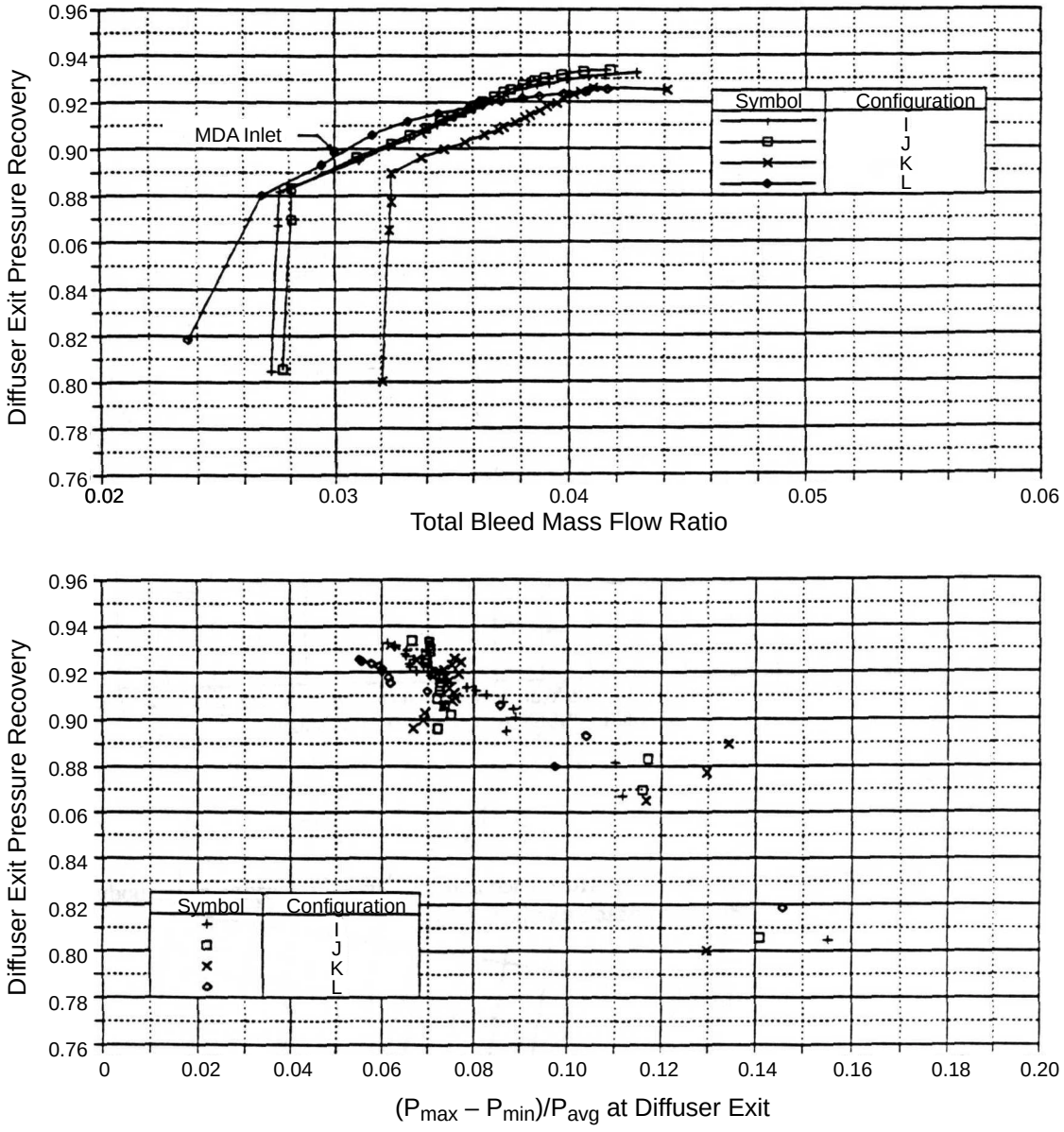

Figure 36. Inlet Performance with Varying Centerbody Geometry, Free-Stream Mach Number = 2.325

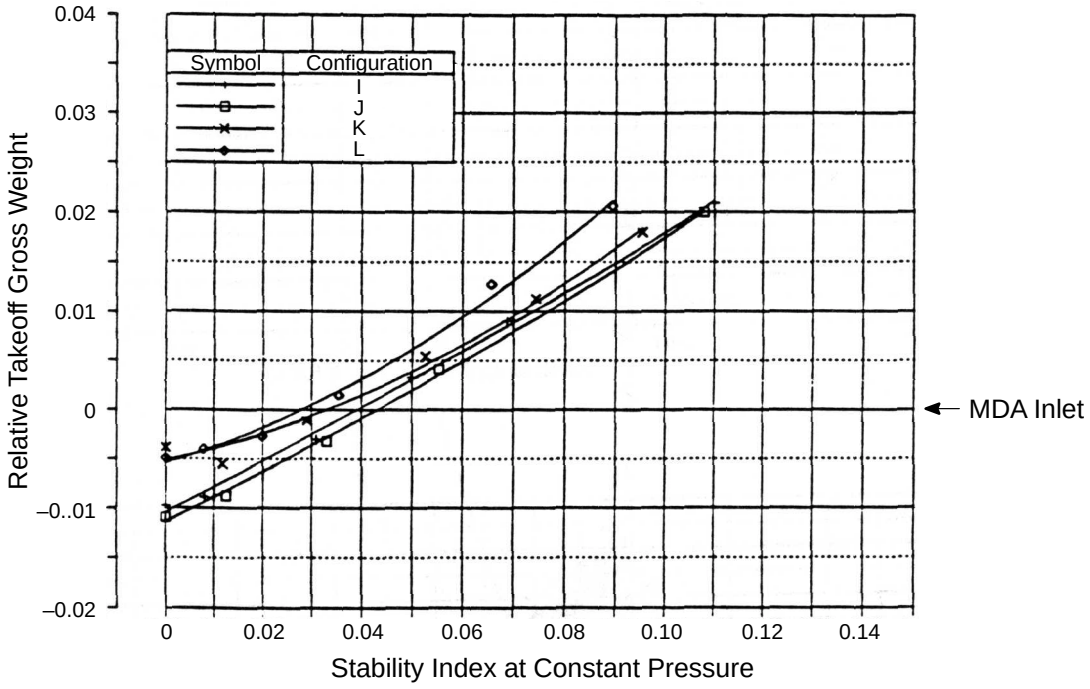

Figure 37. Inlet Overall Performance and Stability with Varying Centerbody Geometry, Free-Stream Mach Number = 2.325

Table 2. Mach 2.325 Inlet Operating Characteristics at SI_{cp} = 0.05

Inlet	NASA VDC Configuration I	MDA VDC Estimate
Diffuser Exit Pressure Recovery	0.912	0.899
Total Bleed Mass Flow Ratio	0.034	0.03
Centerbody Bleed Mass Flow Ratio	0.022	0.020
& Pressure Recovery	0.12	0.22
Cowl Bleed Mass Flow Ratio	0.012	0.010
& Pressure Recovery	0.41	0.22
Relative Takeoff Gross Weight	+0.002	Base

In Reference 3, GEAE analyzed the dynamic engine face data from the VDC test to determine distortion levels. This report details much of the steady-state data and analyzes dynamic data at the inlet Mach 2.325, 0° angle-of-attack operating point. Using the a rough correlation based on this 0° case, the steady-state data can be extended to the angle cases. Eventually, the HSR program adopted standard ARP–1420 dynamic distortion descriptors. The limits for radial distortion, DPR, were 0.03 and 0.05 for cruise and maneuver, respectively. The limits for circumferential distortion (DPC) were 0.05 and 0.08 for cruise and maneuver, respectively. Table 3 lists these results in the context of the ARP–1420 descriptors.

Table 3. Mach 2.325 Inlet Configuration Angle-of-Attack Effects on Distortion and Recovery

Angle of Attack	Recovery	DPR		DPC	
		Steady State	Dynamic	Steady State	Dynamic
0°	0.925	0.014	0.0175	0.008	0.021
3°	0.922	0.025	0.031	0.020	0.052
5°	0.901	0.035	0.044	0.038	0.100
7°	0.862	0.054	0.068	0.064	0.168
Cruise Goal	*0.92*		*0.03*		*0.05*
Maneuver Goal	*N/A*		*0.05*		*0.08*

Therefore, the VDC inlet had acceptable performance well beyond 2° angle of attack and could operate to about 5° during planned vehicle maneuvers.

In general, the VDC inlet proved to have excellent aerodynamic and operability characteristics. Mechanical complexity/durability issues remained a concern to be addressed by a subsequent test program (Subsection 6.9.2, page 54).

6.5.3 2DB Inlet

The 2DB inlet was tested with fixed as well as variable bleed exits. For fixed-bleed testing, the exit areas of the various bleed regions were adjusted for the best total pressure recovery and were kept fixed at that value while data were recorded at various positions of the primary-flow plug valve. For variable-bleed testing, the exits for the forward bleed were fixed at the predetermined value and the throat bleed exits were continually varied to maintain a constant pressure ratio (with respect to the tunnel total pressure) in the throat bleed plenum while varying the primary plug valve position.

Figure 38 shows the excellent total pressure recovery and flow stability demonstrated during cold-pipe testing of the 2DB inlet. At the nominal operating point, the model has 93% total pressure recovery with 3% bleed and approximately 0.5% spillage. Controlling the throat bleed exit area provides stable inlet operation over a wide mass-flow range. Figure 38 also illustrates the substantial inlet performance improvement realized by optimizing the inlet bleed and subsonic diffuser vortex generator configurations between the beginning and the end of the wind tunnel experiments.

Figure 39 shows hub and tip distortion values calculated from the 2DB inlet experimental data using the procedures of Aerospace Recommended Practice 1420. The results indicate that the radial values are near the preliminary limits established by the CPC Inlet ITD Team.

Figure 40 shows that the variable-bleed mode of operation almost doubles the tolerance of the inlet to excursions in pitch, yaw, and local Mach number from the nominal operating values. The figure indicates the required tolerance levels of 1° pitch and 2° yaw at –0.05 ΔMach tolerance are (1) just met with fixed-bleed exit operation and (2) are easily met with variable-bleed operation. Simply controlling the bleed is not adequate to meet the maneuver requirements set as 4° yaw while maintaining a –0.05 ΔMach tolerance. Since airplane maneuvers occur at a relatively slow rate, the required tolerance during maneuvers may be obtained by activating the inlet compression ramps.

Results of testing with the three mixing length configurations (see Figure 28, page 26) are shown in Figure 41. These data indicate that the subsonic diffuser mixing length did not have a significant

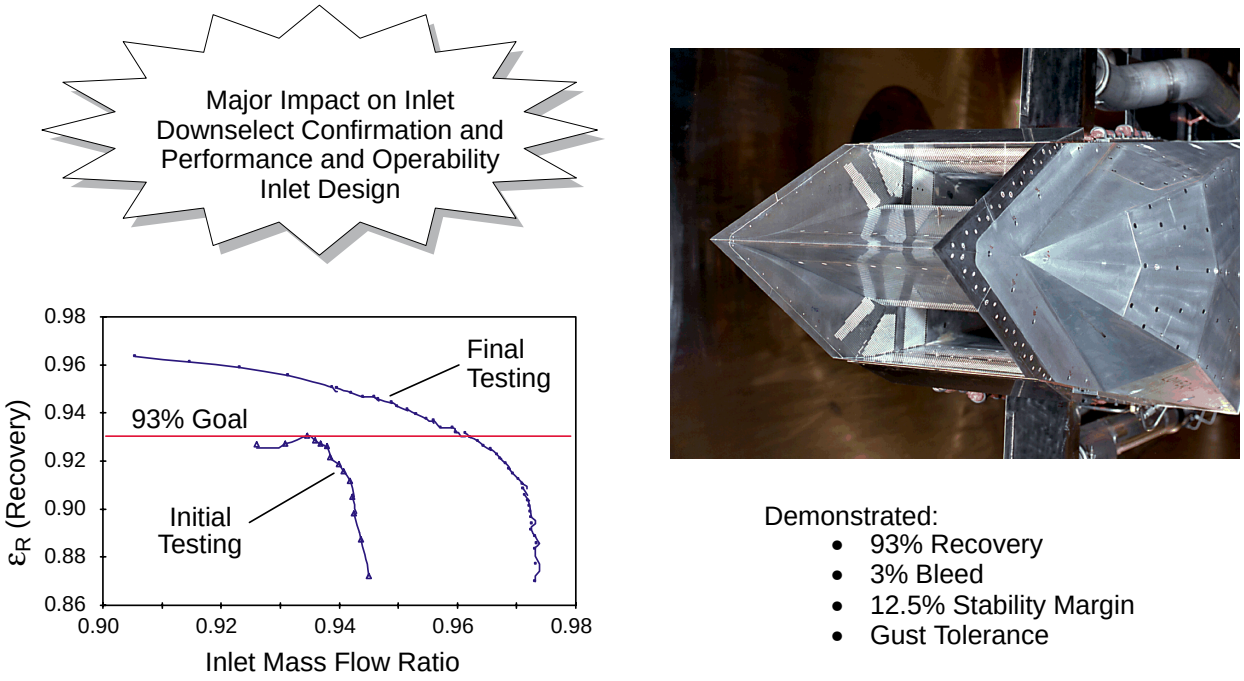

Figure 38. Testing 2DB in 10x10 SWT

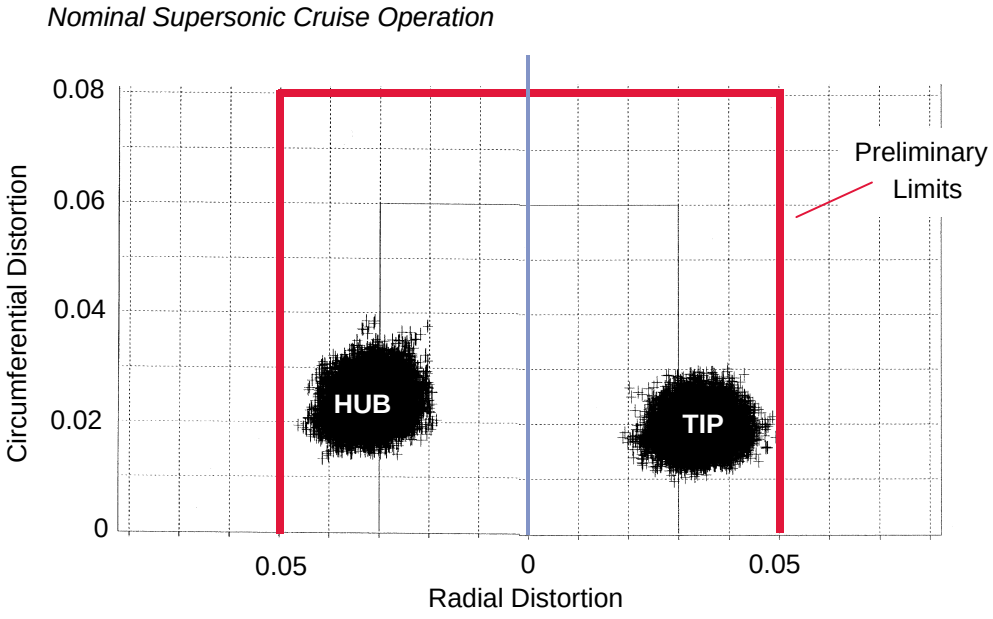

Figure 39. Dynamic Distortion – 2DB Inlet *Total pressure distortion per Aerospace Recommended Practice 1420.*

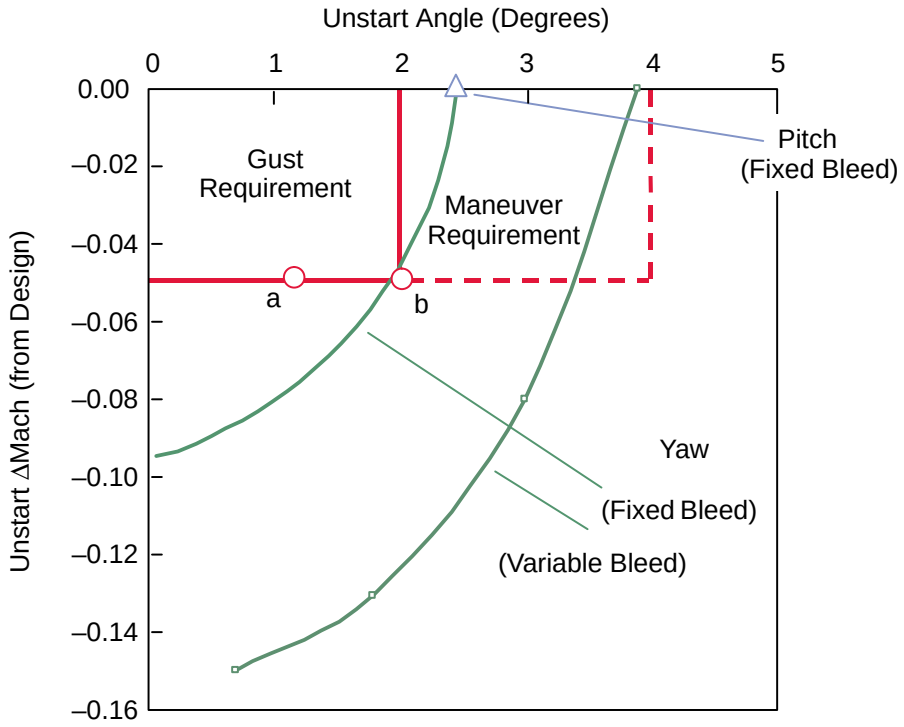

Figure 40. Pitch, Yaw, and Mach Tolerance of 2DB Inlet (10x10 SWT Test)

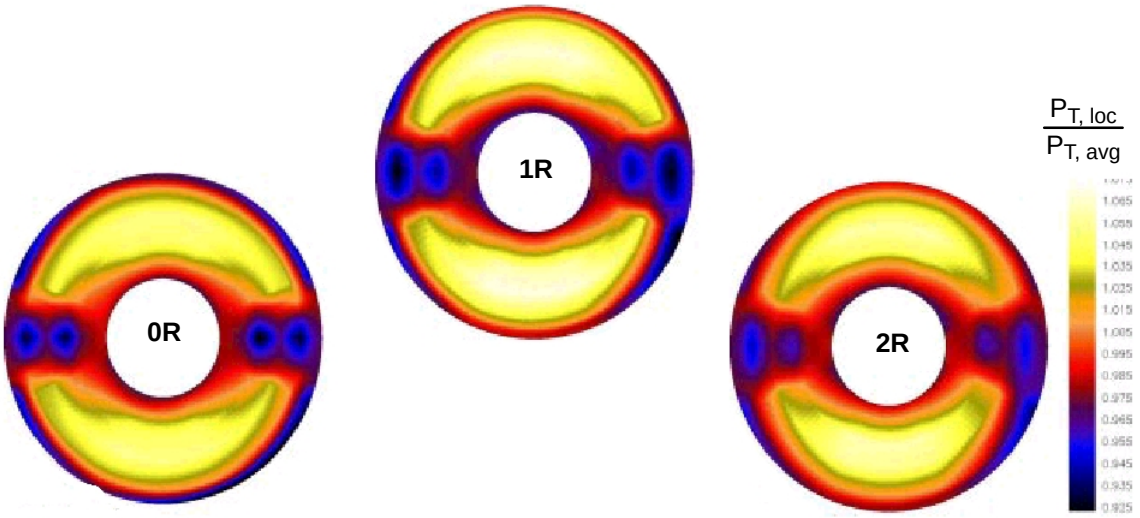

Figure 41. Steady-State Distortion Contours with Different Mixing Lengths
Mixing length effect on distortion is unclear.

effect on total pressure deficit in the wake of the bifurcation as measured at the engine face. Based on these results, the one-radius (1R) mixing length was selected as the preferred configuration. The 0R length would not result in a savings of overall inlet length due to a requirement of 1R length for the bypass system downstream of the station where the diffusion of the primary air stream is completed.

Subsequent to completion of testing with the cold pipe, a J85 engine was installed behind the inlet. For part of the testing, the flow ducts controlling the throat bleed were replaced with fast-acting poppet valves. Figure 42 shows the increased stability available with the poppet valves compared to operation with fixed bleed exits. The results obtained during the cold pipe testing are shown for comparison. With additional experimental work, the inlet performance with the engine and poppet valves should be equal to the performance obtained with the cold pipe and variable bleed.

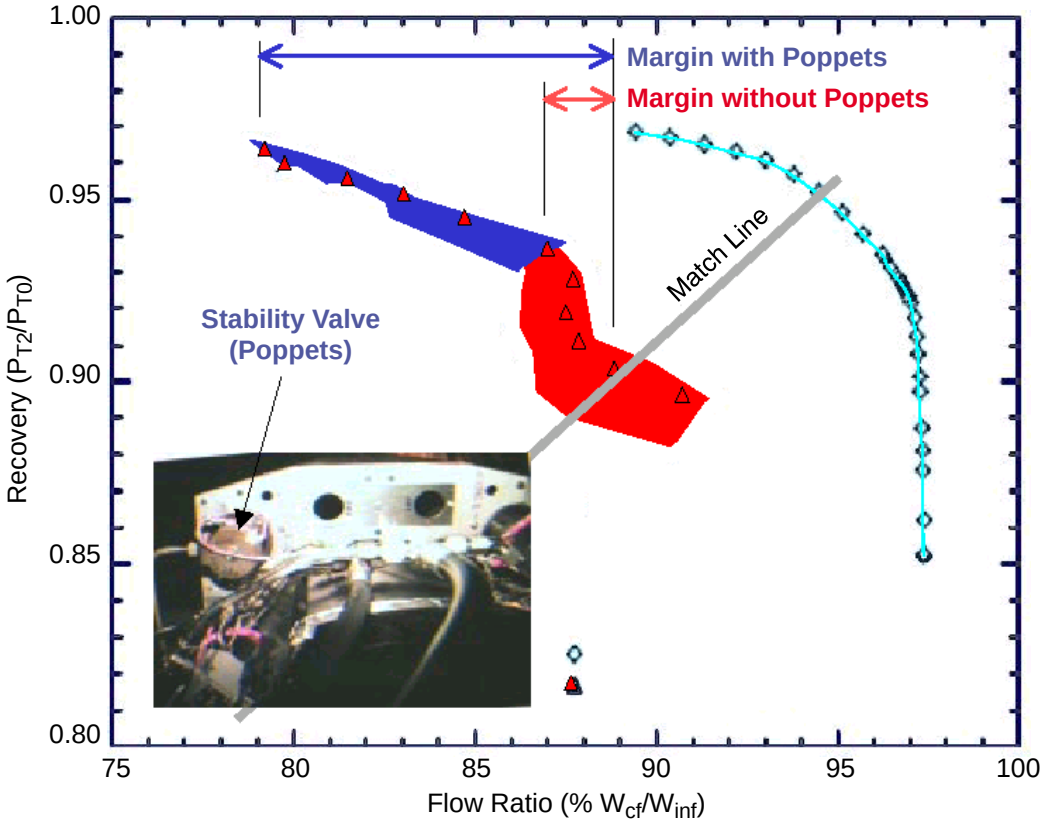

Figure 42. Stability Margins for Engine with and Without Poppet Valves

6.6 Controls Technology

6.6.1 Component Development

Shock Sensor – Two shock-sensing methods were evaluated, and development of a third method was partially started. The first method was an optical density gradient sensor using a linear-variable spectral filter. The second method was based on hot-film flow sensor technology. These two methods were compared with conventional pressure transducer approaches, of which there are several. The last method that began development was an optical/mechanical, laser-scanning, spatial filter. The linear-variable spectral filter approach was demonstrated in wind tunnel testing and successful-

ly incorporated in a simple, closed-loop, normal-shock control system. The hot-film system results were inconclusive, and loop closure was never preformed. The scanning spatial filter was demonstrated on the bench, but no opportunity was available to prove it further.

Pressure Transducers – Crane Eldec manufactures "silicon on sapphire" high-temperature (150°C) pressure transducers. These transducers were evaluated for application in the HSCT aircraft. The evaluation goal was to understand the implications of using high-temperature transducers in a "to be developed" *smart* transducers package capable of operation in the thermal environment of an inlet. It was concluded from wind tunnel model usage that the Eldec's and associated systems, with thermal compensation, nonlinear curve fitting and in a benign environment, exhibited a 0.1% full-scale output (FSO) tolerance. This tolerance is comparable to the 0.02% to 0.3% FSO exhibited by modern air-data systems in a controlled environment, while current technology for thermally compensated transducers operating up to 200°C is around 1.5% FSO. It was shown that to maintain the expected inlet operability and stability margins the control system requires 0.1% or better FSO tolerances.

Atmosphere – A common HSCT atmospheric model for gust loads and inlet unstart calculations was developed. This model used an eddy dissipation rate and allows unstart calculations to be preformed with (effectively) only one free parameter. With this model, inlet unstart margin control strategies and the effect of these strategies on inlet pressure recovery ratio were studied to see if inlet margins could be reduced between turbulent patches, as well as studying the unstart margin required to compensate for angular misalignment, flow distortions, and other airplane-installation effects.

Controller – Many approaches were studied to improve the atmospheric-disturbance rejection capabilities of the inlet controller. Using developed nonlinear (LAPIN), linear transfer function and state-space inlet models, various controllers ranging in approach from conventional *proportional plus integral* control to more advanced multiple input/multiple output (MIMO) and *fuzzy logic* control were compared and refined. Inlet modeling was also approached from the standpoint of providing system redundancy for fault detection and accommodation, as a means of reducing system required redundant sensors.

Stability Systems – A study was performed to develop a design database for mechanical bleed valve systems for supersonic cruise mixed-compression inlets. This database was founded on present and prior research studies on shock stability for mixed-compression inlets. The study included valve characteristics such as type (automatic or controlled), airflow characteristics, weight and envelope, time response, pressure characteristics, failure modes and detection, and reliability. The valves of interest were limited to chopper valves, poppet valves, butterfly valves, and external doors.

6.6.2 Simulations and Modeling

In support of the HSCT inlet control high-fidelity simulations, three-dimensional CFD proof-of-concept bleed hole modeling demonstrations were conducted using the WIND CFD code. The analyses computed the flow in and around a nine-bleed-hole surface and plenum in the presence of an incident shock. The computation provides better understanding of the underlying physics involved in shock/boundary-layer interaction with bleed. The computed solutions indicated recirculating regions in the 90° bleed hole as well as the plenum. The computation also showed that, under certain plenum geometry and flow conditions, blowing occurred from the bleed holes forward of the incident shock. All analyses used an inlet inflow profile to better simulate the in-flow conditions.

A preliminary plan for further development of a time-accurate bleed model using *design of experiments* was planned. The goal was to develop a state-of-the-art, time-accurate bleed model using table-look-up procedures that correctly and efficiently capture the underlying physics.

Recommendations were made to use a more detailed 3D geometry with finer and possibly adaptive mesh to capture flow details better and to improve the simulation accuracy of this complex, highly turbulent, 3D flow.

6.7 Inlet Engine Operability Technology Development

The work accomplished in this area was primarily dynamic inlet/engine modeling and engine stability audits. The purpose of the dynamic modeling was development of improved analytical tools in support of the high degree of inlet/engine integration required to achieve the HSCT design goal of no more than "one unstart per fleet per year." The engine stability audits supported this HSCT design goal through periodic tracking of engine cycle stability margin available relative to estimates of stability margin required. The latest inlet distortion-level windtunnel results were used in the stability-margin-required estimates.

6.7.1 Inlet/Engine Simulation and Modeling

This modeling effort was accomplished through coordination with the *Inlet Controls Team* and was based primarily on use of the LAPIN model. Results from inlet scale-model testing (6.5, page 29) and inlet controls results (6.6, page 37) enabled subsequent enhancements to the LAPIN model. The initial version of a mixed-compression-inlet/compressor transient simulation was operational by mid-1996, prior to scheduled CPC Program mixed-compression-inlet/engine testing. Consequently, earlier NASA data were used, involving an axisymmetric inlet and a J85 engine. Figure 43 is a typical comparison of the test data with model-simulation predictions. The transient tracks a surge induced in the J85 engine followed by surge recovery at a free-stream Mach number of 1.98. Inlet total pressure recovery at the AIP and compressor pressure ratio results are compared over the same 80-ms time interval. This early simulation is seen to model the initial inlet and compressor transients better than those in the latter part of the interval and also to predict less time required for surge recovery than indicated by the test data.

Figure 44 compares simulation results from the final version of the transient inlet/compressor model with CPC program data from 2DB inlet/J85 engine tests at Mach 2.35. The partially opened inlet bypass was rapidly closed, to induce engine surge, then fully opened. Initiation of inlet unstart lagged the initial bypass closure by nominally 50 ms. The subsequent initial compressor pressure ratio overpressure and the magnitude and frequency of the immediately following low-pressure transient predicted by the simulation appear to be in close agreement with the test measurements. Nominally 150 ms after the peak surge overpressure, the simulation damps out to the near-periodic pressure ratio frequency of the stalled compressor. Comparisons such as Figure 44 were considered to document validation of the transient inlet/compressor model.

6.7.2 Inlet/Engine Compatibility

Figure 45 illustrates the dynamic distortion limits for the inlet, used through most of the CPC program, derived from the indicated circumferential and radial total pressure distortion descriptors of Reference 6. The lower "cruise" levels ($DPC/P_{max} = 0.06$ and $DPR/P_{max} = 0.03$) apply throughout

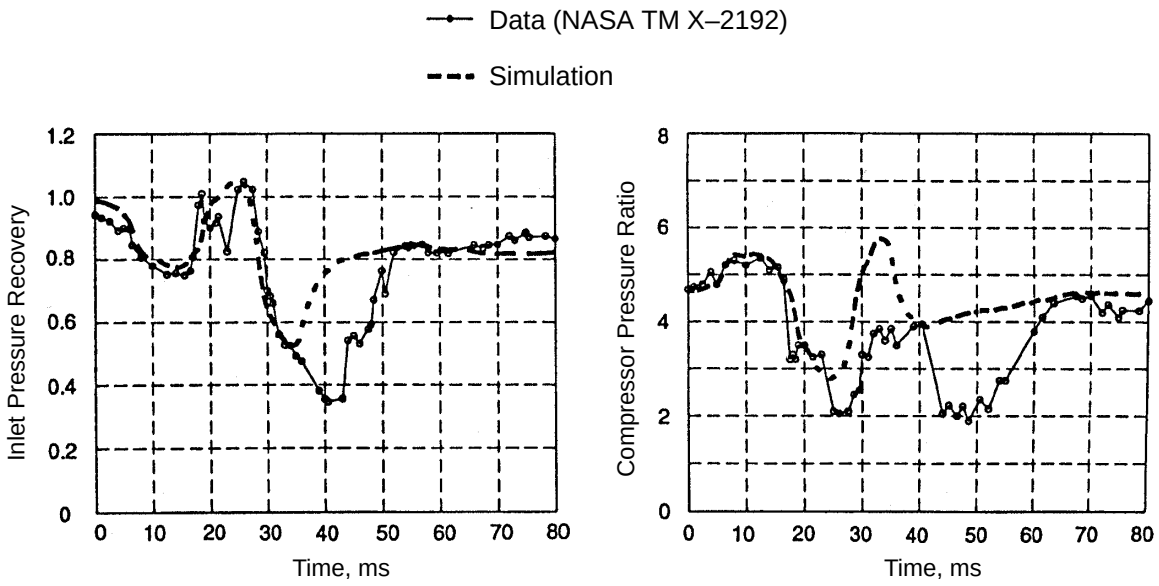

Figure 43. Mach 1.98 Surge with Recovery Simulation with Initial Version of TIC Model

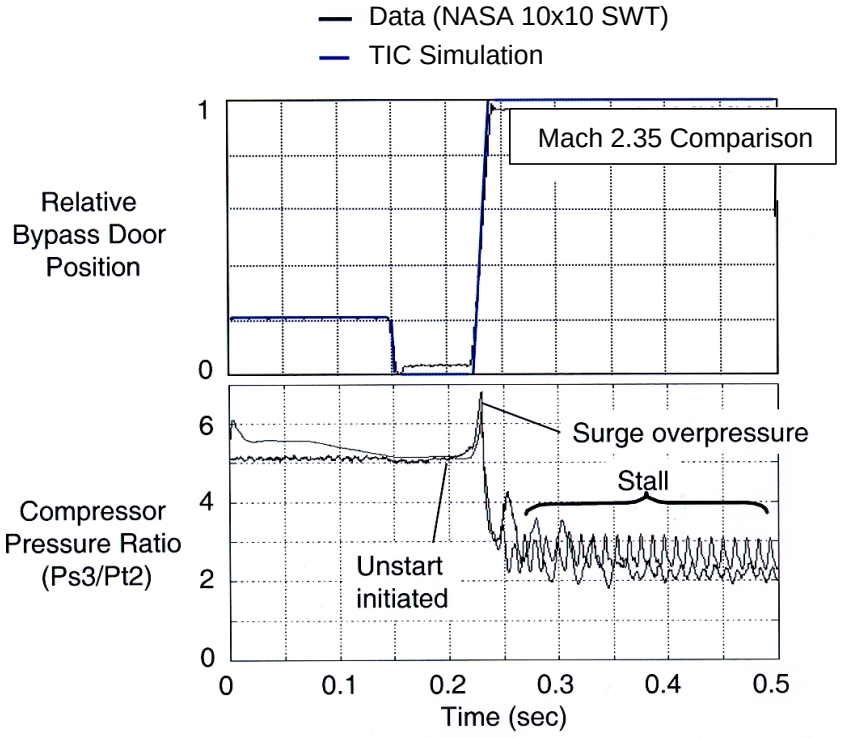

Figure 44. TIC Simulation of 2DB Inlet/J85 Engine Unstart/Surge

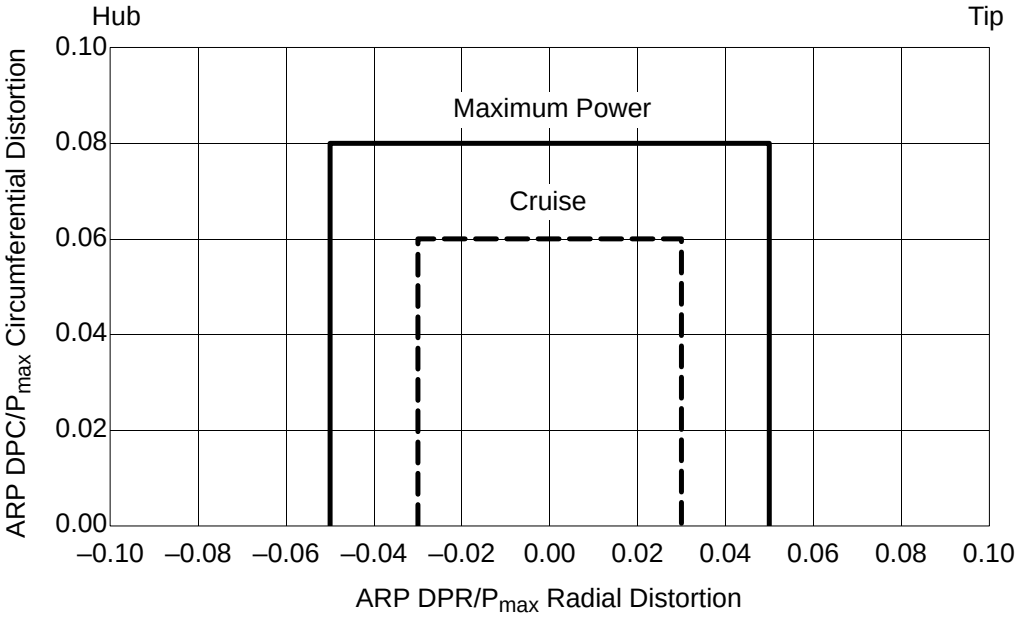

Figure 45. Recommended Dynamic Distortion Limits

the "static" box of Figure 12 (page 12) — ΔM as high as 0.05 and Δangle up to 2°. The higher "maximum power" levels apply throughout the "maneuver" box of Figure 12 (ΔM at least as high as 0.05 and Δangle at least as high as 4°). Thus, these higher levels include takeoff in crosswind conditions as well as aircraft maneuvers resulting in high interim values of angle of attack and yaw.

Figure 46 summarizes peak calculated levels of dynamic distortion based on measurements taken during 2DB inlet/J85 testing. (These levels were used in the engine stability audit.) The measured data were filtered at the cut-off frequency relevant to the model scale such that only pertinent data are used, and peak calculated values of DPC/P_{max} (solid symbols)and DPR/P_{max} (open symbols) are extracted from each record length. Such procedures assure that all reported peak values of dynamic distortion are of sufficient duration to be significant to engine operability. The supersonic cruise peak circumferential dynamic distortion levels of Figure 46 are within the corresponding limits of Figure 45, but the supersonic cruise peak radial distortion limits are exceeded.

Figure 47 illustrates the large number of items accounted for in an engine stability stack. On fan and compressor maps of component pressure ratio versus corrected flow, engine-induced "internal" items that tend to raise the nominal steady-state operating line are evaluated and "stacked" to establish the highest (worst case) operating line. In a similar manner, both engine-induced and externally induced items that tend to lower the engine nominal stability line are stacked down from it to establish a worst case (lowest value). The distance of the resulting lowest stability limit line above the highest resulting operating line then represents the "remaining margin." Thus, at a specific operating condition the engine stability margin available is defined by the difference in nominal stability limit and nominal steady-state operating line component pressure ratios. The corresponding engine stability margin required is then the margin available less the remaining margin.

Figures 48 and 49 summarize maximum power (PC50) fan and compressor stability audit results, accounting for all of the items in Figure 47 and using the 2DB inlet distortion levels of Figure 46. At all six operating conditions, both fan and compressor stability margins available are higher than

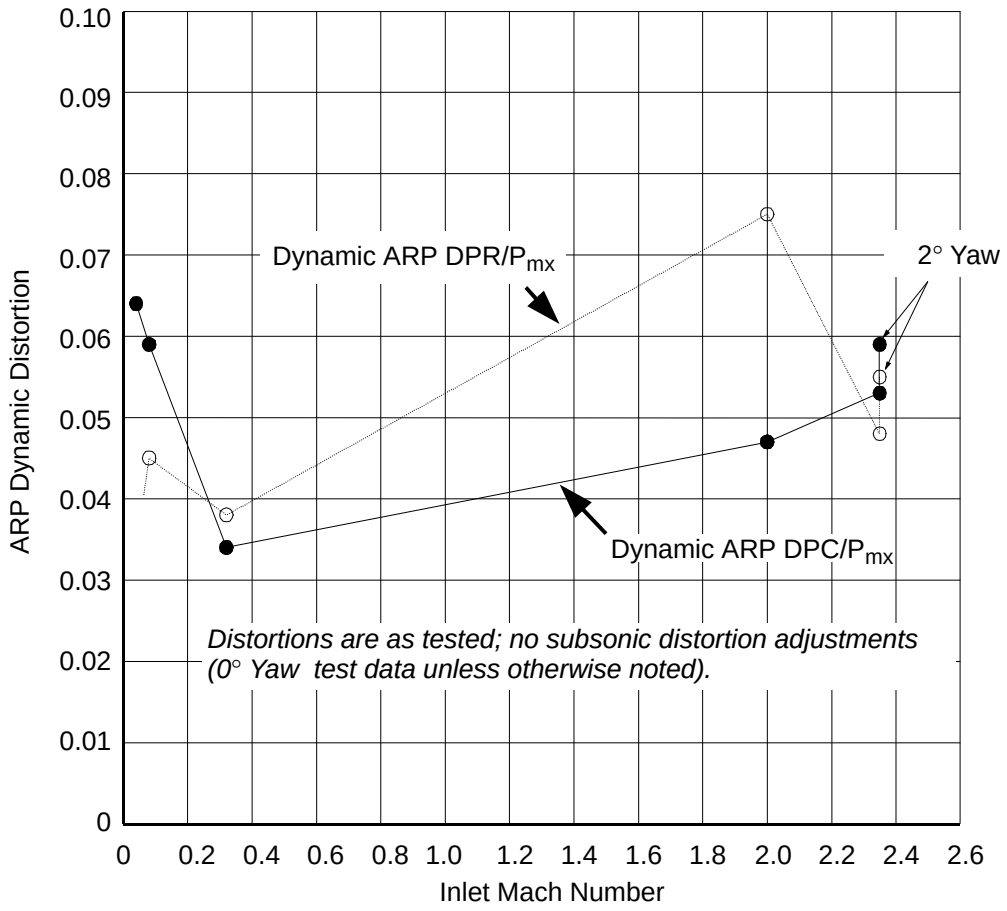

Figure 46. Dynamic Distortion Test Data for 2DB Inlet

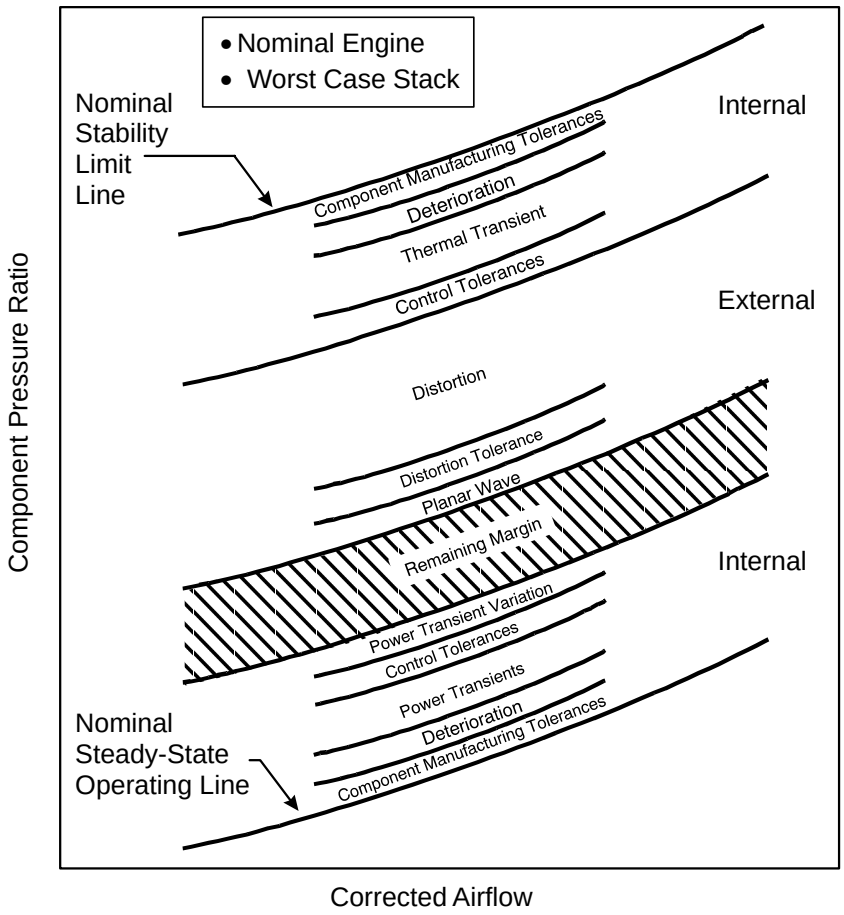

Figure 47. Stability Stack Schematic

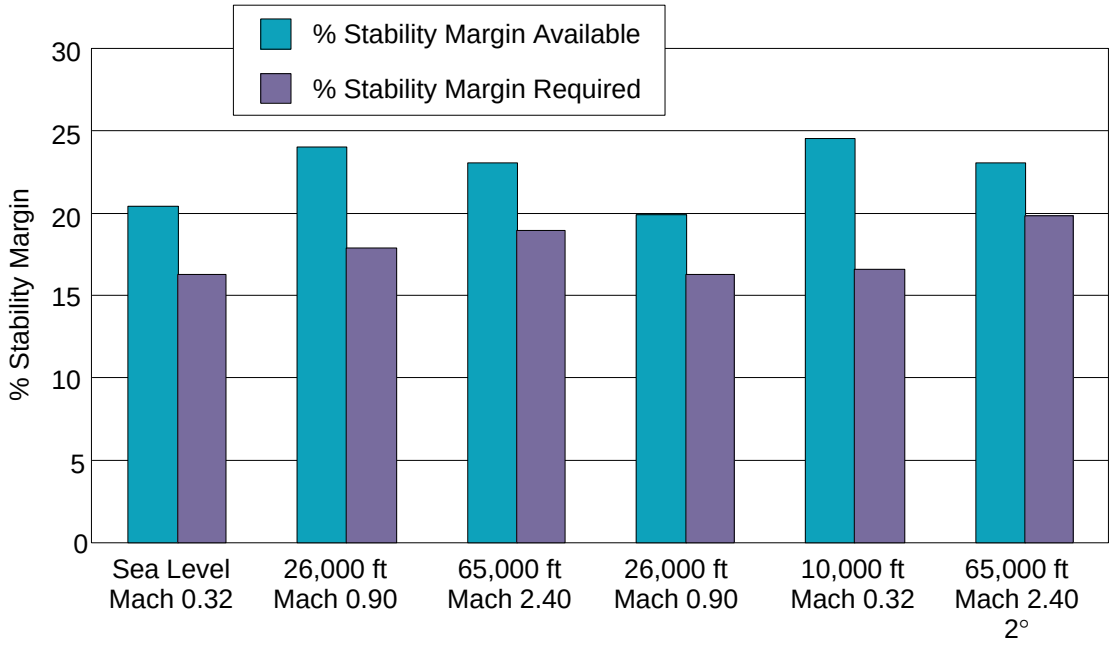

Figure 48. Stability Audit Results: PC50 Fan and 2DB Inlet

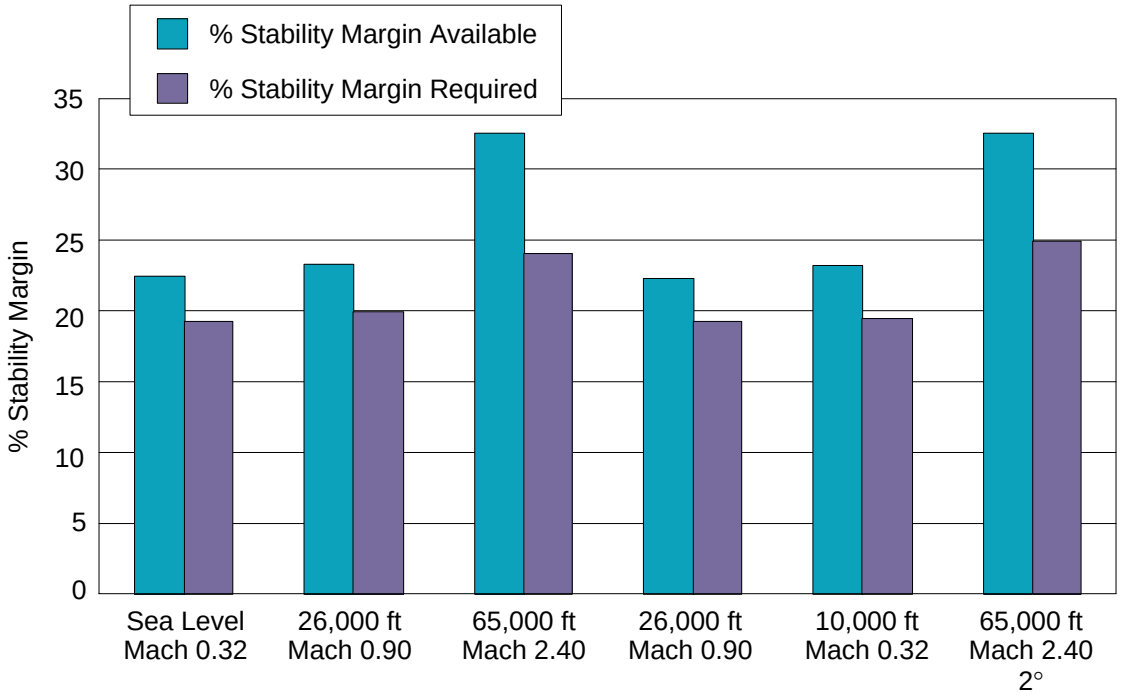

Figure 49. Stability Audit Results: PC50 Compressor and 2DB Inlet

the corresponding estimates of stability margins required. Thus at the assumed distortion sensitivities, even though the supersonic cruise 2DB inlet radial distortion levels of Figure 46 were in excess of the Figure 45 limits, the engine cycle is operating with enough stability margin available to provide positive values of remaining margin.

6.8 Subcomponent Experiments

In addition to the integrated inlet design and test programs, the CPC contract supported development of inlet technology and components. Experiments in four areas were directly supported: (1) microporous bleed experiments, normal-shock stability experiments, (3) subsonic-diffuser experiments, and (4) auxiliary inlet experiments. The results of these experimental studies may have more lasting value than the near-term focus of the rest of the inlet program.

6.8.1 Microporous Bleed

Microporous honeycomb composite materials offer two potential advantages over conventional perforated-solid-plate material when applied to bleed regions in a supersonic inlet. First, porous honeycomb composites (porous backing skin + honeycomb + porous backing skin) may provide sufficient stiffness to eliminate the need for the hole-blocking backing stiffeners that are normally required when using thin perforated-solid-plate material in bleed regions. Second, for a given porosity and bleed rate, microporous material may yield fuller boundary-layer profiles since flow removal is more uniform across a bleed region.

An experimental investigation to assess the performance of three microporous-bleed-region configurations was conducted to address the latter benefit. Flow coefficient and the boundary layer profile downstream of the bleed region were measured and compared to those of a baseline perforated-sol-

id-plate bleed configuration for free-stream Mach numbers of 1.27 and 1.98. The flow side of the baseline bleed plate (C1, hole diameter = 6.35 mm, porosity = 20%) and one of the microporous configurations (MP2, hole diameter = 0.368 mm, porosity = 21%) are shown in Figure 50.

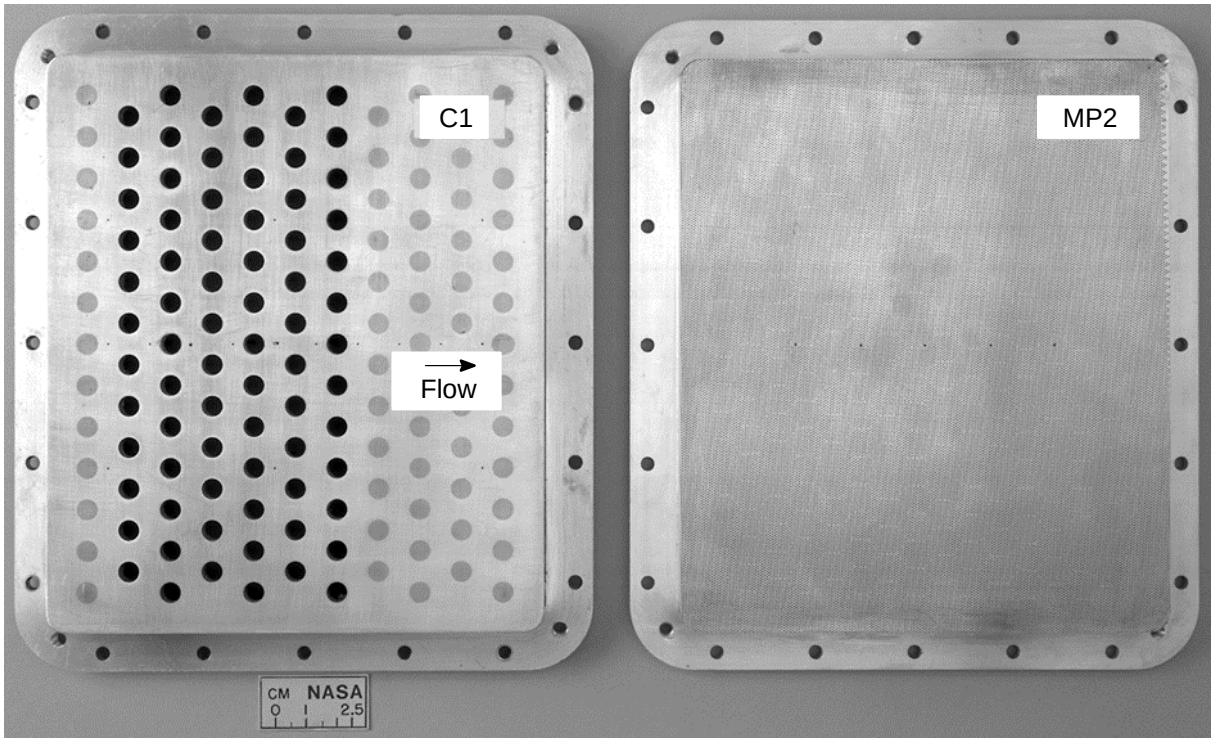

Figure 50. Baseline Bleed Plate (Left) and Microporous Configuration MP2

The investigation found that the microporous configurations exhibited flow coefficient behavior that was equal to or higher than the baseline configuration. Also, for a similar porosity and bleed mass flow rate, the microporous configuration yielded a fuller boundary-layer profile downstream of the bleed region than the baseline configuration, as shown in Figure 51. Further information may be found in AIAA Paper 97–3260.

6.8.2 Shock Stability

A subsonic diffuser test rig was designed, fabricated, and operated to emulate the subsonic diffuser located in the aft section of the bifurcated, two-dimensional, supersonic inlet. This rig is described in the following subsection (6.8.3). A terminal shock in the throat of the diffuser model was stabilized with the various techniques listed in Figure 52. The shaded regions in Figure 52 represent the recovery performance of the subsonic diffuser test model, each region corresponding to a different shock-stabilization technique or a variation in geometry of the diffuser model. The shock-stabilization techniques tested included bleed through normal holes or “standard plates,” bleed through microporous surface plates, and tangential blowing through slotted nozzle plates. In addition to testing a diffuser with a length-to-diameter (L/D) ratio of 3.0, a shorter model with L/D = 2.0 was also tested using standard plate.

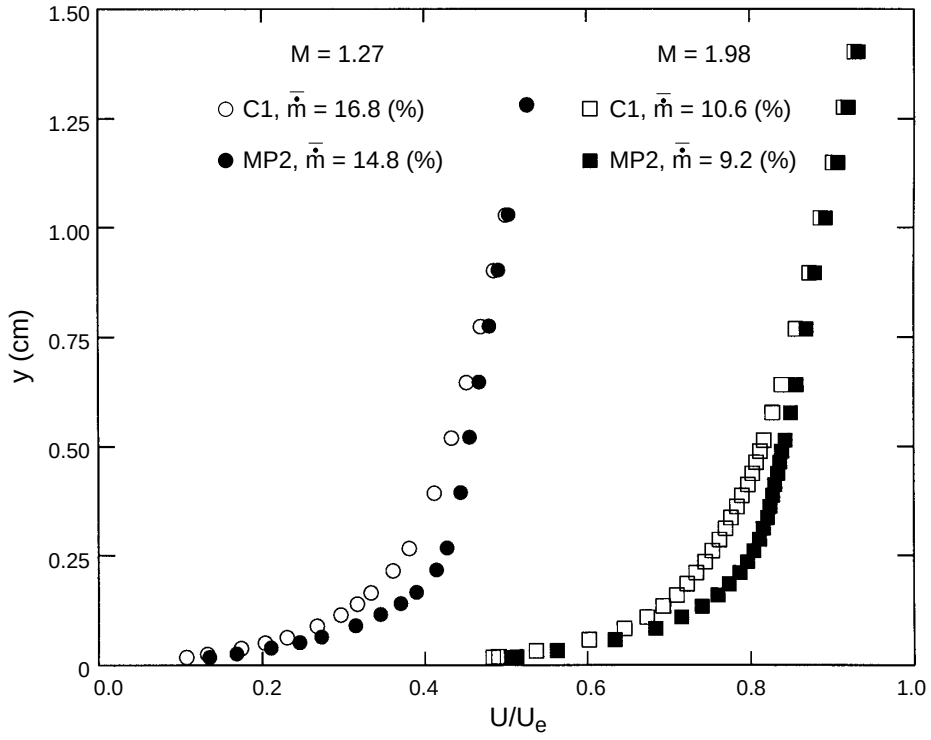

Figure 51. Boundary-Layer Profiles Downstream of Bleed Region

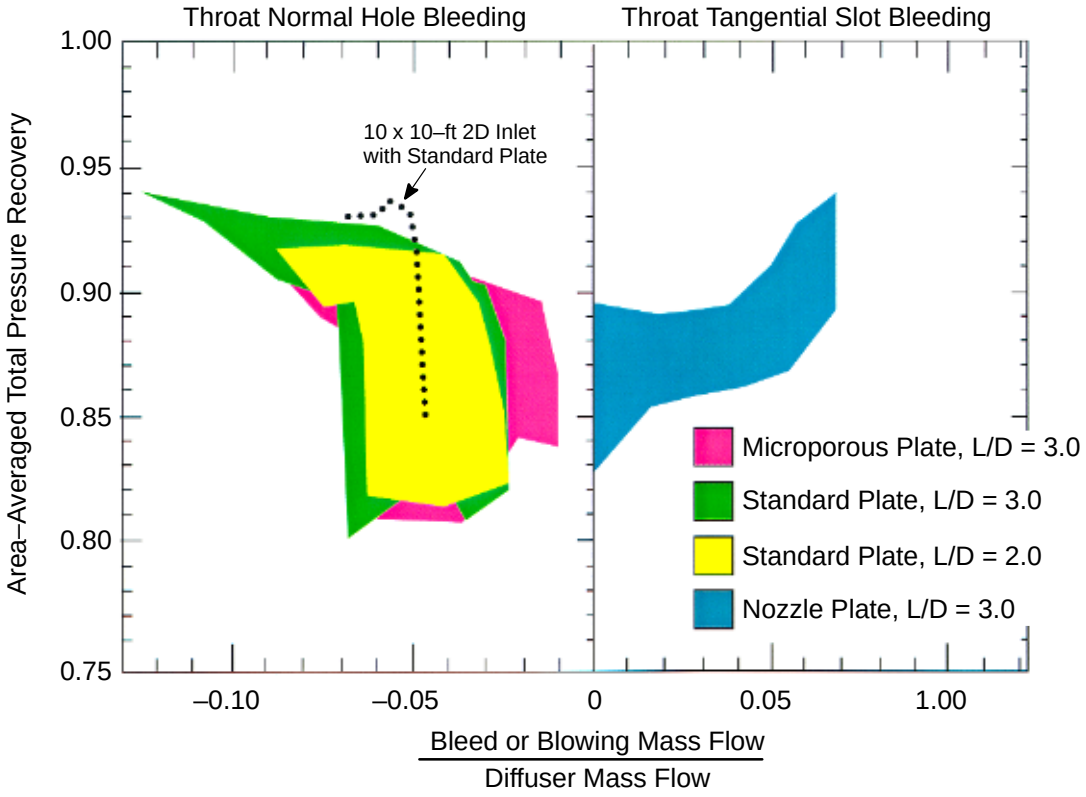

Figure 52. Effects of Shock-Stabilization Techniques

6.8.3 Subsonic Diffuser

Figure 53 illustrates the features built into the subsonic diffuser test rig (DTR) as installed in the NASA–Glenn W1B test cell. Downstream of the diffuser throat, the flow surface geometry is scaled precisely between the 2DB mixed-compression inlet and the subsonic diffuser model installed in the DTR. The DTR model is 62.2% scale with respect to the 2DB model or about 1/6 of full scale. A pair of two-dimensional converging/diverging nozzles induce supersonic inflow (at a Mach number of 1.3, a flow feature also occurring in the prototype inlet) into the throat of the model. Terminal shock stability issues are addressed with an elaborate seven-channel bleed system that can independently control bleed flow rates to the six sets of bleed surfaces in the model throat. The subsonic diffuser model may be detached near the throat, thus allowing installation of alternate diffuser candidates. Flow control features include three sets of surface-mounted vortex generators, louvers in the bypass cavity, and various bypass cavity surface treatments. Rake probes with unlimited cross-stream resolution can be installed in the engine face plane of the model. These rake probes include Pitot pressure probes and a similar five- and seven-hole set of directional probes. The rakes probes can be interchanged with a standard 72-port Pitot rake for performance data.

Figure 54 is an example of the results obtained using the DTR. In Figure 54, plots of total pressure ratio define the diffuser performance in terms of total pressure recovery and total pressure distortion. Improvements achieved by using flow control (such as vortex generators) can be quantified and studied before costly trials are attempted in the 2DB integrated inlet system. The more extensive data sets acquirable in the DTR are useful in validating corresponding computational design studies, thus allowing improvements in the capabilities of computational diffuser design codes.

Figures 55 and 56 further illustrate the correspondence between test results achieved in the mixed-compression 2DB inlet system and the DTR. The plots in Figure 55 compare total pressure recovery versus engine mass flow ratio between the two models, and Figure 56 compares total pressure results at the engine face. The DTR test model simulates the results obtained in the integrated mixed-compression 2DB inlet (as tested in the 10×10-ft SWT) to within 30% for all significant steady-state performance descriptors. These results are obtained in the DTR at approximately 4% of the operating test cost required by the SWT testing of the 2DB inlet system. However, facility modification and model design and fabrication costs are similar between the SWT and DTR tests, so the overall cost reduction of the DTR tests may be 20% to 50%. Thus the DTR allows testing and development of the subsonic diffuser independent of the full 2DB inlet system, at a reduced cost, with higher resolution flowfield measurements. Care must be exerted in designing the experimental hardware to ensure a realistic simulation.

6.8.4 Auxiliary Inlet

Providing adequate airflow to the engine at off-design conditions, with acceptable distortion and pressure recovery, is a key requirement for the inlet of a HSCT propulsion system. Mission analyses of the HSCT propulsion system indicated that an auxiliary inlet system would be required to augment the primary inlet system during off-design operation. An experimental program was planned to test and evaluate auxiliary inlet concept configurations using an existing inlet model as a test-bed. The initial test-bed selected was the VDC inlet model. The planned test facility was the 10×10-ft SWT at NASA–Glenn. The VDC was selected based on low-speed flow capacity and the existing bypass configuration. The 10×10-ft SWT was selected based on facility capability; however, modifications were needed to enable adequate flow through the model. Seventeen auxiliary

Subsonic Diffuser – Test Facility Features

- Rake probes mounted in the diffuser exit plane (engine face plane) provide recovery and distortion performance of the subsonic diffuser.
- Vortex generators are mounted in various configurations on the diffuser flow surfaces to enhance performance.
- Diffuser throat bleed surfaces and bypass air cavities are modeled with an elaborate, 7-channel bleed system to study terminal shock stability and boundary layer control and blockage issues.
- The subsonic diffuser model is interchangeable with a shorter version to study the effects of reducing axial length.

The HSR Bifurcated Inlet

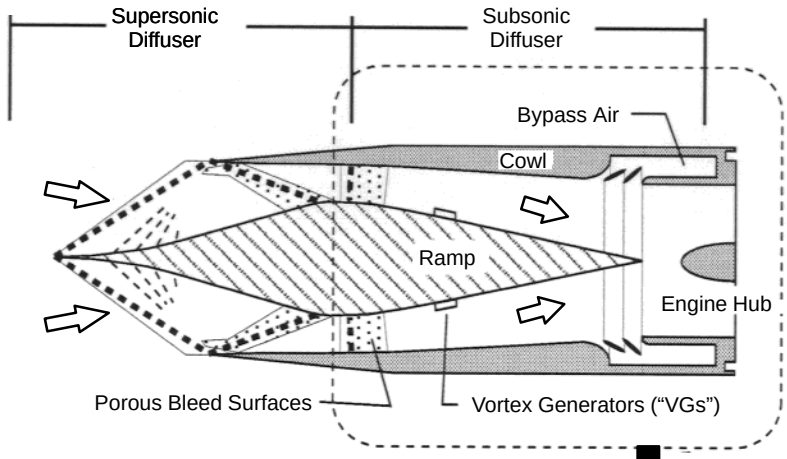

W1B Test Section

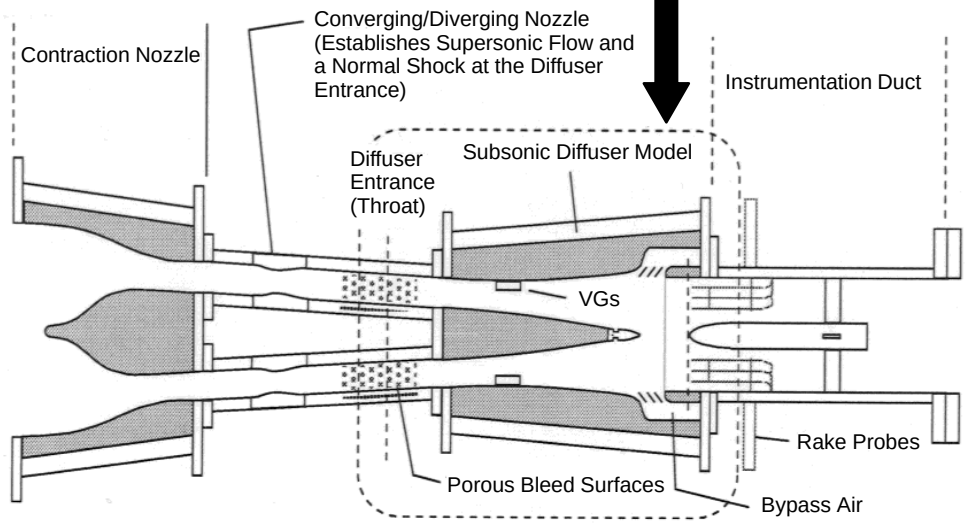

Figure 53. Subsonic Diffuser Technology Development

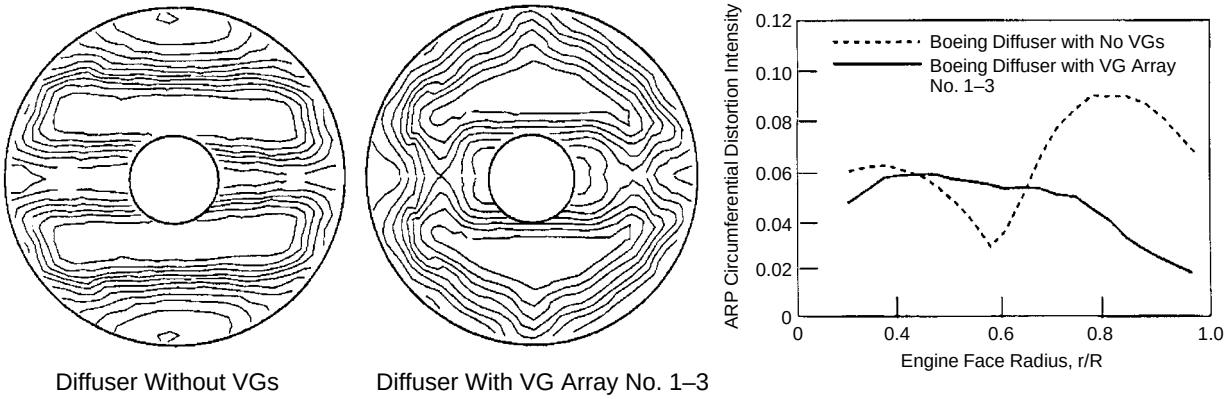

Diffuser Without VGs
Pressure Recovery = 0.918

Diffuser With VG Array No. 1–3
Pressure Recovery = 0.925

Distortion Performance

- Subsonic diffuser flow features are tested ahead of the integrated inlet system to identify and address potential flow problem areas.
- By controlling boundary layer thickness and flow separation, VG's improve diffuser recovery and distortion performance, allowing consideration of shorter designs.
- Extensive parametric testing develops VG configurations for use in larger scale testing, saving valuable test time.
- Data are used to validate corresponding computational codes to improve and expand design capabilities.

Figure 54. Total Pressure Contours at Engine Face and Total Pressure Distortion Performance

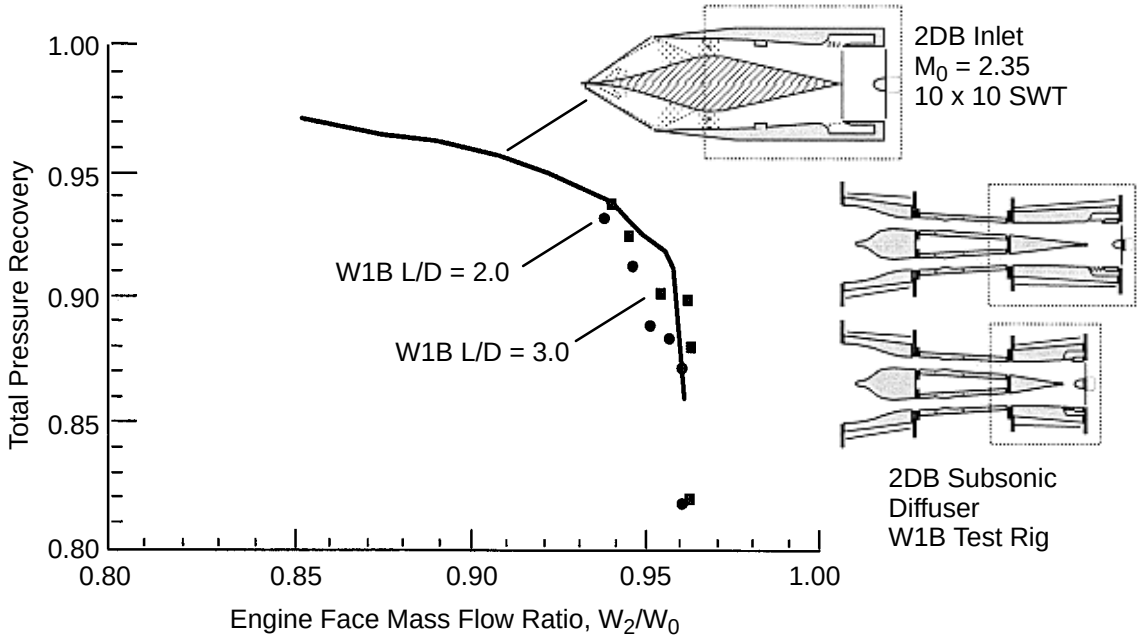

Figure 55. Subsonic Rig Test Results: Varying L/D

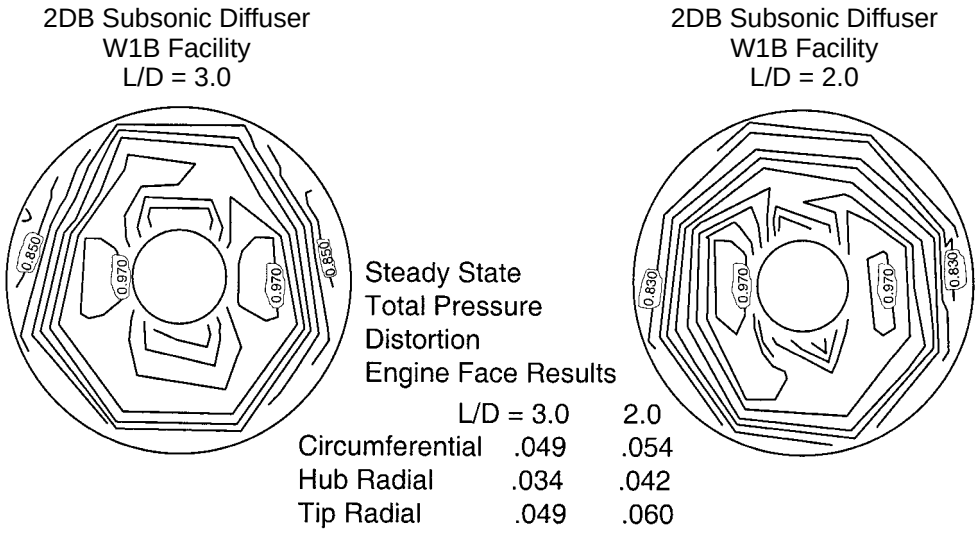

Figure 56. Subsonic Rig Test Results: Effect on Distortion of Reducing L/D *Total pressure distortion per Aerospace Recommended Practice 1420.*

inlet configuration concepts were considered through a brainstorming and evaluation process. The concepts were evaluated on the basis of complexity, performance, acoustics, controls, cost, and realism. Project plans were to evaluate up to three different configurations by designing interchangeable hardware to integrate with the test-bed inlet.

Due to cost and schedule constraints in the HSR program, a decision was made to combine the auxiliary inlet test program with the fan inlet acoustics test (FIAT). This fan inlet acoustic test was to be conducted in the 9×15-ft low-speed wind tunnel at NASA–Glenn. Provisions were incorporated into the FIAT model design to accommodate interchangeable auxiliary inlet configurations as well as the baseline auxiliary inlet/bypass configuration. The baseline configuration and the leading alternate configurations were all variations of shared-cavity designs. The design approach employs a shared cavity within the inlet, near the fan face, that provides both auxiliary inlet flow and bypass flow capability. The function of the configuration for both requirements is accomplished by incorporation of moveable doors or louvers to direct flow through the cavity. As plans for the combined test effort were formed, an alternate approach to providing auxiliary flow capacity to the engine was identified. This approach separated the function of the auxiliary and bypass systems, thus reducing the complexity inherent with a shared-cavity configuration. The alternate approach provided auxiliary flow capability by using rotating or variable cowl lips to increase the effective mass flow rate of the inlet and reduce flow separation (Figure 29, page 26).

A test was conducted to evaluate the effectiveness of variable cowl lips at increasing the mass flow rate (and pressure recovery) and reducing flow distortion of the 2D bifurcated inlet at static conditions. Figure 57 shows the 60° cowl lip installed on the 2DB inlet. Tests were conducted with and without a flat trapezoidal plate mounted near the inlet top side, simulating an under-wing aircraft installation and with cowl lips in the baseline (0°) and rotated (30°, 45°, and 60°) positions. Oil-flow studies were conducted to qualitatively examine flow structure associated with sharp leading-edge

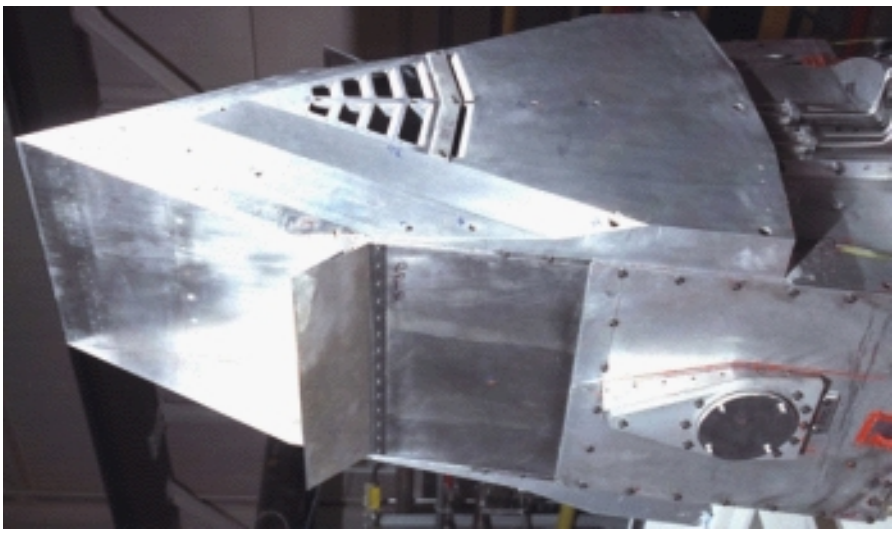

Figure 57. Photo of 2DB Inlet with Variable Cowl Lips Installed

cowl lips. Preliminary analysis of qualitative data indicates symmetric and nonseparated flow with rotated cowl lips installed. Quantitative data indicates as much as a five-count gain in pressure recovery over the baseline inlet configuration. Flow inside the inlet was very unsteady and dynamic; mass flow rate, steady-state pressure recovery, and distortion levels fluctuated significantly. Figure 58 compares the ring circumference radial distortion plots of the baseline and 60° cowl lip configurations. Both measurements were taken at maximum flow conditions. The data indicate that the distortion with the 60° cowl lips falls within allowable engine limits.

6.9 Full-Scale Design

Unlike most other propulsion system component areas, the CPC program initially had no full-scale inlet design activity. Replan work in 1995 added such effort in support of the mid-1997 inlet downselect confirmation milestone and provided full-scale designs for the TCB, VDC, and 2DB inlets. Consistent leakage airflow, weight, manufacturing-cost, and maintenance-cost estimates were part of this effort. In addition, based on the full-scale VDC inlet design, critical component hardware was designed, fabricated, and tested for structural integrity.

6.9.1 Inlet Evaluations

The full-scale TCB, VDC, and 2DB inlets were designed to the same groundrules. Highlights of the mechanical-design groundrules were:

- Sizing
  - Design Mach = 2.35
  - Maximum Airflow = 800 lbm/s (3770 Cycle)
- Control System
  - 1-Second Full Stroke
- Structures
  - Ultimate Load ΔP = 38.2-psi Hammer Shock with 1.5 Safety Factor
  - Limit Loads with Safety Factor = 2.66
  - Vertical Inertial Load = 6.2 G's Down; 3.4 G's Up
  - Side Inertial Load = ±2.8 G's
  - Material: Ti 64

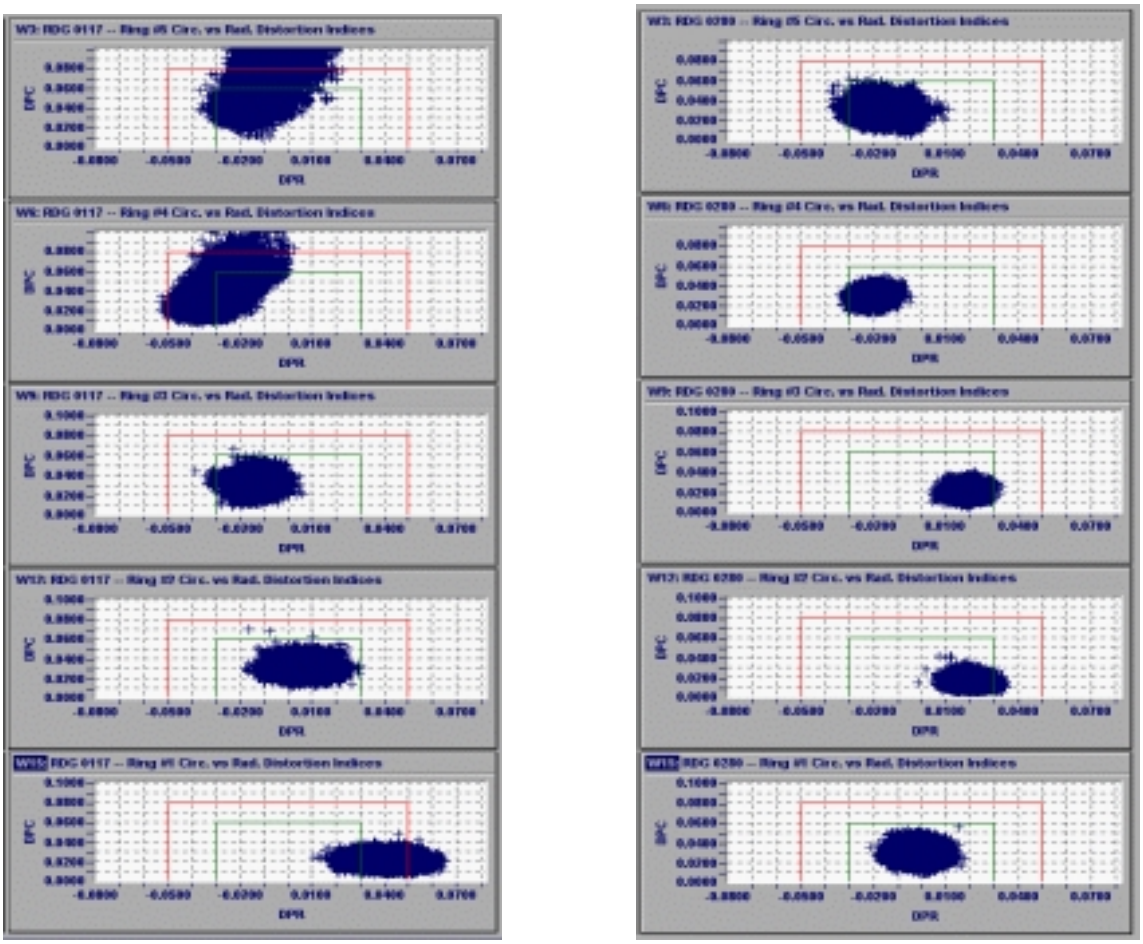

Baseline Cowl Lip (0°) Variable Cowl Lip (60°)

Figure 58. Comparison of Dynamic Distortion Data

All three full-scale inlet designs were sized for a supercruise local inlet Mach number of 2.35 (corresponding to an aircraft flight M = 2.4) to accommodate the flow lapse rate from 800-lbm/s maximum airflow at takeoff of the 3770 mixed-flow turbofan cycle. Full-stroke actuation (max/min "throat" area change) was specified at 1 second. Design loads considered inertial and aerodynamic inputs at eight points in the flight envelope, including hammer-shock conditions resulting from inlet unstart and engine surge. Structural analyses for all three inlet concepts included inlet-to-wing interface loads, maximum bending stress, deflections and natural frequencies, and bulkhead load. Unique for the TCB inlet were roller loads and bearing stress, for the VDC inlet were diffuser leaf analysis and link loads, and for the 2DB inlet were diffuser ramp analysis and link/hinge loads.

Figure 59 summarizes the initial length (L) to engine diameter (De) results and the initial weights for each of the three inlet concepts. The 2DB inlet was significantly longer than the two axisymmetric inlets, and the VDC inlet had significantly lower weight. These lengths (and thus, to some extent, also these weights) were set from flowpath considerations driven primarily by the aerodynamic performance metrics (pressure recovery, bleed, and distortion) of Subsection 6.1.3 (page 3). Acoustic-suppression panels were installed where internal surface area was available for, and

Two-Dimensional Bifurcated (2DB)

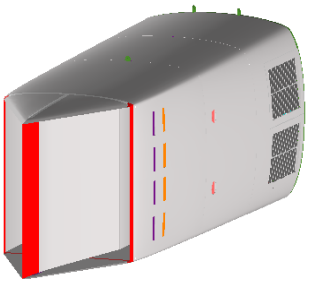

Costs in 1999 $

Initial Design	
L/De	Weight, lbm
2.9	3880

Redesign			
L/De	Weight, lbm	Manufacturing Cost at100th Unit	Maintenance Cost ($/FH)
2.93	4070	$1.42M	21

Variable-Diameter Centerbody (VDC)

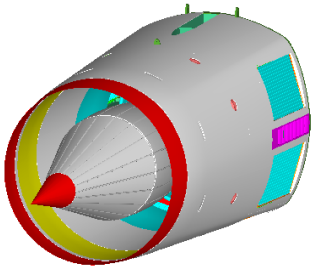

Initial Design	
L/De	Weight, lbm
2.1	3840

Redesign			
L/De	Weight, lbm	Manufacturing Cost at100th Unit	Maintenance Cost ($/FH)
3.15	5520	$1.99M	212

Translating Centerbody (TCB)

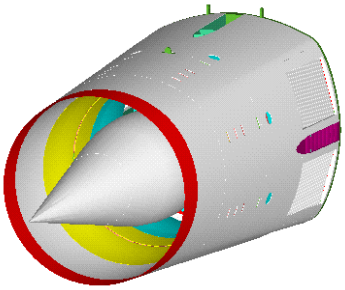

Initial Design	
L/De	Weight, lbm
2.3	3310

Redesign			
L/De	Weight, lbm	Manufacturing Cost at100th Unit	Maintenance Cost ($/FH)
2.95	4270	$1.28M	47

Figure 59. Full-Scale Inlet Initial Designs and Redesigns for Same-Approach Noise Suppression
Significant differences in not achieving approach-noise goals with each initial design.

amenable to, allocation. Subsequent approach noise estimates by FIAT indicated none of the three inlet concepts met the noise reduction goal; each missing it by a different amount. FIAT was then requested to estimate the increase in surface area required for each inlet concept to be within 3 ΔEPNL of the approach noise suppression goal (remaining 3 ΔEPNL reduction to be achieved later from the *Low-Noise Fan* program). Based on these FIAT estimates of additional surface area required for each of the three inlet concepts, the full-scale designs for each were revised accordingly.

Figure 59 lists the length and weight differences for the three inlet concepts after each was redesigned to accommodate the required additional acoustic panel treatment. The lengths of the two axisymmetric inlets increased to nominally that of the 2DB inlet, and the VDC inlet, instead of remaining the lightest, became the heaviest concept by substantial poundage. Manufacturing and maintenance cost estimates are also listed in Figure 59. Major drivers in the manufacturing cost results were parts count and weight. The VDC inlet was not only the heaviest, it also had the highest parts count; the latter driven primarily by the actuators, linkage subassemblies, and leaf sections required to accomplish centerbody diameter change. Similar considerations drove the maintenance cost results, in addition to accessibility. On the 2DB inlet, appropriately located panels provide relatively quick access to most actuation, seals, etc. Access to internal centerbody components requires centerbody removal for the TCB and VDC inlets. The need for accessibility was estimated to occur at smaller intervals between flight hours for the higher parts count VDC inlet centerbody.

6.9.2 Inlet Component Testing

The complex and unproven VDC inlet actuation mechanism was a major concern. To determine if such a variable-geometry (VG) was practical for HSCT application, tests of the mechanism were conducted at simulated flight conditions. A 60% scale flight type structure of the aft variable-diameter centerbody leaf assembly was designed and fabricated. A heated and pressurized test chamber was designed and fabricated at NASA–Dryden to simulate the defined HSCT flight-type duty cycle environment. Instrumentation enabled evaluation of seal integrity, seal wear, concentricity, and diameter positioning throughout the scheduled cycles of aft centerbody leaf assembly diameter change. A life requirement of 15,700 cycles was established; failure occurred early in the testing at only 784 cycles. Figure 60 sums up this effort and the results.

The indicated two leaf trunnions that failed were test rig components and not part of the flight-type hardware. The occurrence of such a failure so early in the cyclic testing, however, was interpreted as an indication of the potential “unknown unknowns” associated with this rather unorthodox and relatively complex mechanical design. Consequently, it was concluded that the development cost of the VDC inlet was beyond HSR scope, and this effort was promptly terminated.

6.10 Unstart PAI Test

6.10.1 Test Configuration and Installation

For an under-wing supersonic propulsion system pod installation, adverse transient phenomena (such as engine compressor stall and inlet unstart with subsequent shock wave/boundary layer interactions and flow field degradation) are important parameters to investigate before beginning a realistic propulsion airframe integration effort. The purpose of the inlet unstart propulsion/airframe integration (PAI) test program was to acquire transient aerodynamic data in the vicinity of a representative HSCT propulsion system during an engine stall and inlet unstart sequence. Informa-

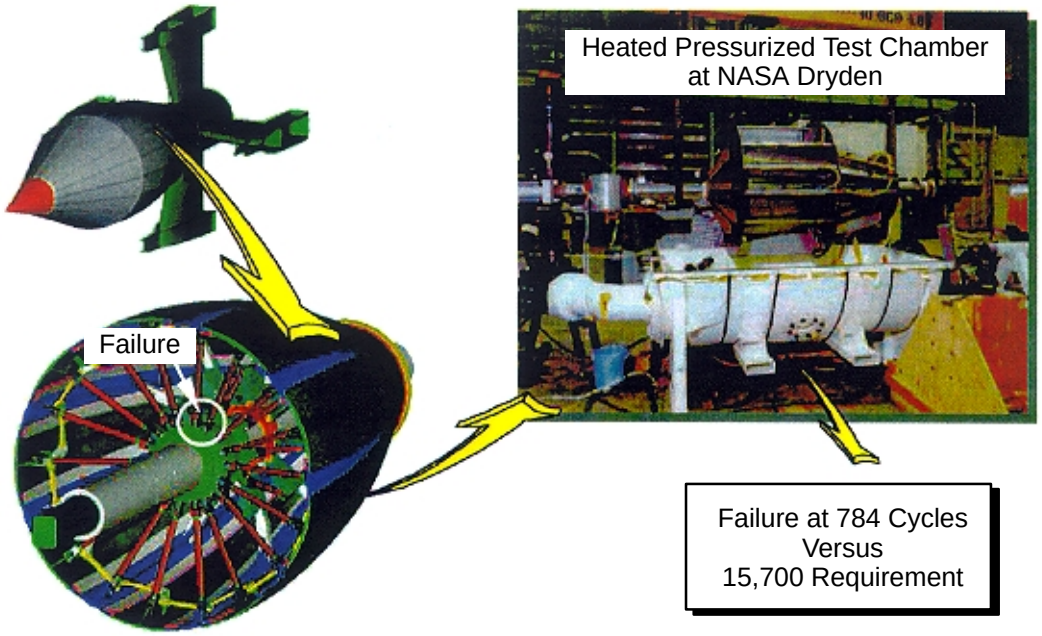

Figure 60. VDC Inlet Component Durability Test

tion such as transient pressure wing loading and extent of flowfield influence due to a propulsion system unstart is important in determining parameters such as the minimum lateral separation between adjacent propulsion systems.

The unstart PAI test program objective was to assess the under-wing flow field of a HSCT propulsion system during an engine stall and subsequent inlet unstart. The program approach was to conduct experimental research testing in the NASA–Glenn 10×10-ft SWT (Figure 61). The test configurations include a representative propulsion pod consisting of the 25% scale HSCT 2DB inlet mated to a GEAE J85–13 turbojet. The propulsion pod is mounted below a large flat plate that acts as a wing simulator. The plate has nominal dimensions of 10-ft wide by 18-ft long; the length allows realistic, thick, boundary layers to form at the inlet plane. Transient instrumentation is used to document the aerodynamic flowfield conditions during an unstart sequence. Flow surface information is acquired via static pressure taps installed in the wing simulator, and intrusive pressure probes are used to acquire flowfield information. These data are extensively analyzed to determine the impact of the unstart transient on the surrounding flow field.

The wing simulator is instrumented with an array of 143 static pressure taps arranged in a nominal 5×5-inch grid. These taps are designed to be interchangeable with steady-state or dynamic pressure measurement devices. Typically, 40 static pressure taps are configured to acquire dynamic pressure measurements.

Attached to the wing simulator are a pair of instrumentation struts that contain the flow field pressure measurement instrumentation. These struts have 22 ports spaced 2.5 inches apart in the Z direction. Depending on the test run objective, each strut port could be configured with a dynamic pitot, static, or flow-angularity pressure probe. The strut configuration shown in Figure 61 is set up for flowfield Mach number measurements. Alternating pitot and static probes are spaced 5 inches apart with a dummy probe between at the 2.5-inch location. This spacing is necessary due to mutual interference

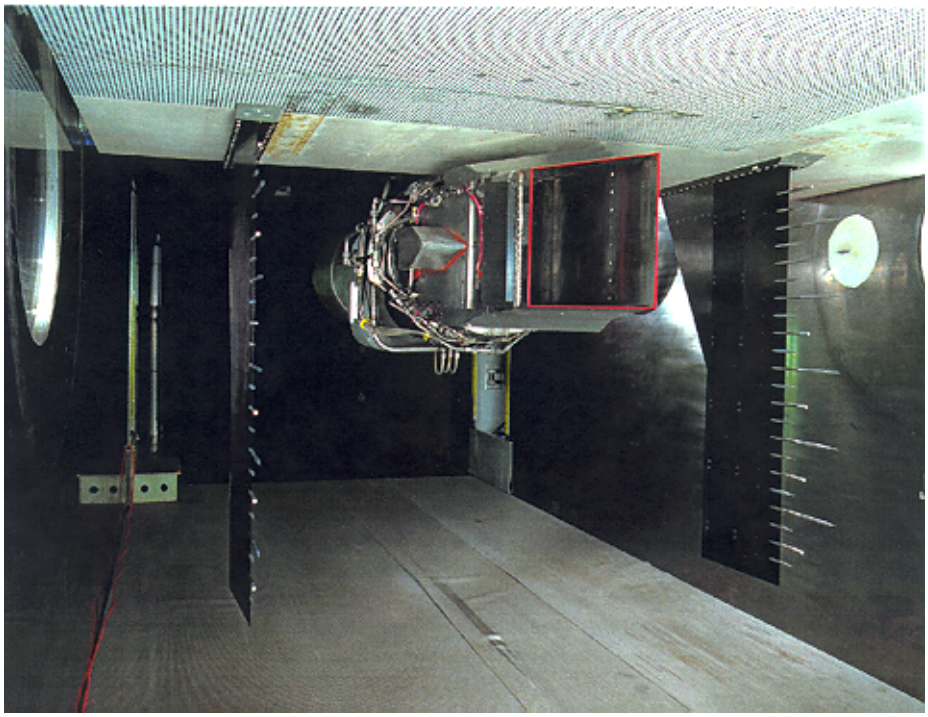

Figure 61. Wind Tunnel Model and Instrumentation Installation

effects of the long static pressure probes. The instrumentation struts are placed at five separate axial and spanwise locations relative to the model centerline to characterize the extent of the flowfield influenced by the unstart events.

6.10.2 Test Results

The data presented in this section are for the case when the engine experiences a compressor stall and subsequent inlet unstart that expels a high-pressure disturbance, called a hammer shock, into the surrounding propulsion system flowfield. The inlet and engine are running at design conditions: free-stream Mach number (M_o) = 2.35, 40 tube inlet recovery (Rec40) = 0.924, corrected engine speed (N_c) = 92%.

The compressor stall is induced by slowly closing the variable exit nozzle (VEN) of the turbojet while holding the corrected engine speed constant. Shock control is maintained during this event, which keeps the inlet recovery constant. The VEN closure at constant N_c causes the compressor pressure ratio to increase along a constant speed line until stall occurs. A dynamic ΔP transducer senses stall in the compressor and triggers a 4-second recording trace of dynamic data centered about the stall event. For all data presented in this report, the wing simulator boundary layer thickness at the inlet axial plane is $\delta/L_c = 0.238$, where $L_c = 16$ inch. The inlet ramp tip is positioned just beneath the wing simulator boundary layer, $Z_r/L_c = 0.265$.

Figure 62 shows typical flowfield measurements obtained during an unstart sequence. In this case, the instrumentation struts are configured to acquire pitot pressure measurements during a VEN stall and inlet unstart sequence. This configuration is optimum for determining how far the transient disturbance propagates at a specific axial and spanwise location in the flowfield. In this particular

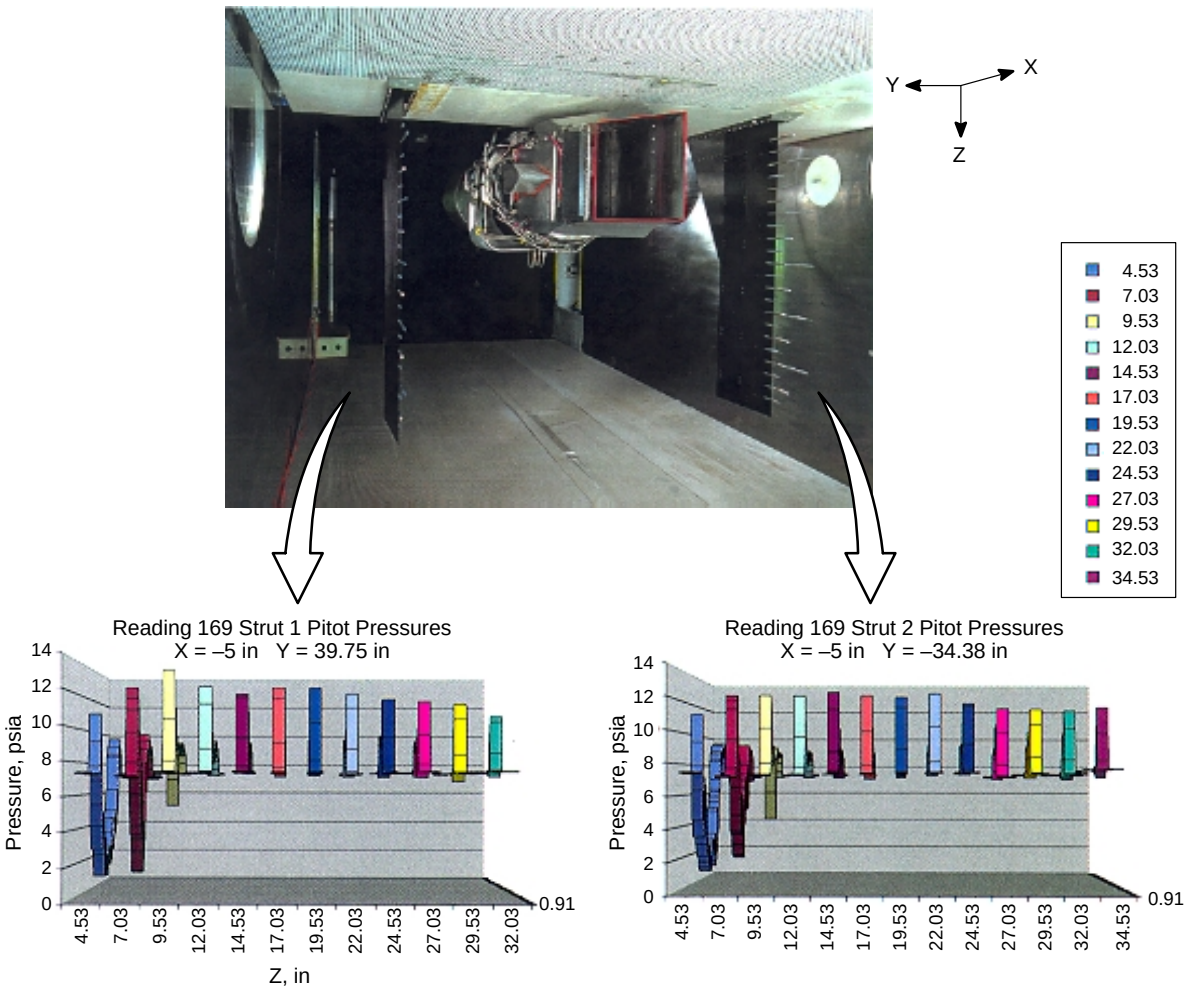

Figure 62. Typical Spanwise Variation in Hammer-Shock Propagation

case, the instrumentation struts are located at two spanwise locations, Y = 39.75 and –34.38 inch, about the model and wind tunnel spanwise centerline. Both struts are at the X = –5 inch axial measurement plane. The inlet cowl leading edge is located at the X = 0 axial station.

The three-dimensional perspective view plots in Figure 62 show the individual pitot pressure time histories during a specific VEN stall unstart sequence. For the starboard strut (Y = 39.75 in), the flowfield pressure disturbance (hammer shock) propagates 32 inches below the wing simulator, while the flowfield pressure disturbance propagates downward 34.5 inches below the wing simulator at the port strut (Y = –34.38 in) measurement plane. For reference, the characteristic height of the inlet, L_c, is 16 inches and is located 4.24 inches below the wing simulator surface.

Figure 63 shows the observed maximum extent of hammer-shock disturbance propagation below the wing simulator surface for multiple VEN stall/inlet unstart sequences. Pitot pressure data similar to those presented in the Figure 62 are used to determine the maximum extent of disturbance propagation. Data are presented at two spanwise locations and three axial locations. The coordinates are nondimensionalized by the inlet characteristic height, L_c = 16 inch. The inlet cowl lip axial station is located at $X/L_c = 0$. Limited spanwise data acquired at the $X/L_c = –0.3125$ axial location

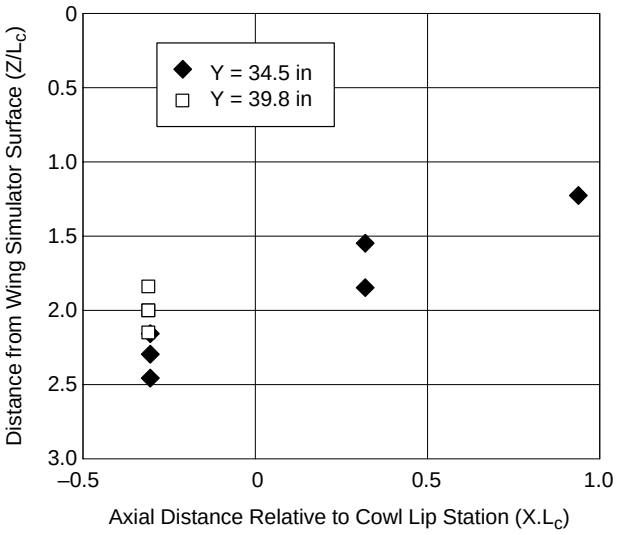

Figure 63. Observed Extent of Hammer-Shock Disturbance Propagation

indicate that the observed extent of disturbance propagation is greater at the spanwise station closest to the model centerline. Axial disturbance propagation information at the Y = 34.5 inch location indicate that maximum propagation below the wing simulator occurs at the axial measurement plane behind the cowl lip and progressively decreases as the disturbance moves upstream.

The two plots in Figure 64 show flowfield pitot pressure time-history traces during a VEN stall and inlet unstart sequence. The left-side plot shows the pitot pressure distributions at selected distances below the wing simulator during the same VEN stall/unstart sequence. Notice the pressure time history trace at $Z/L_C = 0.28$, which is just above the wing simulator boundary layer. The rapid drop in pitot pressure is an indication of flow separation on the wing-simulator surface. This evidence of flow separation at this Z location is seen at all flowfield measurement stations during this test.

Inspection of all the Z-direction pitot pressure time-history traces indicates that the hammer-shock disturbance propagates outward in the flowfield at the beginning of the unstart event. This is shown by the progressive time delay of the onset of pitot pressure increase for each successive Z pressure measurement station. At the end of the unstart event, there is evidence of a distinct disturbance propagating inward towards the wing-simulator surface. The last measurement port affected by the

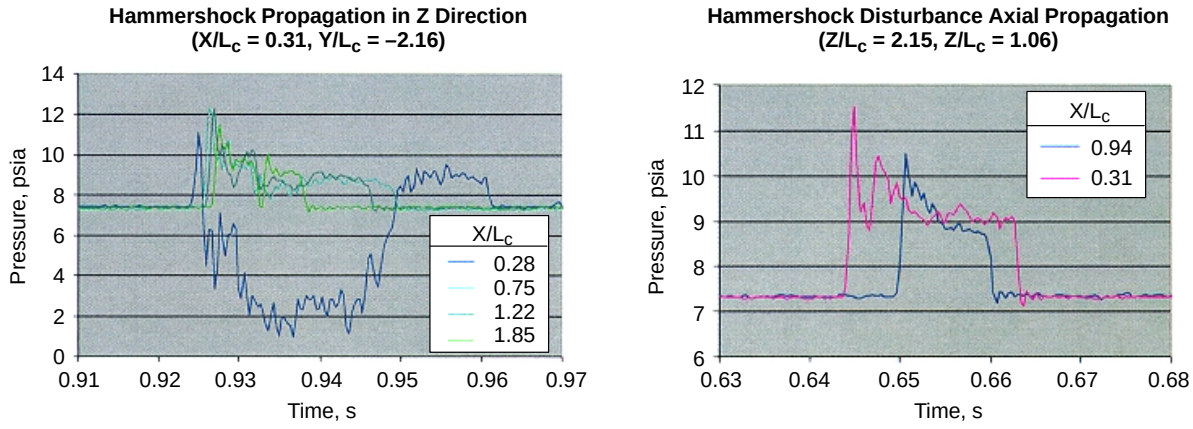

Figure 64. Details of Hammer-Shock Disturbance Propagation

unstart disturbance on this plot, Z/L_C = 1.85, is the first port to recover to the free-stream pitot pressure. The same trend is visible at all measurement stations; that is, the measurement ports recover to the free-stream pitot pressure inversely to the order initially affected. It is interesting to note that as the hammer-shock disturbance propagates outward, the flowfield behind the disturbance is affected until the disturbance propagates inward; then the affected flowfield recovers to the original free-stream conditions.

The hammer-shock disturbance propagation trends also are seen in the axial direction. The plot on the right-hand side of Figure 64 shows two pitot pressure time-history traces acquired simultaneously at constant Y and Z locations but different X (axial) locations. In this case, the Y (spanwise) measurement locations were positioned symmetrically about the test model. The pitot pressure traces clearly substantiate that a disturbance propagates outward, comes to some type of equilibrium, and then propagates inward. This plot indicates a period of time when the entire flowfield is affected by the disturbance — in this case, the 10-ms time span from 0.65 to 0.66 seconds where the pitot pressure levels at each axial station are elevated.

These data indicate that the hammer-shock disturbance due to an engine compressor stall and subsequent inlet unstart causes a three-dimensional disturbance to propagate outward from the inlet. A “bubble” region forms behind this outwardly propagating disturbance where the local flowfield properties are affected. This hammer-shock disturbance and corresponding “bubble” region keep expanding outward until some type of equilibrium process occurs within the free-stream flowfield. Then the disturbance collapses and the affected flowfield returns to free-stream conditions. This whole process occurs on a time scale of about 40 ms.

Local flowfield Mach numbers during the engine stall/inlet unstart transient can be determined when the instrumentation struts are instrumented with alternating pitot and static pressure probes as shown in Figure 65. The plots on the right side of the figure are local transient Mach number calculations based on the measured flowfield transient pitot and static pressures. The arrows show which pressure ports are used for the corresponding calculation. For the case shown above, the measurement station is at X/L_C = –0.312 and Y/L_C = –2.15.

The results for ports 1 and 3 (Z/L_C = 0.28, 0.60) are shown in the top plot of Figure 65. The pressure data and Mach number calculation indicate flow separation at Z/L_C = 0.28. At the beginning of the unstart sequence, it appears that the local Mach number exceeds the free-stream Mach number. This does not physically happen. There are two factors that cause the Mach number to be incorrectly calculated in this region: (1) The probes are spaced 5 inches apart, so the top pitot pressure probe reacts to the hammer-shock propagation before the static pressure probe, and (2) the frequency response of the pitot pressure probes, about double that of the static pressure probe, induces an additional slight time lag before the static pressure probe responds to the hammer shock. Also, at the end of the disturbance propagation, the Mach number data must be interpreted judiciously due to the spatial resolution and frequency response of the pressure probes.

A typical data set for the flowfield out of the separation region is shown in the lower plot of Figure 65. Ports 3 and 5 (Z/L_C = 0.60 and 0.91) are used for this Mach number calculation. For these data, the lower frequency response in the static pressure probe is just enough to cancel-out the spatial resolution error due to the shock propagation. Note that the calculated Mach number drops smoothly at the beginning of the interaction, with no artificial increase in Mach number. The calculated Mach number decreases from the free-stream value of 2.35 to a minimum of about 1.8 during the hammer-

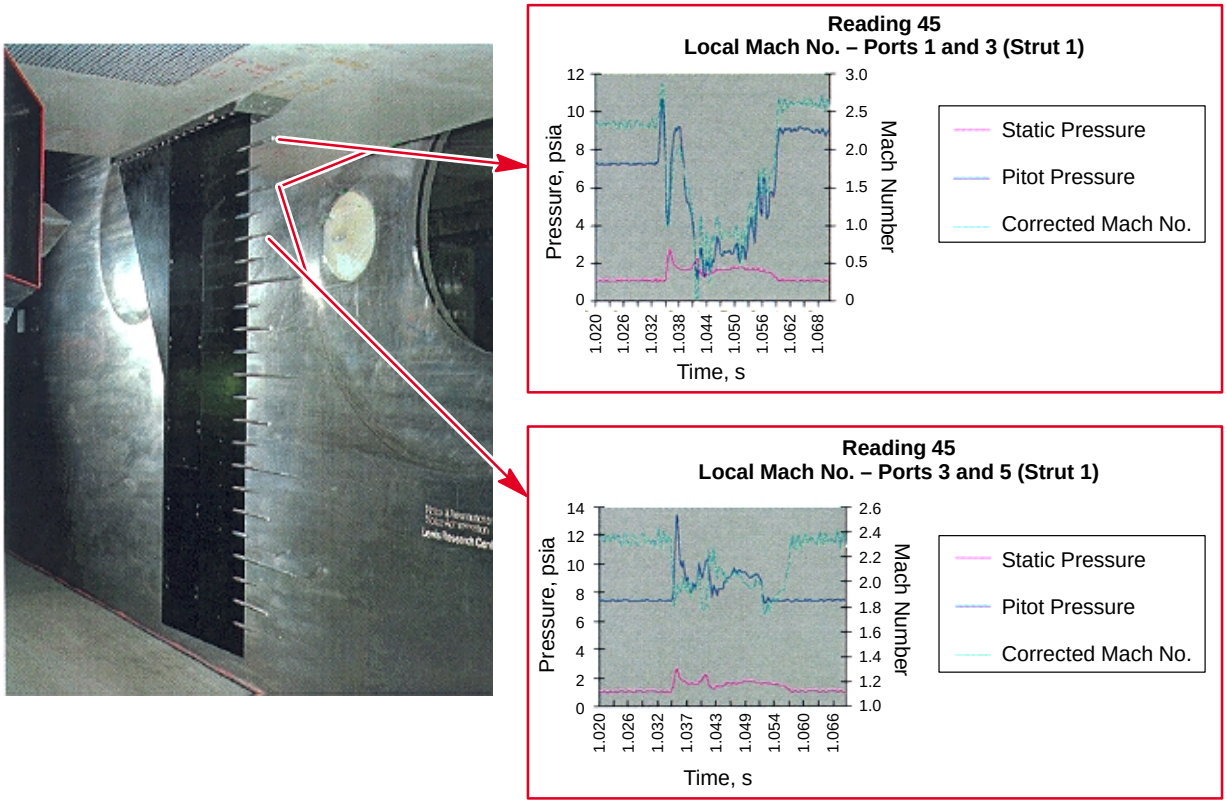

Figure 65. Local Flowfield Properties During Hammer-Shock Transient

shock propagation transient. After the transient passes, the Mach number increases back to the original free-stream value of 2.35. The duration of the total transient interaction is about 30 ms.

By using the results of the flow field Mach number calculations as discussed in Figure 65, we can judiciously estimate the local Mach number decrement in the region influenced during the hammer-shock transient. In Figure 66, a plot of Δ Mach ($M_{local} - M_o$) versus distance below the wing-simulator surface summarizes these results. The free-stream Mach number (M_o) is 2.35 and $X/L_c = 0$ at the inlet cowl lip axial plane. All data were acquired at the $Y/L_c = 2.15$ spanwise location relative to the model centerline.

In general, for a given distance below the wing-simulator surface, the observed Mach number decrement is least at the axial station farthest upstream from the inlet cowl. At the axial station just downstream of the cowl, $X/L_c = –0.31$, the data suggest that the greatest Mach number loss during the hammer-shock transient occurs near $Z/L_c = 1.0$; the losses progressively lessen for increasing distances from the wing-simulator surface. An anomaly seems to occur at $Z/L_c = 0.75$. At this measurement station, the calculated maximum Mach number loss during the hammer-shock transient is less than what is seen in regions farther away from the inlet.

6.11 Wing/Diverter Simulator

Inlet approach flowfield can have a significant impact on propulsion system performance and operation. Ideally, the approach flowfield to the inlet is uniform in Mach number and direction.

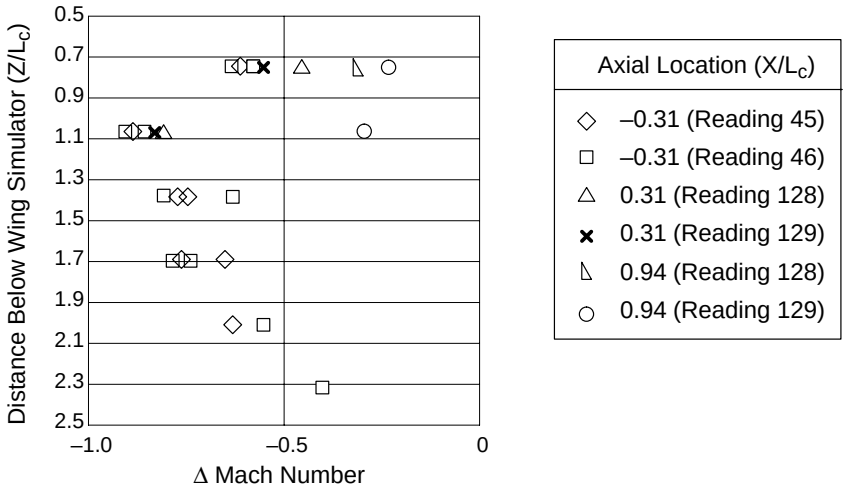

Figure 66. Maximum Observed Flowfield Mach Number Loss During Hammer-Shock Transient

Uniform approach fields present a maximum average total pressure to the inlet aperture. Thrust is sensitive to total pressure, so as average inlet total pressure decreases due to nonuniformities thrust produced by the propulsion system is also decreased. Additionally, inlet pressure recovery and drag performance are sensitive to the interactions among inlet supersonic diffuser geometry and approach Mach number and flow direction. Uniform approach fields are needed to allow proper operation of inlet supersonic diffusers and to promote uniform flow at the engine face for robust inlet/engine operability. Nonuniformities can also reduce the margin between optimum inlet operating conditions and conditions that lead to inlet unstart, decreasing the robustness of propulsion system operation.

The inlet approach flowfield is sensitive to airframe geometry and changes with aircraft design iterations. Changes in aircraft forebody or wing shape change the character of the flowfield approaching the inlet. Aircraft design iterations typically change wing shape and dimensions, as well as wing location with respect to the fuselage, in an effort to optimize aerodynamic performance and thereby change the pressure and flow directional field in the region of the inlet. Integrated aircraft design solutions require that propulsion system performance be compatible with air-vehicle aerodynamics. The influence of the flowfield generated by an air vehicle on the propulsion system is critical to an efficient and functional propulsion system design.

A simulator was designed to permit high-fidelity simulation of such aircraft installation effects, and hardware was fabricated for testing in the NASA–Glenn 10×10 SWT. By inducing the effect of nonuniform Mach number and flow angularity approaching the inlet aperture, this simulator provides test results that more accurately reflect full-scale, integrated-propulsion-system performance.

6.11.1 Simulator Design Configuration

Figure 67 illustrates the concept selected for simulation of a nonuniform inlet approach flowfield for the 2DB inlet installed in the SWT. This concept was selected as a result of a study investigating the use of simple bodies to produce a range of Mach number and flow angularity changes across the 2DB inlet aperture. Aerodynamic design requirements were defined in terms of parametric flow variations, such as mean Mach number and Δ Mach range desired.

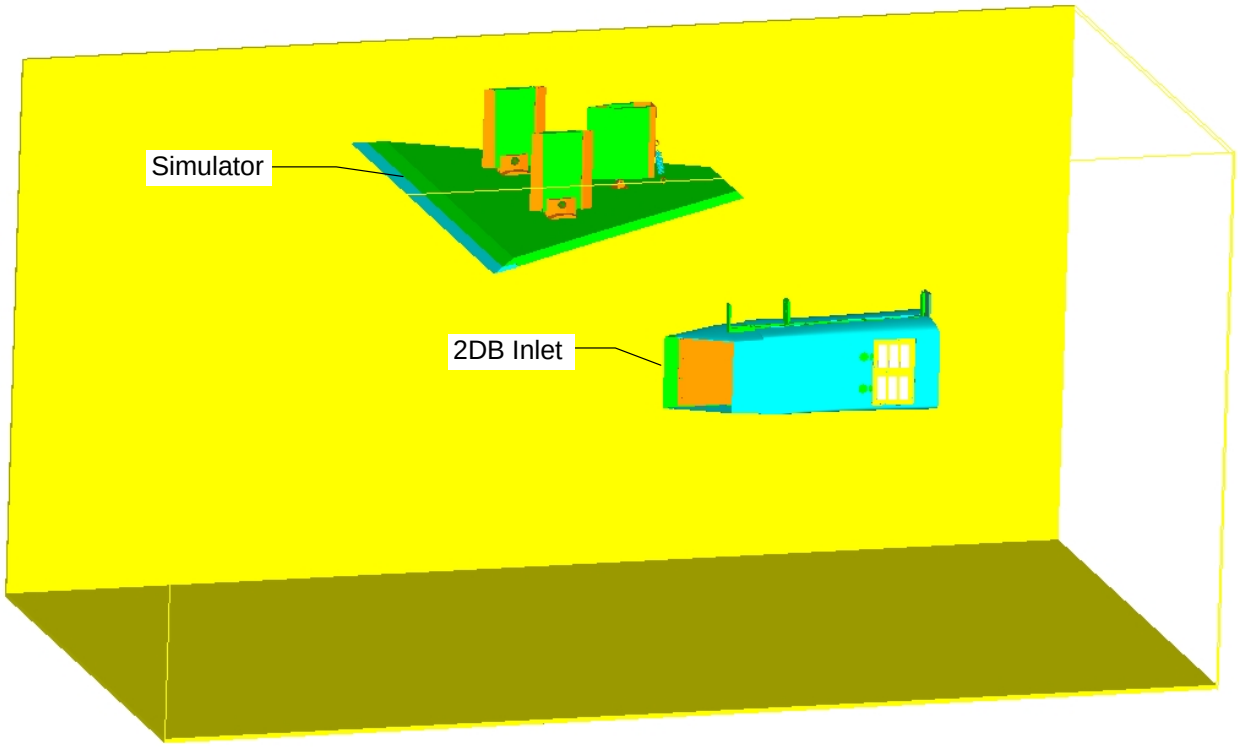

Figure 67. Wing Simulator Using Expansion Plate Concept in NASA 10x10-ft SWT

The concept selected was an expansion plate because it could meet desired combinations of Mach number and flow angularity and the contoured surfaces are easy to produce. Cones and ogives were also investigated but were found to produce undesirable radial flow properties across the inlet aperture. Two expansion plates were produced to allow inlet test investigations at two levels of flow angularity across the inlet aperture.

6.11.2 Analytical Simulation Results

The flowfield produced by the simulator was analyzed. The desired flowfield properties produced by the simulator were first developed from an analysis of flowfield properties produced by the Technology Concept Aircraft (TCA) at the inlet station. Mach number and flow angle fields at the inlet station were determined using a computational fluid dynamics analysis. Figure 68 illustrates the Mach number contours at the inlet station produced by the TCA. The Mach contours represent a supercruise condition at cruise angle of attack with no sideslip. Inboard and outboard inlet aperture locations are shown underneath the wing. The maximum Mach number variation across an inlet aperture is 0.040 Mach number.

Figure 69 illustrates the local upwash contours at the inlet station produced by the TCA. The local upwash contours represent a supercruise condition at cruise angle of attack with no sideslip.

The maximum flow-angle variation across an inlet aperture is the combined angle due to upwash and outwash. Figure 70 illustrates the local outwash contours at the inlet station produced by the TCA.

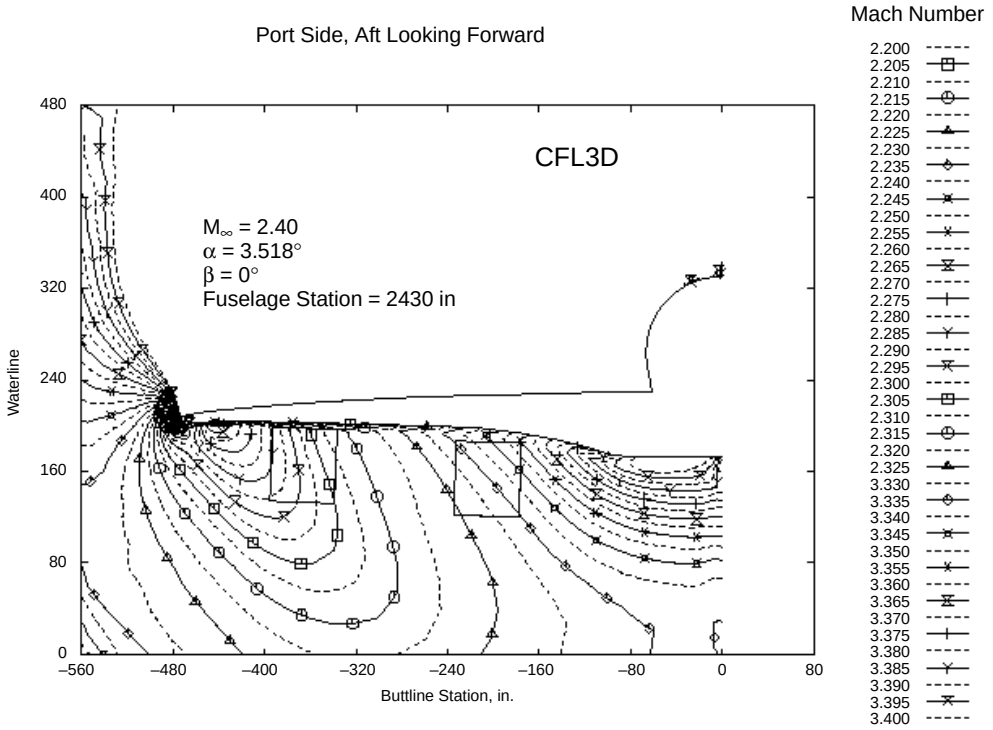

Figure 68. Mach Number Contours at Inlet Aperture

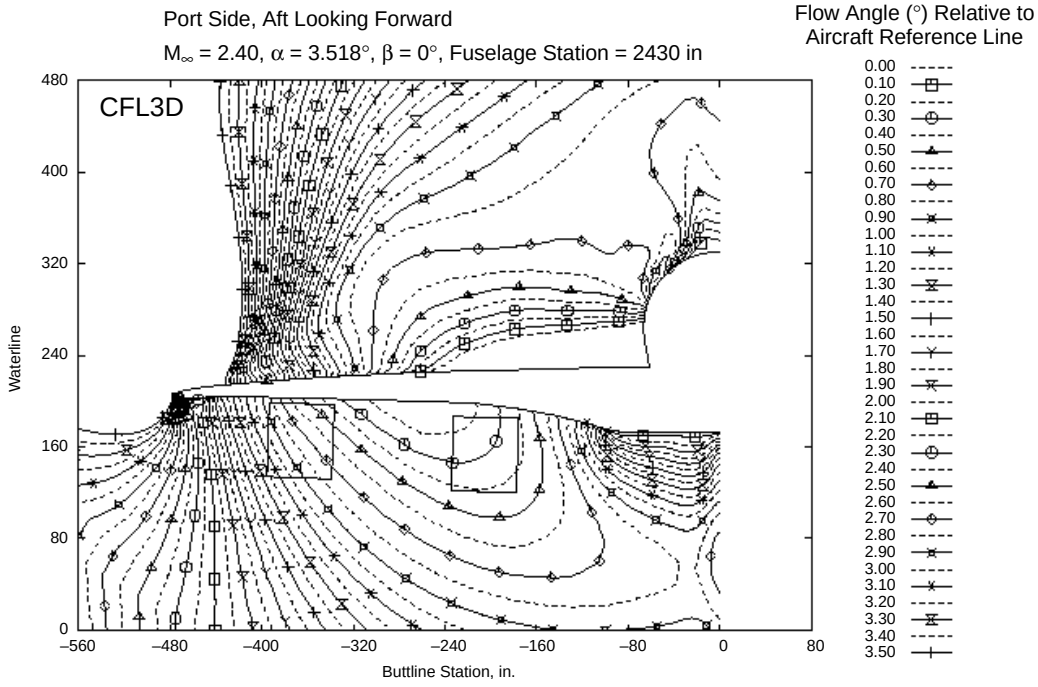

Figure 69. Local Upwash Contours at Inlet Aperture

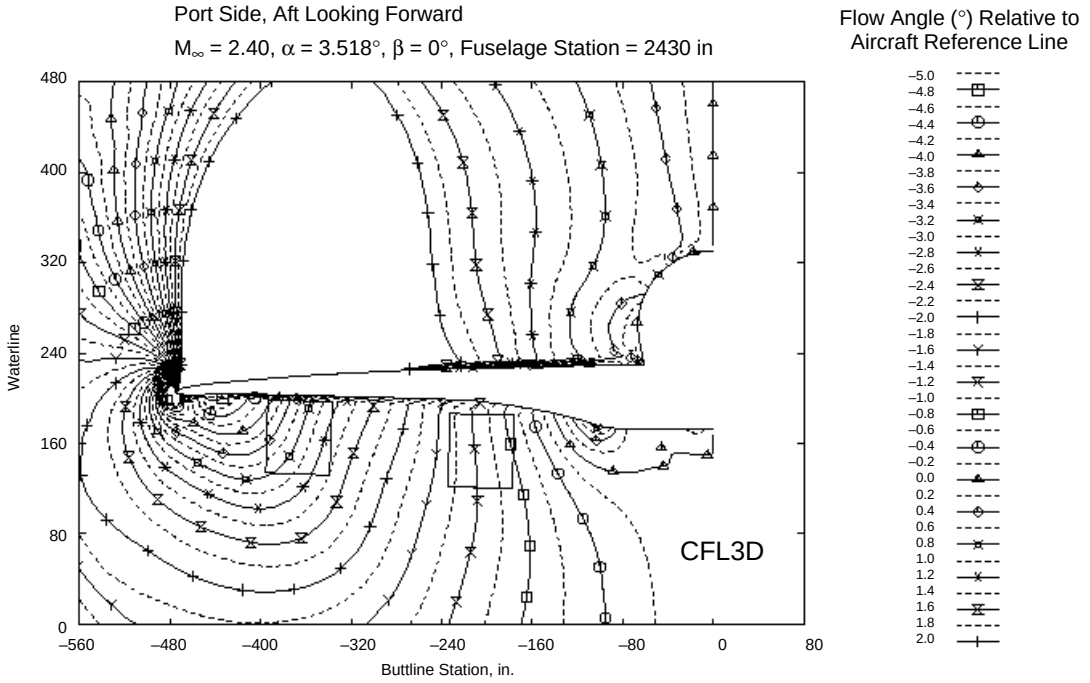

Figure 70. Local Outwash Contours at Inlet Aperture

The maximum variation in flow angularity across an inlet aperture as a result of flow upwash and outwash is 2.5°. Figure 71 illustrates the combined variation in Mach number and flow angularity for the supercruise condition.

The expansion plate concept produces a variation in inlet approach Mach number and flow angularity similar to that produced by the TCA. An analysis of the flowfield generated by an expansion plate was performed using computational fluid dynamics, and the expansion plate was found to provide Mach and flow angularity variations representative of the TCA flowfield. The analysis also indicated the appropriate location of the test inlet in the expansion plate flowfield with respect to the inlet aperture to achieve desired approach flowfield characteristics described in Figure 71. Figure 72 illustrates expansion plate Mach number and flow angularity contours.

6.11.3 Simulator Hardware

Two expansion plates were produced as shown in Figure 73. Plate "A" produces a flow turning angle of 1.3° and plate "B" a flow turning angle of 3.5°. The mechanical design features of the plates are as follows.

- Assumptions:
  - Existing support legs, locations, and spacing are used
  - Minimum clearance between edges of plate and tunnel wall is 6 inches
  - Tolerance on plates is $\Delta y = \pm 0.005$ in
- Two fixed-geometry simulators with radius of curvature:
  - 2203 inches (Plate A)
  - 819 inches (Plate B)

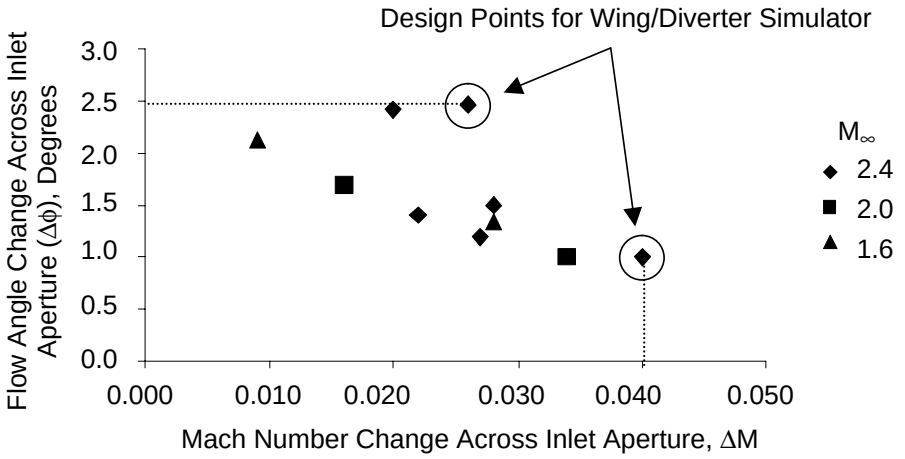

Figure 71. Summary of Mach Number and Flow Angularity Changes Across the 2DB Inlet on the TCA for Supercruise

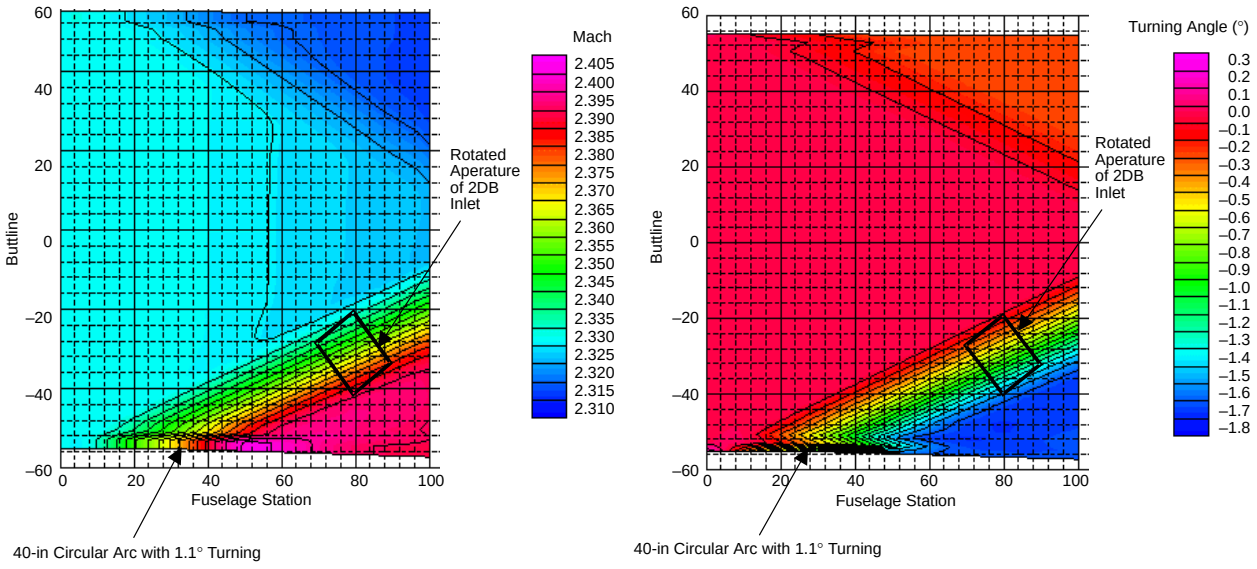

Figure 72. Expansion Plate Mach Number and Flow Angularity Contours
Goal is to meet M_{avg} = 2.35 with ΔM = 0.04 and $\Delta\phi$ = 1.05.

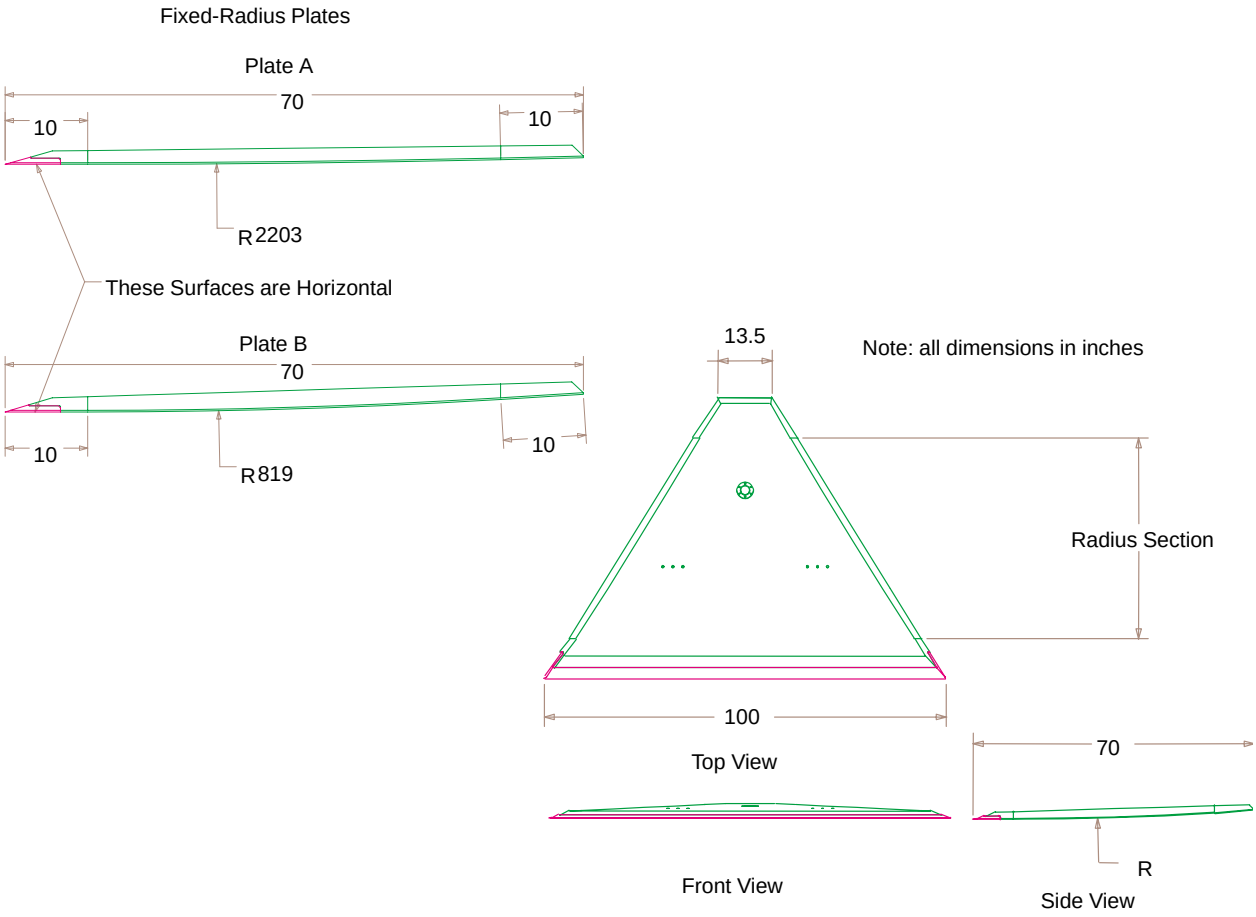

Figure 73. Expansion Plates A and B

- Design load conditions:
  - M = 1.98, α = 0.3° (Plate A); M = 2.18, α = 0° (Plate B)
  - M = 2.30, α = 0.6° (Plate A); M = 2.40, α = 1.9° (Plate B)
  - M = 2.40, α = 1.9° + Tunnel Unstart (Plate A)

Figure 74 illustrates the geometric relationship of the expansion plate and inlet mounted in the SWT. The expansion plate is mounted horizontally while the inlet is rotated and positioned for the range of Mach number and flow angularity variation representative of the TCA inlet approach flowfield as shown in Figure 72. This arrangement allows direct attachment of the plate to existing tunnel support legs.

Two expansion plate simulators were fabricated and delivered to NASA–Glenn for use in advanced inlet testing of the two-dimensional bifurcated concept along with analysis and design reports. Subsequent to simulator manufacture, inlet testing was discontinued; consequently the simulators were not tested. It is recommended that the flowfield produced by the simulators be quantified by test since they produce a range of Mach numbers and flow angularities that may be useful in representing approach flowfields to other integrated inlet concepts.

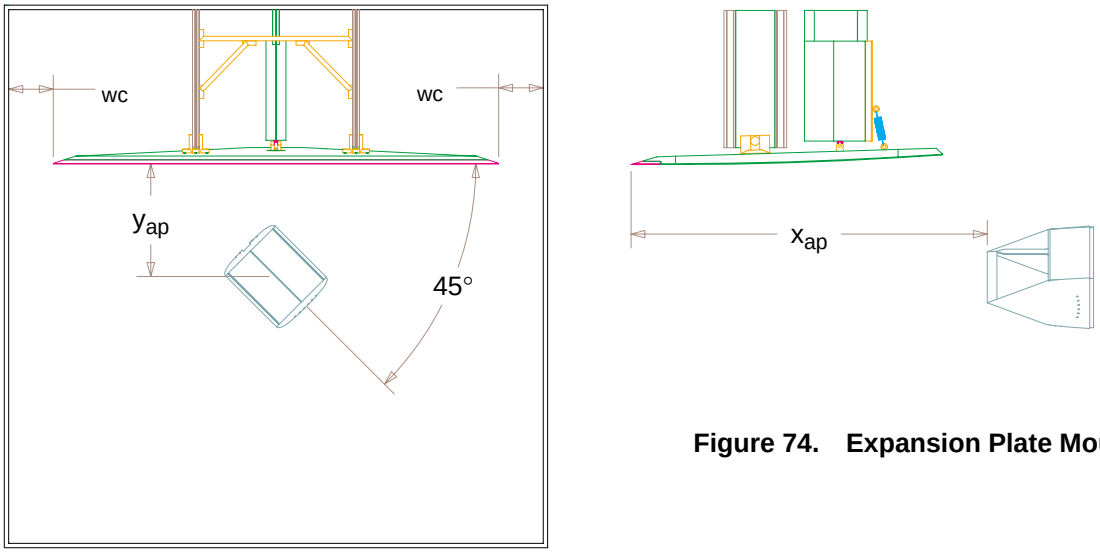

Figure 74. Expansion Plate Mounting

6.12 Lessons Learned and Recommendations

The HSR technology development program for the HSCT inlet was very successful, delivering and surpassing the goals. During the course of the HSR inlet program, many lessons were learned and recommendations formulated. Some are listed below for posterity.

1. Large radial distortion is generally present in mixed-compression supersonic inlets. This distortion is probably due to the typical (long) lengths of these inlets. Fan design can accommodate radial distortion if it is characterized early in propulsion system development.
2. Stability valves are critical for successful mixed-compression inlet operation. Design and integration into the inlet system should be addressed early and throughout any future program.
3. Acoustic requirements can drive inlet design. Research in fan/inlet noise reduction should be continued, and future inlet design should carefully incorporate the appropriate acoustic research to minimize or eliminate any performance degradation.
4. Soft-choke operation of the inlet has severe safety concerns. To seriously incorporate soft-choke benefits, robust control schemes must be devised.
5. Distortion goals are very difficult to set, particularly for a project with an engine that is concurrently being defined. Physics-based model of the interaction (and the whole propulsion system) is an important future goal.
6. CFD tools have matured to the state of augmenting advocacy for an inlet design philosophy. Attempts should be made to work CFD towards making significant advances in viscous inlet design.
7. Control design and engine stall prediction can be enhanced with high-fidelity, two-dimensional, time-accurate CFD. Three-dimensional analyses remain a challenge to computer resources — particularly in the time-accurate domain.
8. Advances were made towards accurate prediction of inlet stability based on atmospheric characterization. Pulling this tool together with CFD analyses of the integrated inlet system was planned but not implemented prior to program cancellation.

9. Bleed boundary layer control may be further reduced with enhanced physics-based modeling and active flow control.
10. The 2DB inlet is a well-developed, third-generation, mixed-compression inlet. Performance and operability met the challenges of the HSCT requirements. The concept is well-posed to continue research in system controls and flight testing. The inlet is the best choice for a near-term program to develop a supersonic transport.
11. Longer term development of supersonic propulsion should continue to consider the axisymmetric options for inherent performance or engine-matching benefits. Other novel concepts and technologies should also be considered so as not to create a narrow focus that burns away radically better paths.
12. A waverider external compression inlet concept holds promise of dramatically enhancing the stability and safety of supersonic propulsion while maintaining adequate performance for a supersonic cruise vehicle. Significant three-dimensional viscous flow present a defining challenge for CFD design methods.
13. A three-dimensional data set and understanding of the underwing-inlet unstart process was acquired. This information is critical to pod spacing and integration issues of novel aircraft configurations.
14. Auxiliary inlet development was directed to the 2DB inlet concept and specifically to a variable cowl-lip geometry. Data were acquired, and preliminary assessment showed promising results. Full engine compatibility assessment was not completed prior to program termination.
15. Judicious use of shock stability/throat geometry subcomponent testing can have cost and insight benefits to mixed compression inlet development.
16. Inlet technology should be contracted with primes not subcontractors. More specifically, airframers should be the direct contractor unless the engine contractors assume the active role in inlet development. Mutual respect between the industry partners and NASA technical staff should be encouraged through shared funding directed in the interest of the nation's taxpayers with a clear set of objectives.

6.13 References

1. Girvin, R., Austin, T.R., and Jones, J.R., "Aerodynamic Characteristics of the NASA Mach 2.5 Variable-Diameter-Centerbody Inlet," McDonnell Douglas Aerospace – Transport Aircraft, NAS3–25965, November 1993.
2. Saunders, J.D., "Operability and Performance of a Variable Diameter Centerbody, Mixed Compression Inlet," NASA TM (publication pending), January 31, 1994.
3. Schultz, J.J., "HSCT–CPC Axisymmetric Inlet Compatibility Report, Translating Centerbody and Variable Diameter Centerbody Inlets, Analysis of Steady-State and Dynamic Data," GEAE, CPC contract NAS3–27235, November 15, 1996.
4. Jones, J.R., Culbertson, C.C., and Kwok, D.W., "An Inlet Configuration Trade Study for a High-Speed Civil Transport with FLADE Engine, Phase III," McDonnell Douglas Aerospace – West, CRAD–9011–TR–0139, NAS3–25965, December 1994.
5. Tank, W.G., "Atmospheric Disturbance Enviroment Definition," Boeing Commercial Airplane Company, NAS3–25963, February 1994.

6. *Gas Turbine Inlet Flow Distortion Guidelines,* ARP 1420.

7. Woodward, R.P., Glaser, F. W., and Lucas, J. G., “Low Flight Speed Fan Noise from a Supersonic Inlet,” Journal of Aircraft, V. 21, No. 9, 1984, pp 665–672.

8. Wing, N.G., “Noise Reduction in an Axisymmetric Supersonic Inlet Using Trailing Edge Blowing,” Final Technical Report, Grant NAG3–1539–SUPL#5, 1998.

7.0 Fan/Inlet Acoustics Team

7.1 Overview

7.1.1 Fan/Inlet Program Objectives

The Fan/Inlet Acoustic Team (FIAT) program objectives were to:

- Quantify fan/inlet noise contribution at approach and cutback.
- Establish fan/inlet noise reduction required meeting HSCT airplane noise goals.
- Quantify noise impact of acoustic liners, inlet flow acceleration (soft choke), inlet auxiliary doors, and fan source-reduction concepts.
- Establish fan/inlet acoustic design criteria to support engine cycle and inlet downselects.

Figure 75 outlines the program established to achieve these objectives. The goal was for the aircraft to meet FAR 36 Stage III minus 1 (104 dB) or less at the approach condition. The aircraft was scaled by Boeing to meet the cutback noise requirements. The approach to estimating the aircraft noise signature was to use an existing fan-noise database, build new fan/inlet scaled models to acquire data, and develop analytical tools. This included existing P–Inlet/J85 and YJ101/XF120 data; Virginia Polytechnic Institute (VPI), Florida Agricultural and Mechanical University (FA&M), and Boeing subscale-model test results; and parametric fan/inlet scale-model results from a NASA 9×15-ft low-speed wind tunnel (LSWT) test for improved noise assessments.

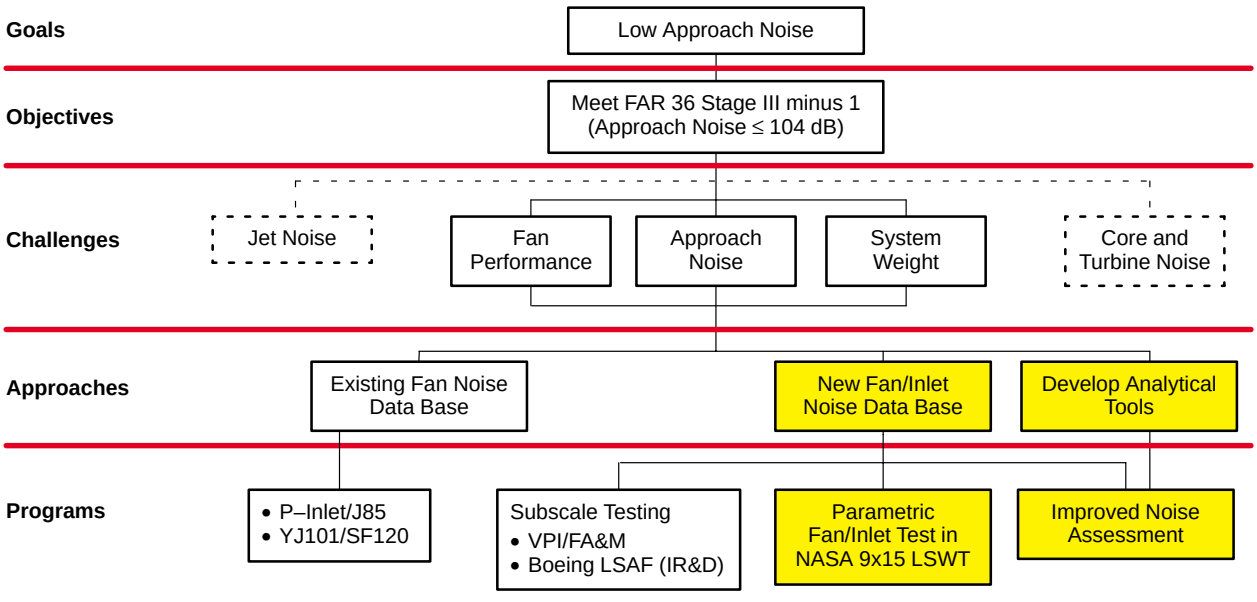

Figure 75. FIAT Programs *Focus was on approach and cutback noise.*

7.1.2 Fan Logic Description

The planned FIAT program schedule to achieve the above objectives is presented as Figure 76. Termination of the overall HSR program at the end of GFY99 precluded the approach noise assessment since the NASA LSWT test has not been conducted; however, fabrication of the fan/inlet scaled rig has been completed. The model design and fabrication tasks among P&W, GEAE, Boeing, and NASA are delineated in Figures 77 and 78. Completing the model hardware fabrication will allow a possible future program to complete the test and approach noise assessment.

7.1.3 Fan Metrics

The basis for the approach noise assessment for the aircraft is as follows:

- FIAT metric: total approach noise $\leq$ Stage III minus 1 EPNdB
- System study performed under HSR technology airframe/engine integration
- *Preliminary Technology Concept* (PTC) airplane
  - Noise-sized for – Stage III minus 1 dB at sideline and
    – Stage III minus 5 dB at cutback
  - Wing aspect ratio = 2.73, Wing area=9200 ft^2
- Mixed-flow turbofan (MFTF) engine
  – 3770.60 engine cycle
  – Three-stage fan, fixed-chute nozzle (135-in mixing length)
- Two-dimensional bifurcated (2DB) Inlet
  – Full acoustic treatment
  – Auxiliary doors closed at approach and open at cutback
- Optimistic auto flap
- Total noise levels include estimated contributions of suppressed jet noise and airframe noise (but not turbine and core noise).

Figure 79 is a breakdown of contributions by engine component to the approach noise. The fan/inlet is the main contributor. At the cutback condition, Figure 80, fan/inlet noise is lower than the jet noise, but the fan/inlet noise still contributes approximately 1 dB to total noise. Since cutback noise sizes the airplane, 1 dB in effect adds 30,000 lbm to the maximum takeoff gross weight (MTOGW). In addition, the estimated approach noise level has great uncertainty (Figure 81) due to:

- Modification to FAR 36 rules
- System design choices
- Performance shortfalls in other technology areas
- Airframe shortfalls
- Fan/inlet prediction tolerance

The status of approach noise absolute level as a function of time with large tolerances is presented as Figure 82.

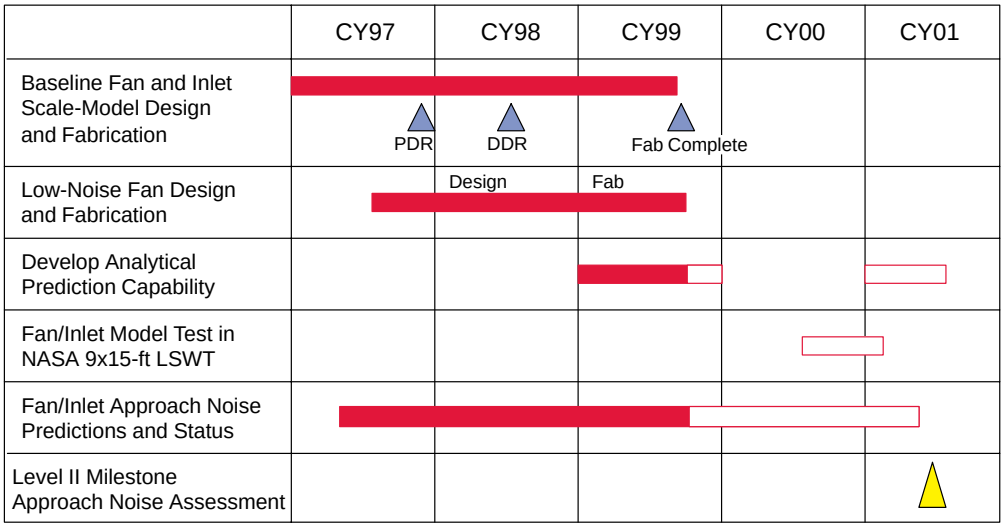

Figure 76. Program Schedule *Model complete, ready for test October 1999; HSR termination halted program before testing began.*

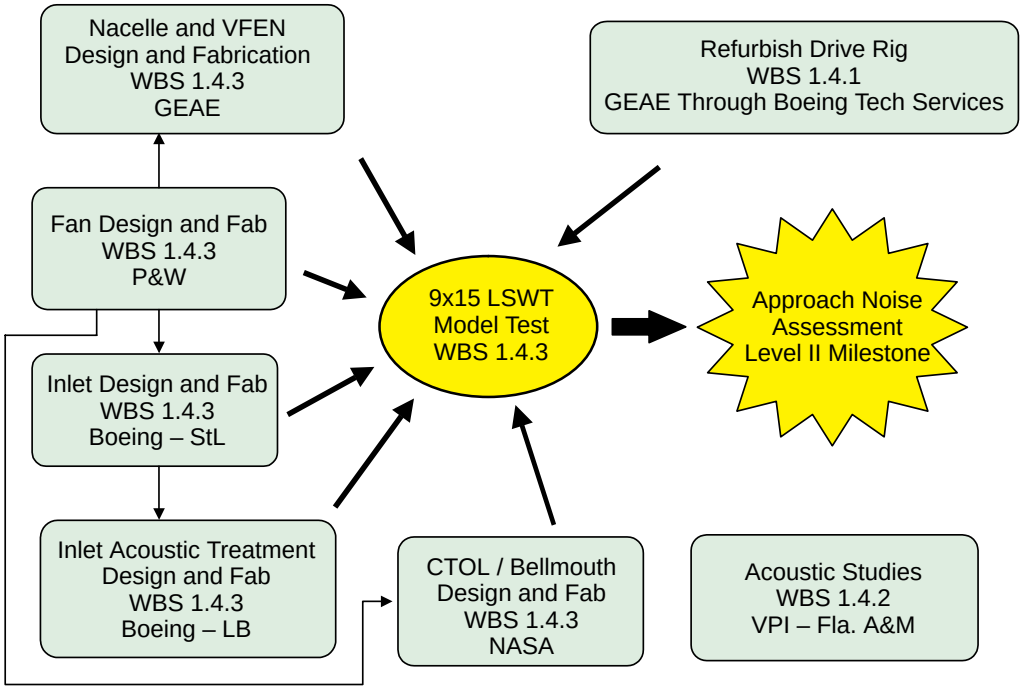

Figure 77. FIAT Program Tasks

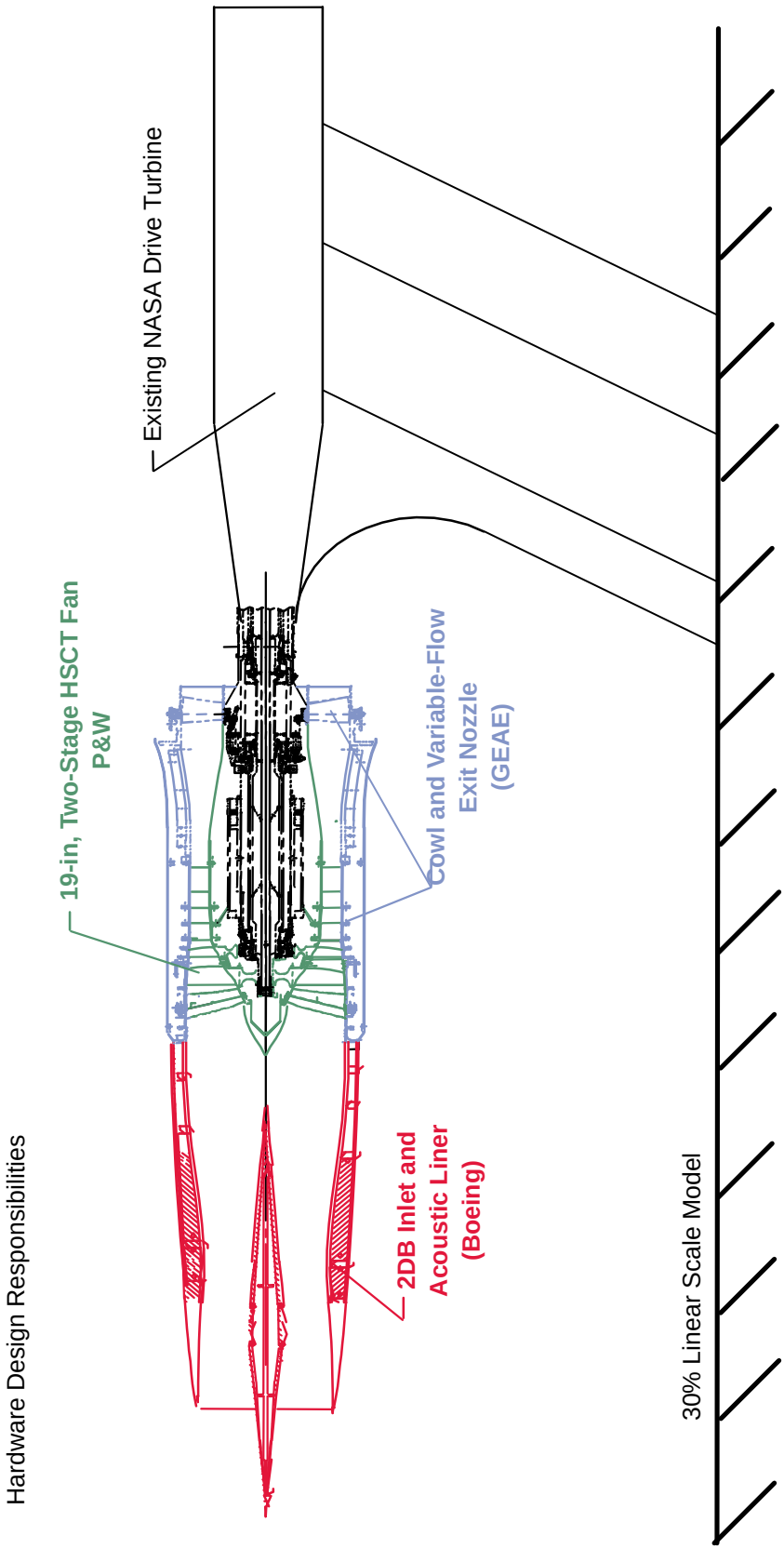

Figure 78. FIAT Model on the Ultrahigh Bypass (UHB) Drive Rig in NASA 9x15 LSWT

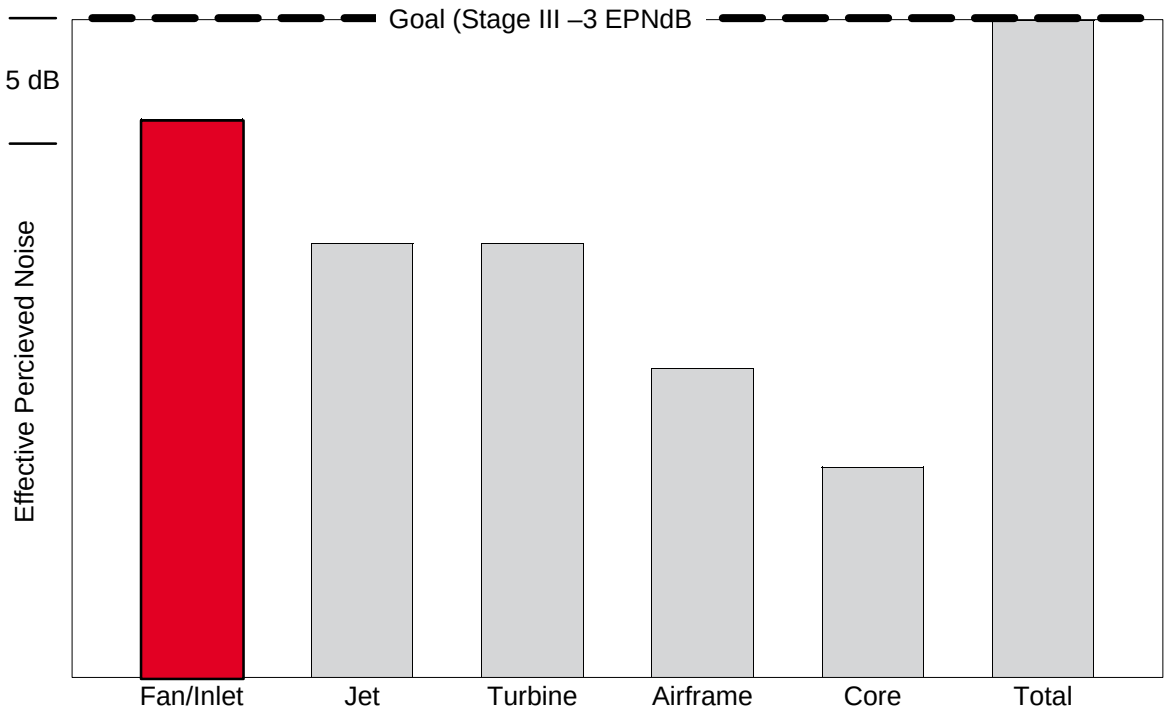

Figure 79. Approach Noise Breakdown *Fan/inlet is the dominant source.*

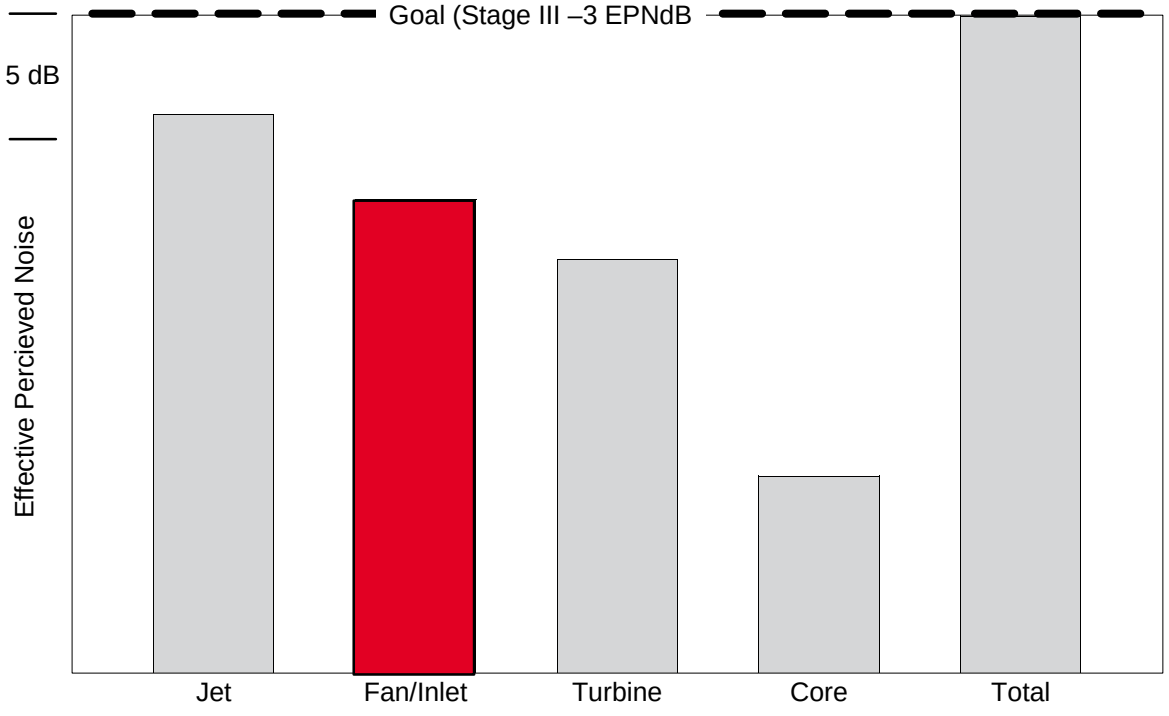

Figure 80. Cutback Noise Breakdown *Fan/inlet is a contributor.*

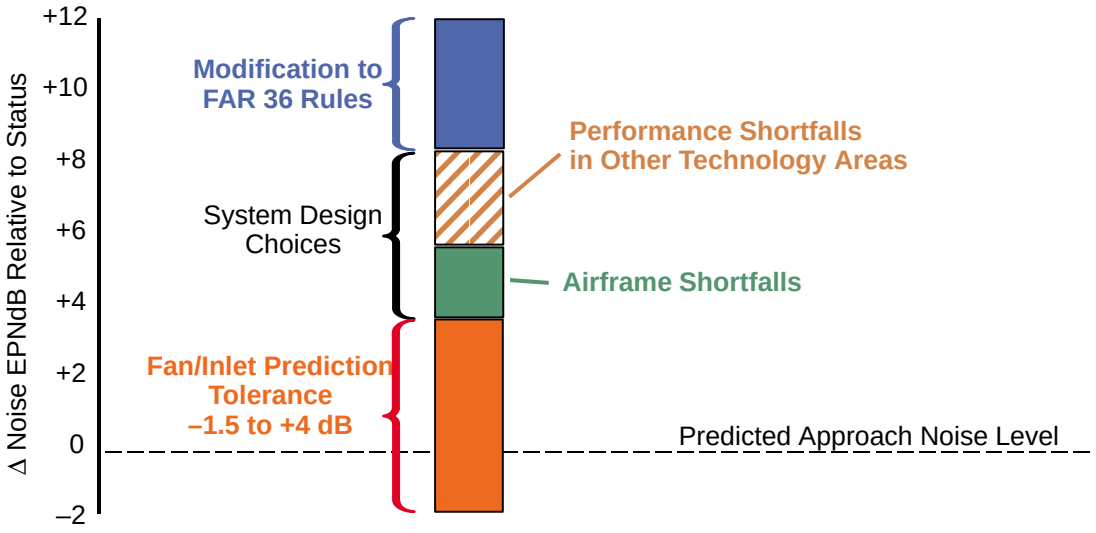

Figure 81. Approach Noise Uncertainty *Many factors contribute to uncertainty; data are needed to reduce prediction tolerance.*

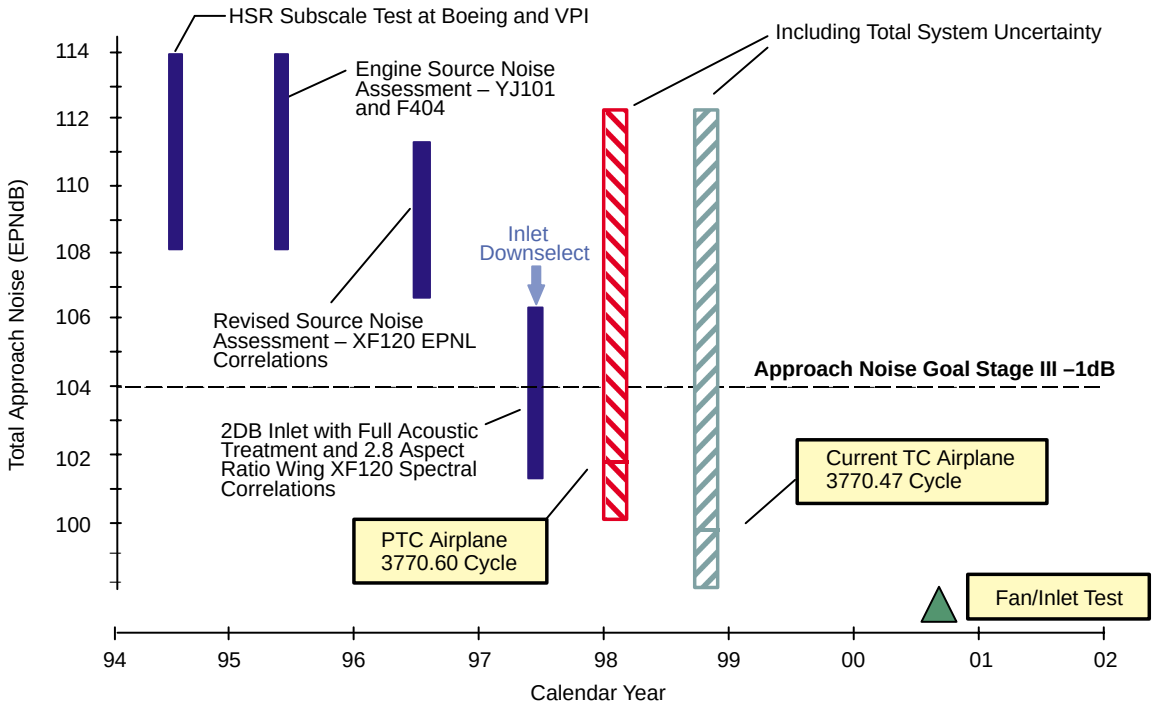

Figure 82. Approach Noise Estimates as a Function of Time

7.2 Fan, Inlet, and Model Support Concepts

7.2.1 Fan

7.2.1.1 Base Configuration

A study was conducted to determine the optimum model fan diameter using the drive rig turbine air pressure, temperature, and flow requirements versus the test facility capabilities. This required evaluating the drive turbine horsepower available as a function of fan size and maximum rotational speed needed to meet test objectives. The fan size chosen, 19-in tip diameter, allows testing of all of the important acoustic test conditions (Figure 83) except for the sideline condition, which was not a requirement of this program.

Only the first two stages of the three-stage, full-size fan are included in the scale model because it was judged that the third stage would not contribute to the forward-radiated fan/inlet noise and because of the drive rig turbine power and RPM constraints. The fan/inlet scaled model mounted on the ultrahigh bypass (UHB) rig in the 9×15-ft LSWT is illustrated in Figure 78 (page 73).

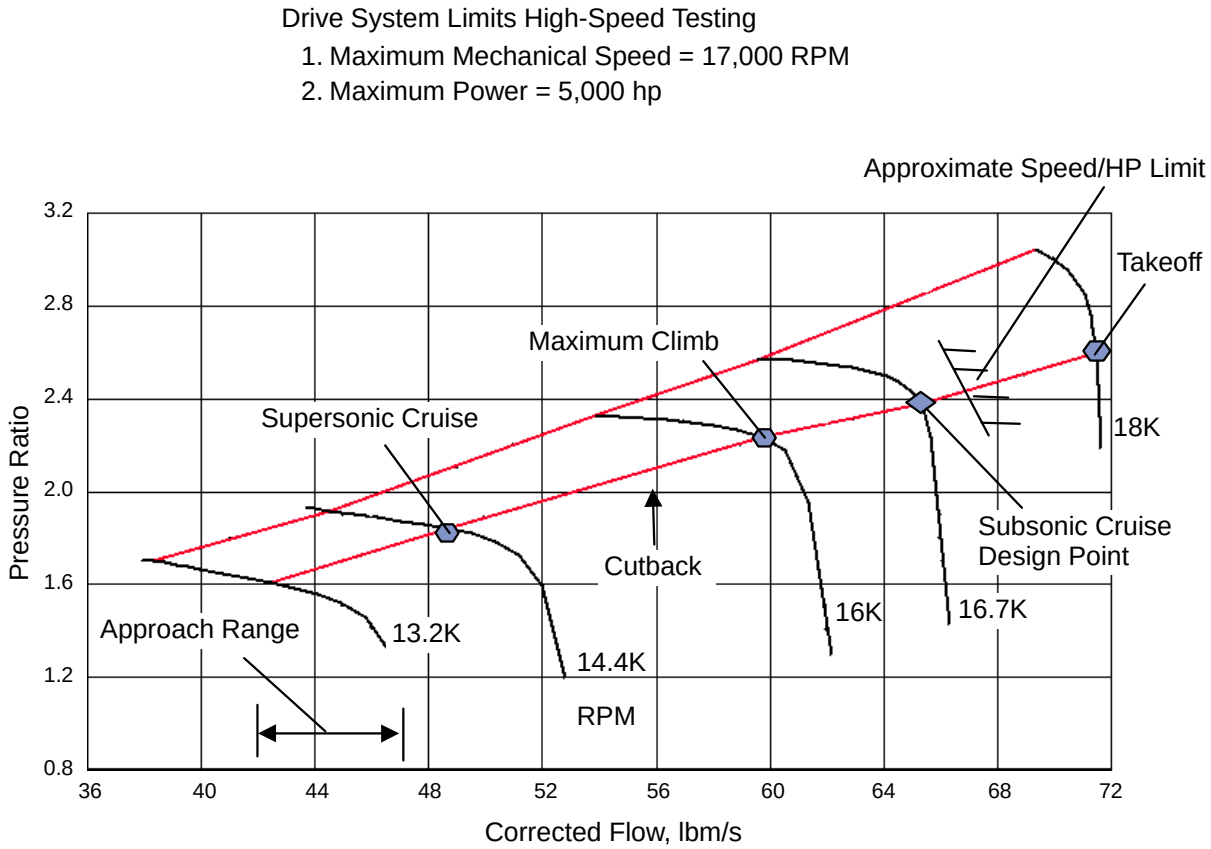

Figure 83. Predicted Fan Map for First Two Fan Stages

7.2.1.2 Low-Noise Fan Configurations

Because of the great uncertainty of achieving the approach fan/inlet noise metric and the need to obtain parametric acoustic data to develop acoustic tools, 17 alternate fan configurations were studied:

1. Increased axial spacing: inlet guide vane (IGV) to rotor 1 (R1)
2. Increased axial spacing: R1 to stator 1 (S1)
3. Increased axial spacing: S1 to rotor 2 (R2)
4. Treatment between IGV and R1
5. Optimized IGV and/or S1 vane counts
6. S1 sweep and/or lean
7. R1 sweep
8. IGV trailing-edge blowing (wake filling)
9. IGV sweep and/or lean
10. Increased axial spacing — inlet bifurcation to IGV frame
11. Bifurcation circumferentially aligned with IGV's
12. Trailing-edge blowing on bifurcation (wake filling)
13. Increased axial spacing — inlet doors to IGV frame
14. Increased inlet acoustic-treatment area
15. Optimized acoustic treatment design
16. Soft choking
17. Increased wing aspect ratio

From those studies, five features were incorporated into the low-noise fan for parametric testing:

1. Increased axial spacing, IGV to R1
2. Increased axial spacing, R1 to S1
3. Treatment for IGV to R1 spacer
4. Reduced IGV count
5. Increased axial spacing, inlet bifurcation to fan face

7.2.2 Inlets

7.2.2.1 HSCT-Type Inlet

The acoustic inlet test module (Figure 84) consists of a subscale HSCT 2D bifurcated inlet supported by a horizontal strut that extends through the wind tunnel wall and attaches to a NASA-provided moveable module support table.

Both inlet and strut structures are semimonocoque designs consisting of stiffened skins, supported by frames, and beams. The inlet is approximately 71 inches long tapering from 17 by 22 inches at the forward end to 25 inches square at the aft end. The strut extends approximately 56 inches from the inlet to the tunnel wall and has a cross section measuring approximately 56-in wide by 8-in high.

The inlet (Figures 85 and 86) consists of four major structural elements: the outer skins, the aft frame (frame 1), the midframe (frame 6, not shown), and the centerbody beam. The inlet outer skins, supported by frames and stiffeners, enclose an acoustically treated cowl liner assembly and a horizontal centerbody assembly.

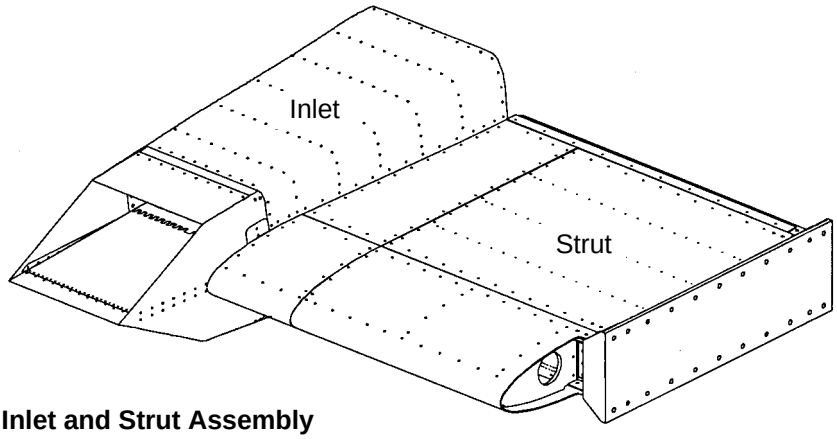

Figure 84. Inlet and Strut Assembly

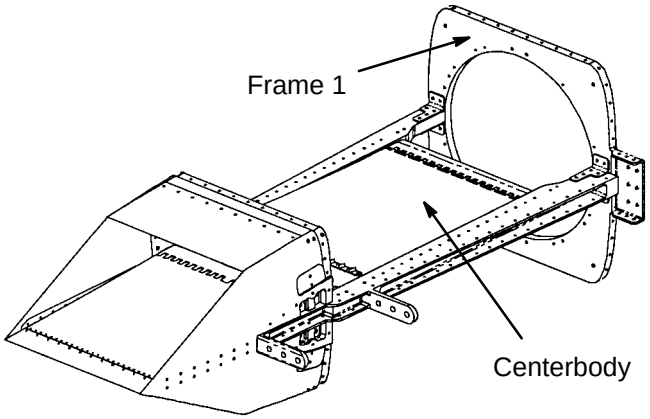

Figure 85. Inlet Assembly Without Skins, Cowl Liners, and Midframe

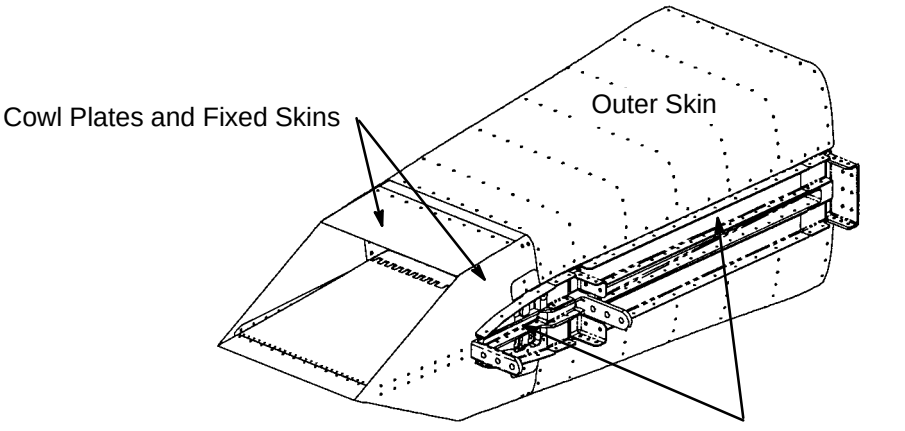

Figure 86. Inlet With Skins Installed

The centerbody assembly, designed to be supported by the strut with the skins and liners removed, contains a centerbody beam with moveable forward, center, and aft ramps. The aft ramps are acoustically treated.

The inlet is fabricated primarily from 7075 aluminum sheet and plate except as follows. The cowl lips and one frame are 15–5PH steel, the forward diffuser ramps are 6AL–4V titanium, and the aft diffuser ramps are 17–4PH steel. The bypass louvers and screens are 304 stainless steel, and the acoustic liners are fiberglass honeycomb sandwich panels with a carbon epoxy facesheet. A 6061–T62 aluminum machining supports each acoustic liner.

The strut structure (Figure 87), without skins, extends between the inlet and the tunnel wall and supports the inlet. It attaches to the inlet skins, frames 1 and 6, and the forward end of the inlet centerbody. The strut assembly attaches through the tunnel wall to a moveable support table, with 5/8-in diameter bolts in the strut mounting plate. The strut is fabricated from 7075 aluminum sheet and plate and 6061 aluminum extrusion.

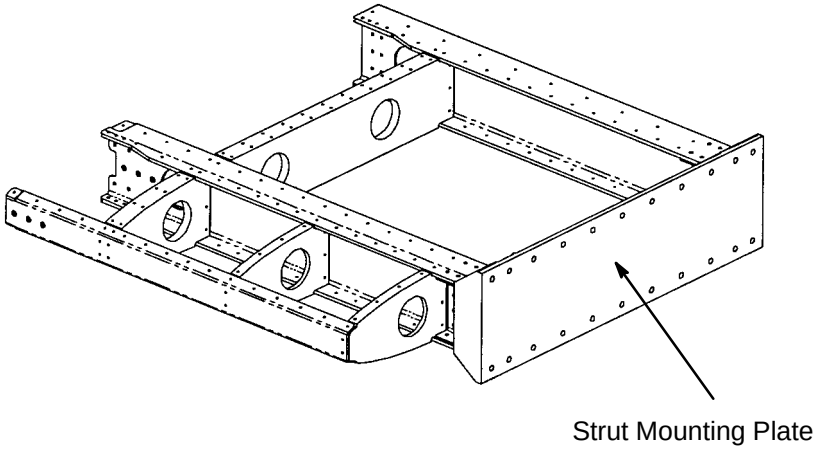

Figure 87. Strut Assembly Without Skins

The outer inlet skins (Figure 86) consist of removable and fixed skins. The outer skin is removable for replacing liners. The cowl plates and fixed skin are not removable. The strut angles provide the forward/aft shear tie for the outer skins and the cowl plate to the strut. The removable inlet skins are fabricated from 0.16-in thick 7075–T76 aluminum sheet with machined aluminum stiffeners.

The inlet is supplied with three sets of acoustic liners, each having a different acoustic configuration. Two sets have carbon epoxy covered honeycomb core panels bonded to the mold-line surfaces for acoustic treatment, and one set (called the “hard wall” set) has no acoustic treatment.

7.2.2.2 CTOL Inlet

The conventional takeoff/landing (CTOL) inlet (Figure 88) will be used to generate the baseline acoustic signature data for the HSCT fans. The inlet must provide a uniform inflow to the HSCT fan across a wide range of fan operating conditions and in a tunnel flowfield environment. This subsonic inlet design has a thick leading-edge lip for flow distortion tolerance and internal and external flow contours that match the new fan hardware lines. The inlet will attach to the fan rig bulkhead for support and be instrumented with 10 wall static-pressure taps.

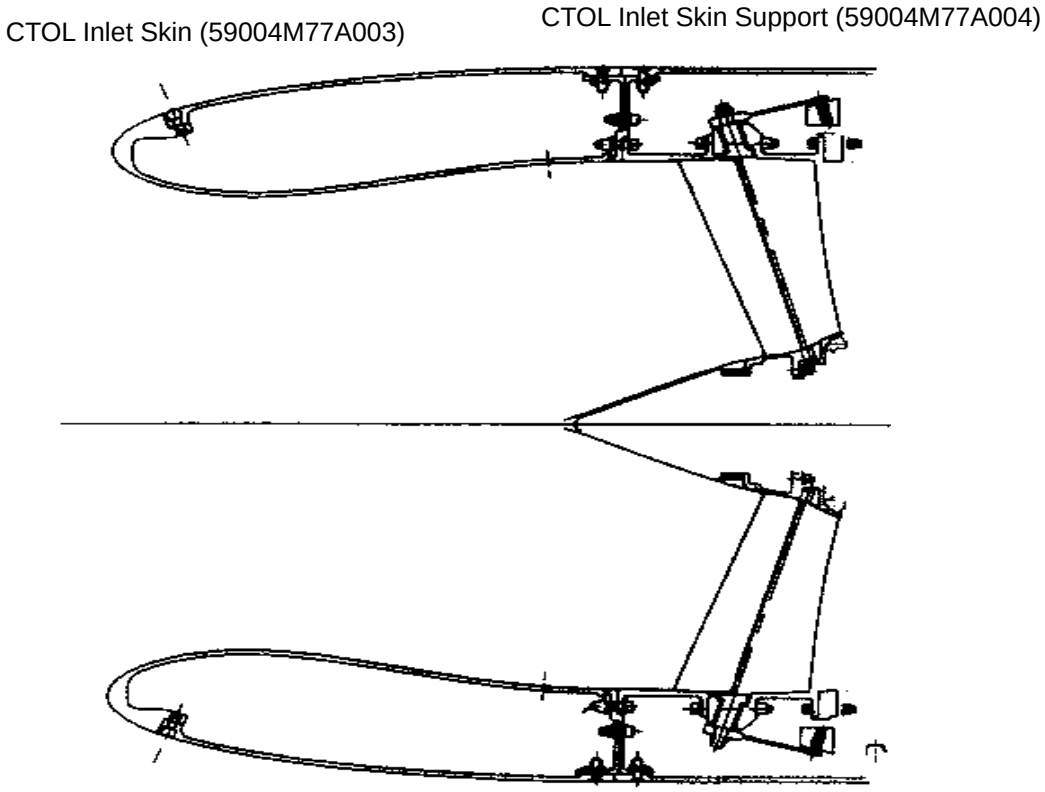

Figure 88. CTOL Inlet (59004M77A002)

7.2.2.3 Bellmouth Inlet Assembly

The bellmouth inlet assembly (Figure 89) will be used to obtain HSCT fan aerodynamic performance data. This inlet must provide a uniform pressure and temperature flowfield to the fan for accurate mass flow and aerodynamic performance determination. The bellmouth inlet assembly consists of an existing NASA 22-inch diameter fan bellmouth and a transition duct that provides flow contours to match with the new 19-in diameter fan hardware. The assembly will be attached to the fan rig forward flange for support and will be counterweighted to relieve fan casing stress. The transition duct will be instrumented with 10 wall static-pressure taps.

7.2.3 Model Supports

7.2.3.1 Inlet Support

The HSCT inlet is “soft” mounted to the fan rig bulkhead with a K-type seal on the inner flowpath and a lap-joint-type seal on the outer flowpath. The inlet has a strut that hard mounts to a three-axis positioning table that is mounted to the tunnel wall structure (see Figure 90). An instrumentation strut is also hard-mounted to the tunnel wall and provides trays for routing model instrumentation and hardware actuation control lines.

The HSCT Inlet is structurally isolated from the fan rig because the weight, approximately 630 pounds, would overstress the fan casing supports. The inlet support is decoupled from the fan drive

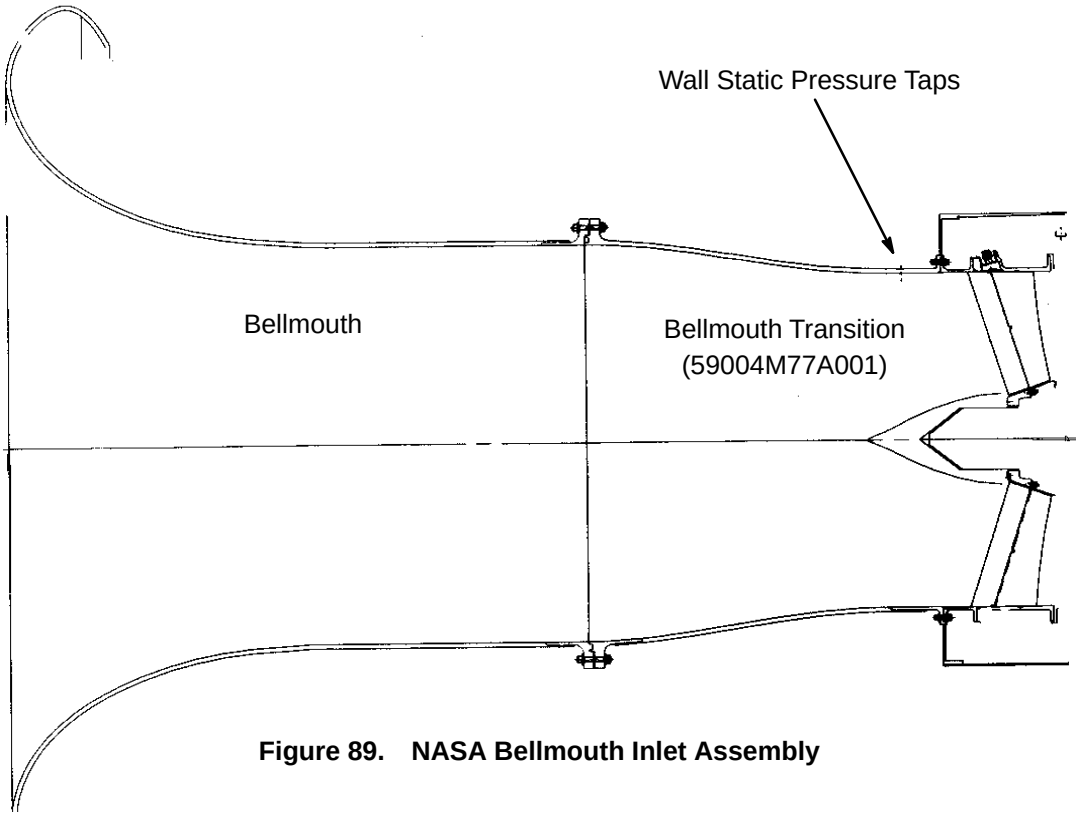

Figure 89. NASA Bellmouth Inlet Assembly

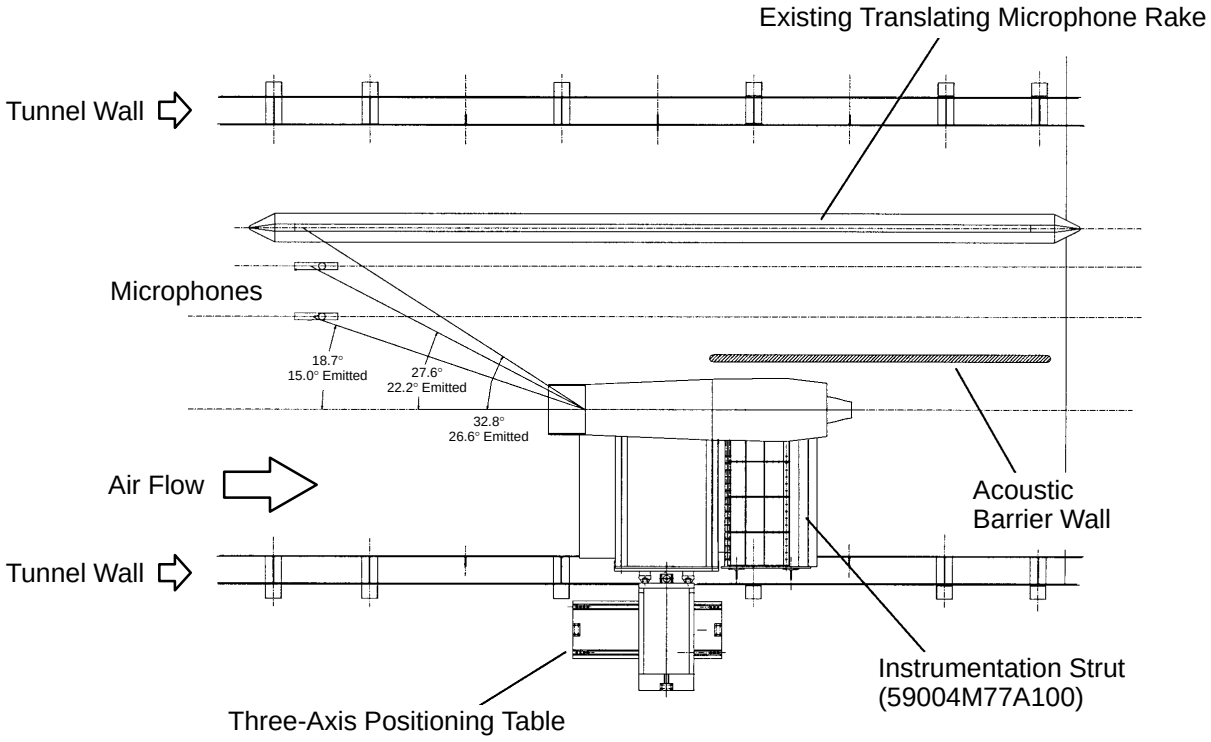

Figure 90. Three-Axis Positioning Table and Microphone Arrangement in the 9x15-ft LSWT

rig, so the inlet and fan rig bulkhead will have a relative motion. As the fan speed increases, thermal growth and thrust forces cause the drive rig to move in three axes. The motion of the fan rig must be matched by the inlet to maintain concentricity. Concentricity is maintained by measuring relative motion between the inlet and fan rig and signaling a three-axis positioning table to align the inlet.

The positioning table (Figure 90) is a custom design made from “off the shelf” commercial parts. Each axis consists of an electric-motor-driven ball screw, an electric brake, two guide rails, and four bearing carriages. Limit switches and hard stops are used to protect against overtravel. Spring-loaded brakes are nominally engaged to hold the table position fixed until motion is required. The brakes are electronically energized to release the drive screws and allow the table to move.

Six position sensors (see Figure 91) will be used to measure relative position between the inlet and the fan rig. Three sensors will act as primary and three will be back up. The sensors will be bracketed to the fan rig bulkhead, and the targets will be mounted to the back face of the inlet. The position sensor is a commercial part. It is a high-precision, inductive type that measures a gap between the sensor head and the target. The sensor has a measuring range of 0.24 inches and an accuracy of ±0.002 in.

Inlet emissions will be recorded using microphone rakes (see Figure 90). An existing translating rake can obtain acoustic data at emission angles (at 0.2 M) relative to the inlet highlight at angles of 26.6° and larger. Two new rakes will be added to record acoustic data at upstream emission angles of 22.2° and 15.0°. The two new rakes will be mounted to a linear actuator that will push the rakes through an opening in the tunnel floor. Both rakes will be vertically translated 44 inches at the same time up to the fan rig centerline. Once data are recorded, the actuator will retract the rakes to a 10-inch distance above the floor. An existing acoustic-barrier wall will block aft-emitted noise.

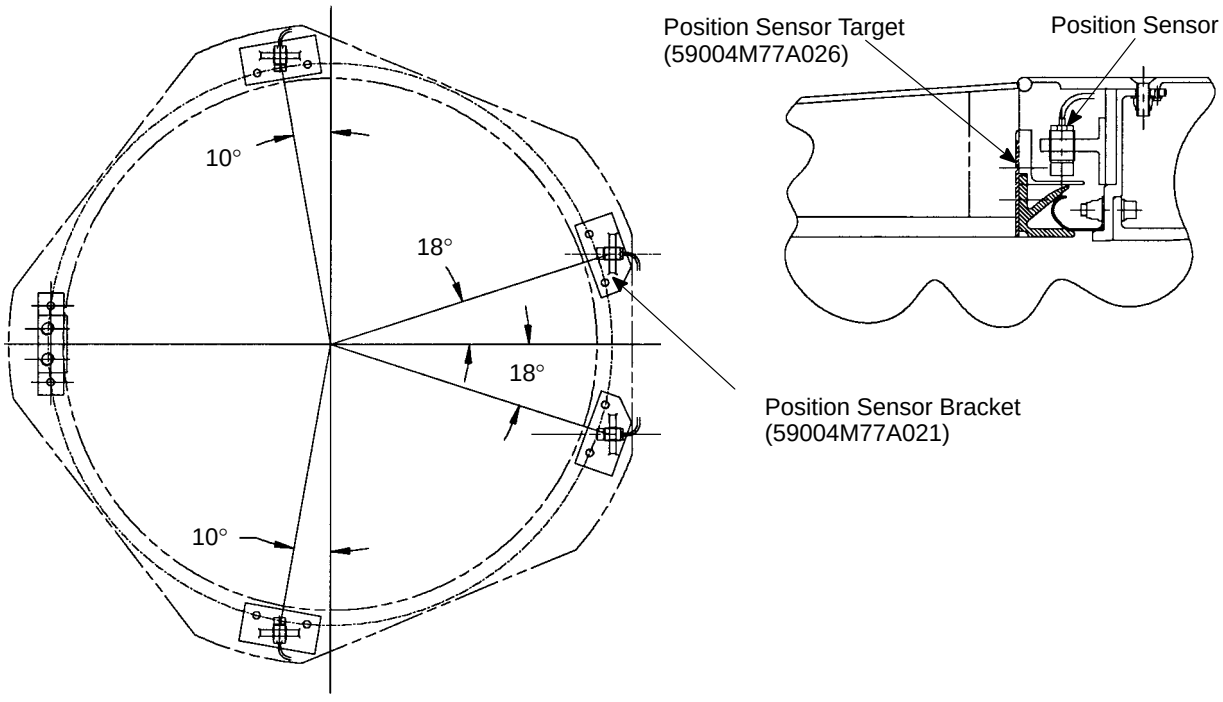

Figure 91. Two-Dimensional Inlet Position-Sensor Arrangement

7.2.3.2 Fan Drive Rig Support

The HSCT fan, stators, fan flowpath, and nacelle are attached to the NASA–Glenn UHB fan drive rig. The drive rig consists of a support strut and turntable, a 4800-hp air turbine and drive shaft, and a stiff sting/housing assembly. The turntable (for angle-of-attack testing) will not be used in the HSCT testing. Tubes in the support strut supply the turbine drive air from the facility 450-psi system. Pressure, temperature, accelerometer, and strain gage instrumentation are routed off the drive rig through strut fairings. Signals from fan strain gages are carried through the drive shaft to a slipring behind the turbine and then down the strut. Rig and fan data are processed by high-speed computer and displayed in the control room.

The drive rig speed is controlled by adjusting the turbine air pressure with hydraulic valves located below the floor of the test section. The speed-control computer is located in the facility control room. The speed-control system is set up to monitor the safety of the drive rig and automatically go to safe condition or shut down if specified limits are exceeded. Overspeed, bearing temperatures, rig vibrations, lube system and slipring health, and fan/stator strain gages are monitored. A history log of selected safety measurements is recorded, as well as safety tapes of selected accelerometer and strain gage signals.

7.3 Fan/Inlet Downselect

As discussed in Section 7.1 and illustrated in Figure 82 (page 75), it is forecast that fan/inlet noise potentially is a primary component of total aircraft system noise at approach and, as suggested in Figure 80, has a significant impact on system community (cutback) noise as well. Because of uncertainty in the nominal noise level predictions, there is a high likelihood that system noise will not meet the program goals at approach and that the aircraft system sizing/performance is significantly impacted by the fan/inlet contribution to community (cutback) noise levels.

It therefore was decided to investigate options for noise reduction of the fan/inlet system for potential evaluation in the scale-model fan/inlet test. As discussed in Section 7.2, many noise-reduction concepts were considered before downselecting to a few. A brainstorming session was held with an expanded team consisting of experts in acoustics, fan and inlet performance, and fan and inlet mechanical design. A ranking system was developed to evaluate the many options that came out of the brainstorming session, and the ranking system was used to downselect to a few noise-reduction options which, based on the ranking methodology, had the greatest probability of success with the lowest penalties in performance, weight, and complexity.

This section describes the fan/inlet noise-reduction concepts downselect criteria, process, and results, as well as the quantitative assessment of the benefits of the “final few” selected for evaluation on the scale-model fan/inlet test.

7.3.1 Concept Selection Criteria

The criteria for ranking the various ideas from the expanded team brainstorming sessions are listed in Table 4. Team members were asked to rank each noise-reduction criteria according to the four categories listed in Table 4 and to rank them with scores of 1, 3, or 5, corresponding to the relative impact the idea or concept might have in each of the four categories. The results of the rankings of the team members were tallied to prioritize the proposed concepts.

Table 4. Brainstorm Concept/Idea Ranking and Scoring Criteria

Category	Description	Scoring
1	Noise-Reduction Potential	L = 1
		M = 3
		H = 5
2	Adverse Performance Impact	L = 5
		M = 3
		H = 1
3	Adverse Weight/Length/Complexity Impact	L = 5
		M = 3
		H = 1
4	Probability of Successful Evaluation/Demonstration	L = 1
		M = 3
		H = 5

Nine team members submitted ballots, but not all team members ranked all concepts, so scoring had to be done by averaging over the number of votes per concept. Some 50 concepts were proposed, many of which dealt with airframe configurational changes (such as high-aspect-ratio wing) or were similar concepts applied to different components in the inlet, fan frame, or fan blade rows.

7.3.2 Concept Downselect Process

The criteria described above were used by team members to evaluate the various fan/inlet noise-reduction ideas, and the results of their assessments were submitted via ballot. The ballots were tallied to generate a ranking for the ideas. Several ranking systems were proposed, including:

1. Weighting all categories equally
2. Weighting category 1 (noise reduction) twice as high as the others
3. Weighting categories 1 through 3 equally, then sorting by average score and category 4
4. Weighting category 1 twice that of 2 and 3, then sorting by average score and category 4

In general, the “top 20” ideas tended to be the same for all ranking systems, with one or two exceptions, but the order in which they appeared moved up or down on the priority list.

For several selected concepts, quantitative estimates of the noise-reduction benefits were attempted. The process used was to establish reference estimates of fan/inlet noise using an empirical, multistage-fan, noise-prediction model and then exercise the model with various assumptions regarding the impact of a given noise-reduction feature on the fan-noise characteristics.

Using the empirical multistage-fan noise model developed by GEAE from prior military engine acoustic test results, estimates of the fan noise at conditions corresponding to the FAR36 certifica-

tion approach, flyover, and sideline points were made. The predictions were then rerun with three amounts of suppression of the first stage fan blade-passing frequency (BPF) tone noise levels. These cases corresponded to 3-dB reduction, 6-dB reduction, and total elimination of BPF tones.

Three additional scenarios were predicted wherein all fan tones were reduced by 3 dB, 6 dB, and complete elimination, respectively. From these various scenario calculation results, and with some reasonable assumptions about the important mechanisms contributing to the fan tone levels, it was possible to evaluate several of the highly ranked noise-reduction concepts, based on the mechanism they were intended to affect.

7.3.3 Downselect Results

The highest ranked noise-reduction concepts are listed in Table 5 for ranking system number 2, which weights the noise-reduction score twice as much as the other category scores. There were actually two brainstorming or "ideas" lists generated during the course of the program, so in Table 5 those with the label "A" correspond to the first list, produced earlier in the program in the course of formulating the low-noise fan plan, and those with the label "B" correspond to the ideas from the brainstorming session. In addition, some ideas may have had two or three parts and so may have an a, b, or c ending to the concept identification. For example, concept B3b is part b of idea number 3 generated at the brainstorming session.

Table 5. Noise-Reduction Concept Ranking – Weighting System 2, "Top 20"

Concept	Description	Rank	Category				Total
			1	2	3	4	
A17	Increase Wing Aspect Ratio	1	4.89	3.56	2.78	4.89	4.2
A1	Increase IGV–R1 Axial Spacing	2	4.56	4.44	2.44	4.89	4.2
B22	Bulk Absorber Liners	3	3.86	5.00	3.43	4.43	4.1
A15	Optimize Liner Design	4	3.56	5.00	4.44	3.56	4.0
A2	Increase R1–S1 Axial Spacing	5	4.11	4.44	2.44	4.44	3.9
A13	Increase Inlet Doors Spacing	6	3.67	4.11	4.00	3.44	3.8
B3b	Axially Segmented Liners	7	3.13	4.89	4.00	3.38	3.7
B15	Flow Duct Liner Tests	8	2.50	5.00	4.80	3.43	3.6
A16	Inlet Soft Choke	9	4.22	2.00	3.44	4.00	3.6
A10	Increase Inlet Bifurcation Spacing	10	3.44	4.89	2.11	3.78	3.5
B23	Integrated Aero/Acoustic Design	11	3.33	4.17	3.83	3.00	3.5
A4	IGV–R1 Casing Liner	12	3.00	4.89	3.56	3.11	3.5
A5	Optimize IGV and S1 Vane Counts	13	3.44	3.78	3.78	3.11	3.5
B1a	Bifurcation Trailing-Edge Blowing	14	3.38	4.38	2.63	3.63	3.5
A14	Increase Inlet Liner Area	15	3.33	4.22	2.78	3.56	3.4
B16	VPI Screening Tests	16	2.86	4.40	4.20	2.86	3.4
B26	IGV–Less Fan	17	4.57	2.00	2.57	3.43	3.4
A12	Bifurcation T/E Blowing	18	3.33	4.44	2.22	3.78	3.4
A6	Sweep and/or Lean S1	19	3.22	4.00	4.22	2.33	3.4
B3a	Circumferentially Segmented Liners	20	2.63	4.89	3.78	2.88	3.4

Items B15, B16, and B23 are really processes and not noise-reduction concepts, but they were thought to be capable of providing additional insight and information that might lead to enhancing the noise reduction or reducing the penalties of other concepts. Items B1a and A12 are duplicates, coming from different "idea" sources. Item A17 (ranked number 1) is an airframe concept that basically reduces the thrust requirement at approach, hence reducing noise (the fan would operate at lower pressure ratio and tip speed). Item A16 is an inlet operational concept. If the inlet throat can be actuated to a more closed position during approach, the resulting higher inlet throat Mach number might reduce the inlet noise radiation from the fan. It was planned to test this concept in the scale-model fan/inlet test.

Items B22, A15, B3a, B3b, and A14 all have to do with the inlet liner design. All of these were addressed in the liner design studies leading to definition of the liners for the scale-model fan/inlet test program, through liner suppression studies of various liner segmentation patterns and impedance distributions. Item B26 was studied and deemed impractical from mechanical design and operability points of view, so it was not considered further. Increasing the axial distance between the inlet and the fan can accommodate items A10 and A13, and this feature was put into the scale-model fan/inlet test program.

From the list of noise-reduction concepts in Table 5 and the above distillation of concepts, the remaining noise reduction concepts (Table 6) were then considered for experimental evaluation and collectively identified as the "Low-Noise Fan" package option.

Table 6. Downselected Concepts for "Low-Noise Fan"

Concept	Description	Total Score
A1	Increase IGV–R1 Spacing	4.2
A2	Increase R1–S1 Spacing	3.9
A4	IGV–R1 Casing Liner	3.5
A5	Optimize IGV and S1 Vane Counts	3.5
A6	Sweep and/or Lean S1	3.4

Each of the above concepts was evaluated with available prediction model tools and databases, and these assessments are described in the following paragraphs.

Increase IGV–R1 Axial Spacing (Concept A1): If we assume that the vane/blade ratios for R1 and S1 are selected such that the R1–S1 and S1–R2 interactions are cut off, the majority of the BPF tone is produced by the IGV–R1 interaction. The fan noise database used in the HSR fan noise predictions came from tests that employed an aerodynamically clean (no inlet distortions) inlet with a turbulence control structure, so the predicted BPF tones at approach should primarily be from IGV–rotor 1 interaction. Analysis of the influence of tone reduction on fan noise (in effective perceived noise level units or EPNLdB) showed the trends listed in Table 7.

It can be seen from Table 7 that reducing BPF tone has a significant influence on the total fan EPNL and that this influence increases with increasing tip speed, consistent with the assumption that it is primarily caused by IGV–R1 interaction. At approach, the R1–S1 interaction can be assumed cut off, so it is reasonable to estimate that a 5-dB reduction in BPF can be achieved by increasing the axial spacing between the IGV and Rotor 1. This would reduce total fan EPNL about 2.5 dB.

Table 7. Predicted BPF Tone Reduction Effect On Fan EPNLdB

Condition	Tip Speed (ft/s)	Reduced 3 dB	Reduced 6 dB	Removed Completely
Approach	1000	–1.5	–2.7	–3.0
Cutback	1200	–2.3	–5.9	–11.3
Sideline	1400	–2.7	–5.7	–12.4

At cutback, rotor-alone noise and R1–S1 interaction noise are also contributing to the BPF tone, so conservatively it can be assumed that IGV–R1 interaction is only about half the total BPF noise. Thus, if increasing axial spacing reduces IGV–R1 noise by 5 dB, then the net reduction in BPF is only about 2 dB, which, from Table 7, yields a total fan noise EPNL reduction of about 1.5 to 2.0 dB. Similar reductions can be expected at sideline, since the sensitivity to BPF reductions is similar to that at cutback (flyover), and rotor-alone noise is cut on as well.

Increase R1–S1 Axial Spacing (Concept A2): At approach, the R1–S1 interaction BPF is cut off, so this is a higher harmonic tone benefit. The R2 BPF frequency is approximately equal to the R1 2BPF frequency, so only a portion of the "2BPF" of R1 can be impacted. Since S1 has 68 vanes and R2 has 47 blades, (V/B = 1.45), we can assume little transmission loss of the R2–BPF through S1 because counterrotating modes (V/B > 1) will pass right through S1 — no blocking effect. If we assume that the S1–R2 interaction noise is about the same level as the R1–S1 interaction noise, then by increasing the axial spacing ratio between R1 and S1 from about 0.1 to about 0.5 (axial spacing /axial chord), we can achieve a tone-noise reduction of about 5 dB for R1–S1 interaction, based on past experience with axial-spacing effects. This gives a net reduction of the total tone at 2BPF of about 1.8 dB.

At cutback, the R1 BPF tone is cut on. Assuming equal contributions of rotor-alone, IGV–R1, and R1–S1 interactions, reducing the R1–S1 by 5 dB through increasing R1–S1 axial spacing would give approximately 1.1 dB reduction in the total R1 BPF tone, in addition to the 1.8 dB reduction in the 2BPF and higher harmonics of BPF. Rolling these estimates into the empirical fan noise assessment model yielded a projected fan EPNL benefit of 0.6 dB at approach and less than 0.1 dB at cutback and sideline.

Add an IGV–R1 Fan Casing Liner (Concept A4): Because IGV–R1 interaction was assessed to be a strong contributor to the total fan noise, it was felt that significant benefit could be obtained by treating the fan outer wall between the IGV and R1. It could also reduce rotor-alone noise from R1 at transonic and supersonic tip speeds. This option is only viable when the increased-axial-spacing option (A1) is employed. It was estimated that, assuming a spacing increase (model scale) of 2.3 inches, and assuming about 80% effective treated area can be accomplished, a treatment length-to-diameter ratio L/D = 0.13 would be achieved. For this level of treated L/D, approximately 1-dB suppression of tone levels was estimated, which translates to about 0.5 dB in total fan EPNL at approach and to about 1 dB at cutback and sideline.

Optimize IGV and S1 Vane Counts (Concept A5): The IGV is actually a variable-flap vane. The leading edge forms the fan front frame strut and is a structural member. It would be desirable to have an IGV count that is at least twice the number of R1 blades, so as to cut off the R1 BPF. But this would be very difficult to implement because of the IGV flap actuation and clearance complexities. In addition, having a high vane count can cause interference at the hub and introduce flow choking due to the higher blockage, thus limiting fan flow. An alternative to having a cut-off vane/blade ratio is

to select a vane count that provides an increase in transmission loss of the rotor–generated noise. This is accomplished by selecting a vane/blade ratio that provides a positive (in the direction of rotor rotation) spinning mode order between the IGV and R1 so that the reflection off the IGV's when the IGV flaps are partially closed is enhanced. This is because the spinning mode wave front is nearly parallel to the IGV flap surface and provides a greater reflection of the wave front back into the fan stages. It was conservatively estimated that this would provide about 2-dB reduction in R1 BPF tone, especially if the increased axial spacing option was also in place, because the contribution of the IGV (due to rotor leading-edge potential field interaction) would be minimal.

For Stator 1, it was deemed sufficient to specify a vane count that was cut off and hence did not contribute to the R1 BPF tone frequency.

Sweep and/or Lean Stator 1 (Concept A6): Mechanical design constraints prevented increasing the axial spacing between R1 and S1 sufficiently to allow any significant axial sweep of S1. Leaning S1 was possible, however, and a parametric study of the effects of leaning S1 on R1–S1 interaction noise was carried out using the NASA V072 code. Since R1 BPF was cut off, the effects on higher harmonics were evaluated by varying lean angle over a range from 0° to 30°. The impact was found to be very small: no change in 2BPF, 2 to 3 dB reductions in 3BPF, and 1 dB increases in 4BPF were observed. By increasing axial spacing to about 0.6 chords, some additional benefit to 3 and 4BPF were observed, but the baseline levels were substantially lower than 2BPF, so the net impact on total noise level was minimal. Based on these study results, it was decided that S1 vane lean did not offer a significant noise reduction, and was therefore dropped from consideration.

Final Assessment of Noise-Reduction Concept Benefits: It can be seen from the above discussions that a quantitative assessment of each of the concepts is quite complex. There are several mechanisms contributing to the various spectral components of the fan noise, and the relative importance of each mechanism changes with operating condition. In addition, some assumptions about the relative contributions must be made for the reference or baseline case so that the effects of changing these mechanisms via introduction of a noise reduction feature can be quantified; you have to know where your are before you can predict where you will be. This requires some expert judgement; the assumptions for this study were based on the best information available. It is very likely that some of the assumptions can be verified in the planned scale-model fan/inlet test.

A book-keeping model of the various noise generation mechanisms was based on exercising the empirical multistage fan noise model with various amounts of BPF tone reduction, higher harmonic tone reduction, broadband noise reduction, and hypotheses for how much each mechanism contributed to each of these components. Six source mechanisms were identified, and contributions to each of the tone components were assigned. For each noise-reduction concept, a decision was made as to whether it affected a given mechanism and by how much. From these noise-reduction assignments and the previously established sensitivities of reductions of tone components on total fan EPNL, a net effect of each noise reduction concept was calculated. These calculations were done for each concept by itself and then in combination with others. The results are listed in Table 8.

In addition to the four concepts discussed above and listed in Table 7, the IGV-less fan concept was evaluated, for comparison. It can be seen, based on this book-keeping model, that the concept effects are interactive; that is, impact on the total fan EPNL is sometimes a function of whether or not one or more of the other concepts are included. For example, the increase in R1–S1 spacing, concept 4 (A2), has only a small effect if implemented by itself (0.6 dB), but it provides an additional 1.5 dB reduction when added in combination with concepts 1, 2, and 3.

Table 8. Low-Noise Fan Concepts Assessment Summary: Fan Component EPNL Change Re: Baseline, dB

Concept	Idea	Description	Approach	Cutback	Sideline
1	A1	Increase IGV–R1 Spacing	–2.9	–1.1	–1.1
2	A4	IGV–R1 Casing Liner	–1.2	–1.2	–1.2
3	A5	Optimize IGV Count	–0.9	–0.5	–0.5
4	A2	Increase R1–S1 Spacing	–0.6	0.0	0.0
1 + 2		Concepts 1 and 2	–3.7	–2.1	–2.1
1 + 3		Concepts 1 and 3	–3.4	–1.3	–1.3
3 + 4		Concepts 3 and 4	–1.6	–0.6	–0.6
1 + 4		Concepts 1 and 4	–4.1	–1.2	–1.2
1 + 2 + 3		Concepts 1, 2, and 3	–4.1	–2.2	–2.2
1 + 3 + 4		Concepts 1, 3, and 4	–4.8	–1.4	–1.4
All		Concepts 1 through 4	–5.6	–2.3	–2.3
5	B26	No IGV's	–3.7	–1.4	–1.4

It should also be noted that concept 2 (A4) can only be done in conjunction with concept 1 (A1), so any effect by itself is academic. Another observation is that concepts 1 and 2 together provide about the same benefit as removing IGV's altogether, so there is no acoustic advantage to removing IGV's if the increase in axial spacing can be accommodated.

The results listed in Table 8, although based on many assumptions as yet to be verified, provided quantitative assessments that the Low-Noise Fan package could provide significant noise reduction and therefore warranted testing in the scale-model fan/inlet test program.

7.4 Baseline Fan and Low-Noise Fan Development

The XF120 fan was chosen as a reference for acoustic parameters. An attempt was made to be the same as the XF120 fan or better in acoustic cutoff airfoil ratios and axial spacing. Acoustic parameters for the baseline and low-noise configurations relative to XF120 fan are listed in Table 9.

Table 9. Acoustic Parameter Comparisons *Low-noise configuration ratios are in parentheses.*

Parameter	Airfoil Number Ratio		Axial Spacing Ratio	
	HSCT	XF120	HSCT	XF120
IGV–R1	1.1	– – –	44% (100%)	17%
R1–S1	2.8	2.2	23% (50%)	26%
S1–R2	0.6	– – –	33%	– – –
R2–S2	2.5	– – –	24%	– – –
S2–R3	0.6	– – –	30%	– – –
R3–S3	2.0	– – –	30%	– – –

7.5 Fan Design and Analysis Methods and Tools

The aerodynamic design of the fan was done at the full engine size and is covered in Subsection 3.3.2.2 – Fan Aerodynamic and Mechanical Design. For the FIAT model, the first two fan stages were scaled to a tip diameter of 19 inches. A unique fan exit case was designed for the model to turn the air to axial and provide structural support for the outer cases. The mechanical design and structural analysis of the fan model are documented in Deliverable DRD–220–L2 (Fan Detailed Design Review Package). The analysis/methods used included ANSYS, PATRAN, NASTRAN, finite element, 3D CFD, and other proprietary P&W tools.

7.6 Subscale Model Testing

Preliminary aeroacoustic testing has been performed at VPI and Florida A&M using a single-stage turbofan simulator as the fan source. This fan is powered by compressed air. The fan blade tip speed becomes supersonic with associated multiple pure tones above 65,000 rpm. Characteristics of the fan are as follows:

- Rotor diameter 4.1 inches
- Rotor blades 18
- Stator vanes 26
- Design RPM 80,000
- Max. mass flow at design 2.72 lbm/s
- Design stage pressure ratio 1.6

7.6.1 VPI Results

Model testing at VPI was in their anechoic chamber under static conditions. Acoustic data were taken on a 48-in radius from the inlet highlight 0° to 110° from the fan inlet axis in the horizontal plane. The model inflow was not conditioned with a turbulence-reduction device. Exhaust airflow from the research fan and drive turbine was ducted out of the acoustic arena. Limited aerodynamic measurements were made to quantify the flowfield entering the rotor.

Likely candidate turbofans for a supersonic transport would include inlet guide vanes. The turbofan simulator, being representative of modern subsonic engines, does not have inlet guide vanes. A 14-vane IGV was made to investigate inlet noise contributions due to IGV/rotor interaction. The vanes were made of 0.031-in thick steel plate. Data were taken at 30,000, 50,000, and 70,000 rpm, which correspond to 40%, 60%, and 88% design fan speed.

CTOL Inlet – Baseline noise measurements were made with a conventional subsonic inlet. Tests were made with and without the simulated IGV's in place. The IGV were located 0.8 chord upstream from the rotor. At 60% fan speed the fundamental tone level is about 7 dB higher with the IGV in place; the overall sound power level (SPL) was 9 dB higher with the IGV's.

NASA Axisymmetric P–Inlet – Initial tests were conducted with a model of the NASA P–inlet (Reference 7). The P–inlet had a rounded "bellmouth" lip and closed auxiliary doors. Four prominent inlet-support struts were in proximity to the fan face. The simulated IGV was not used for this test. Support-strut, trailing-edge blowing was successfully used to reduce the wake deficit from

these struts, thereby reducing inflow distortion at the rotor face. This trailing-edge blowing reduced fundamental tones as much as 9.5 dB at some azimuthal angles. Lesser noise reductions were seen for the harmonics and broadband noise.

Boeing Axisymmetric Translating Inlet – A representative axisymmetric inlet was made using an inlet bellmouth lip rather than the typical sharp lip to facilitate testing under static conditions (see Figure 92). Auxiliary inlet doors were not present on this inlet. The inlet centerbody was modeled in the fully extended position. Acoustic results showed that strut trailing-edge blowing was somewhat less effective than for the NASA P–inlet — due to the dominance of the closely spaced IGV and reduced profile support struts (Reference 8).

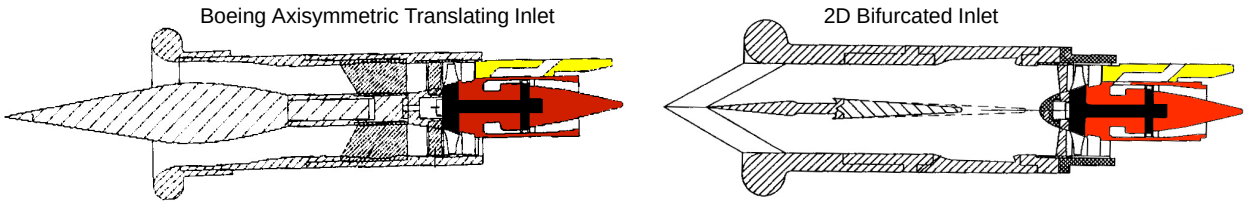

Figure 92. VPI Test Models Schematics

2D Bifurcated Inlet – A representative 2D bifurcated inlet with a bellmouth lip (see Figure 92) was likewise tested in the VPI anechoic chamber.

- The 14-vane IGV was tested at 0.8 and 4.5 chords from the rotor face.
- The inlet ramp was tested at an upstream position and with the ramp trailing edge one fan radius from the fan face. Overall sound level results showed the noise to be largely controlled by the proximity of the IGV rather than by the ramp at either axial position, although changes in ramp position caused significant changes in the fundamental-tone directivity.
- Trailing-edge blowing on the inlet ramp was deemed unnecessary due to the minimal tone contribution from the ramp wake compared to that from the IGV.

7.6.2 Florida A&M Results

A parallel testing effort was initiated with Florida A&M to test selected similar inlets using the same model turbofan simulator in an anechoic tunnel environment. This tunnel provided a Mach 0.2 takeoff/landing environment that should be more typical of aircraft operation than the earlier VPI static results. Acoustic data were likewise acquired on a 48-in radius from the inlet highlight from 20° to 110°. The test plan included the CTOL, axisymmetric, and 2D bifurcated inlets. However, the two supersonic inlets had typical sharp lips because testing was within a tunnel airflow rather than static, as was the case at VPI.

Acoustic data for the CTOL inlet showed good agreement with the previously acquired VPI results at static conditions. Rotor interaction tones showed the expected decrease of about 10 dB with forward flight. Future tests at Florida A&M were expected to extend these comparisons for the two supersonic inlet configurations, further validating the earlier VPI test results.

7.7 Remaining Challenges

Remaining challenges for the fan and inlet acoustic portion of the HSR/CPC program include the following:

- Trial fit of all the fan, nacelle, and inlet hardware
- Maintaining and verifying the position of the 2DB inlet relative to the fan and nacelle module during testing.
- Conducting the test program
- Analyzing the data from the test program
- Developing a empirical fan acoustic code for conducting future trade studies

7.7.1 Trial Fit

None of the scale-model fan and nacelle hardware has been trial fit on the NASA–Glenn drive rig that provides the support and power to drive the fan module. Previous fan/nacelle programs under the Advanced Subsonic Technology (AST) program indicated that trial fit of scale-model hardware is needed to minimize unproductive occupancy time in the test facility — modifying model hardware so that it fits as intended. To facilitate this effort, NASA–Glenn obtained a "dummy" UHB rig for trial fit of scale-model fan/nacelle hardware. Such a trial fit was performed on all of the AST programs. All of the fan (including the variations in rotor/stator spacing), nacelle, variable-area nozzle, bellmouth, and CTOL inlet hardware can and should be trial fit on the "dummy" UHB rig prior to installation in the wind tunnel. During the trial fit, the variable fan nozzle can be assembled and operationally checked. In addition the fan rotor and stator strain gage wire routing can be completed and interfaced with other rig components, and the various other instrumentation (pressure and temperature) can be trial routed within the fan module.

The 2DB inlet probably cannot be easily trial fit to the special support strut (being provided by NASA–Glenn) prior to installation in the wind tunnel. It would be very desirable to do this, if possible, to minimize the unproductive wind tunnel occupancy time. During the trial fit of the fan module hardware, it may be possible to at least check the interfaces between the fan module and the 2DB inlet.

7.7.2 Position of the 2DB Inlet

Probably the greatest remaining challenge for this program was to maintain and verify the position of the 2DB inlet relative to the fan and nacelle module during testing. The UHB drive rig is mounted from the NASA–Glenn 9×15-ft LSWT floor, and the 2DB inlet (too heavy to be supported from the fan module) is supported from a movable and controllable table mounted from the wall of the tunnel. The UHB drive rig moves in all three directions (axial, vertical, and horizontal) as a function of RPM, model and rig temperature, aerodynamic loads, tunnel vibrations, etc. The 2DB inlet will also move in all three directions as a function of various aerodynamic loading and tunnel vibrations. The relative motions of each may be up to 0.25 inches or more. Small misalignments of the inlet internal duct relative to the fan inlet may not be detrimental to the fan system during RPM and free-stream Mach number transients. However, even small misalignments during fan/inlet aerodynamic and acoustic performance testing may contaminate the results. The movable and controllable table has the resolution to maintain extremely good alignment between the inlet and fan, but verifying this position will be the major challenge.

7.7.3 Conducting the Test Program

Conducting any test program is a challenge, but this program will be especially difficult because of the numerous components and the complexity of the model hardware. The NASA and industry personnel assigned to the program must be experts in all aspects of the test planning and actual testing to ensure success. This test program was envisioned to take up to eight months including installation and checkout.

7.7.4 Analyzing the Test Data

Analyzing the data from this program would not be unlike that of any other multiple-discipline programs. However, an extensive amount of data were anticipated from the various combinations of fan and inlet configurations. In addition, the final analyses should include considerations and trades between the fan/inlet aerodynamic and acoustic performance predictions conducted in this program, as well as weight and other system considerations. In addition, the loss of expertise of the original team with regard to the aerodynamic and acoustic design philosophy and expectations from the test results is a challenge in assuring meaningful data analysis and interpretation.

7.7.5 Developing a Semiempirical Fan Acoustic Code

Once all the acoustic data have been obtained and analyzed for the various combinations of rotor/stator spacing, IGV number variations, and inlet variations, a semiempirical fan acoustic code can be developed for use in future design trade studies. It was planned to adapt a GEAE proprietary theoretical multiple-blade-row acoustic code (that was expanded by GEAE under this contract), along with the original empirical fan noise code and the parametric acoustic data obtained from this program, to develop a semiempirical fan acoustic prediction code for multistage fans. Development of the fan acoustic prediction code as planned will require some continuity of personnel from this program if any future fan acoustic code development program effort is to be most efficacious and efficient.

REPORT DOCUMENTATION PAGE

Form Approved
OMB No. 0704-0188

1. AGENCY USE ONLY (*Leave blank*)	2. REPORT DATE	3. REPORT TYPE AND DATES COVERED
	May 2005	Final Contractor Report

4. TITLE AND SUBTITLE

Critical Propulsion Components
Volume 4: Inlet and Fan/Inlet Accoustics Team

5. FUNDING NUMBERS

WBS–22–714–09–447
NAS3–27235

6. AUTHOR(S)

Pratt & Whitney and General Electric Aircraft Engines

7. PERFORMING ORGANIZATION NAME(S) AND ADDRESS(ES)

Pratt & Whitney
Advanced Engineering Operations
P.O. Box 109600
West Palm Beach, Florida 33410

8. PERFORMING ORGANIZATION REPORT NUMBER

E–15051–4

9. SPONSORING/MONITORING AGENCY NAME(S) AND ADDRESS(ES)

National Aeronautics and Space Administration
Washington, DC 20546–0001

10. SPONSORING/MONITORING AGENCY REPORT NUMBER

NASA CR—2005-213584-VOL4

11. SUPPLEMENTARY NOTES

This research was originally published internally in September 2000. Pratt & Whitney, Advanced Engineering Operations, P.O. Box 109600, West Palm Beach, Florida 33410; and General Electric Aircraft Engines, Advanced Engineering Programs Department, One Neumann Way, Cincinnati, Ohio 45125–6301. Responsible person, Diane Chapman, Ultra-Efficient Engine Technology Program Office, NASA Glenn Research Center, organization code PA, 216–433–2309.

12a. DISTRIBUTION/AVAILABILITY STATEMENT

Unclassified - Unlimited
Subject Categories: 01, 05, and 07

Available electronically at http://gltrs.grc.nasa.gov

This publication is available from the NASA Center for AeroSpace Information, 301–621–0390.

12b. DISTRIBUTION CODE

13. ABSTRACT ***(Maximum 200 words)***

Several studies have concluded that a supersonic aircraft, if environmentally acceptable and economically viable, could successfully compete in the 21st century marketplace. However, before industry can commit to what is estimated as a 15 to 20 billion dollar investment, several barrier issues must be resolved. In an effort to address these barrier issues, NASA and Industry teamed to form the High-Speed Research (HSR) program. As part of this program, the Critical Propulsion Components (CPC) element was created and assigned the task of developing those propulsion component technologies necessary to: (1) reduce cruise emissions by a factor of 10 and (2) meet the ever-increasing airport noise restrictions with an economically viable propulsion system. The CPC-identified critical components were ultra-low emission combustors, low-noise/high-performance exhaust nozzles, low-noise fans, and stable/high-performance inlets. Propulsion cycle studies (coordinated with NASA Langley Research Center sponsored airplane studies) were conducted throughout this CPC program to help evaluate candidate components and select the best concepts for the more complex and larger scale research efforts. The propulsion cycle and components ultimately selected were a mixed-flow turbofan (MFTF) engine employing a lean, premixed, prevaporized (LPP) combustor coupled to a two-dimensional mixed compression inlet and a two-dimensional mixer/ejector nozzle. Due to the large amount of material presented in this report, it was prepared in four volumes; Volume 1: Summary, Introduction, and Propulsion System Studies, Volume 2: Combustor, Volume 3: Exhaust Nozzle, and Volume 4: Inlet and Fan/Inlet Acoustic Team.

14. SUBJECT TERMS

High speed civil transport; High speed research; Mixed-flow turbofan; Mixed-compression inlet; Two-dimensional bifurcated inlet; Axisymmetric translating centerbody inlet; Variable-diameter centerbody inlet; Fans; Variable capacity fan; Conventional fan; Oversized fan

15. NUMBER OF PAGES

114

16. PRICE CODE

17. SECURITY CLASSIFICATION OF REPORT	18. SECURITY CLASSIFICATION OF THIS PAGE	19. SECURITY CLASSIFICATION OF ABSTRACT	20. LIMITATION OF ABSTRACT
Unclassified	Unclassified	Unclassified	